

18 Nuclear Cardiology

SHARMILA DORBALA AND MARCELO F. DI CARLI

PRINCIPLES OF IMAGING, 277

Single Photon Emission Computed Tomography, 277
Positron Emission Tomography, 278
Hybrid SPECT/CT, PET/CT, and PET/MR, 279
Radiotracers and Protocols, 280

SYSTEMATIC INTERPRETATION OF IMAGES, 287

Image Quality, 287

Image Display, 287
Image Review and Interpretation, 287
Photon Attenuation and Attenuation Correction, 288

REDUCING RADIATION DOSE, 288

PATIENT-CENTERED CLINICAL APPLICATIONS, 290

Ischemic Heart Disease, 290
Heart Failure and Cardiomyopathies, 298

Infective Endocarditis, 307
Cardio-Oncology, 310

MACHINE LEARNING AND ARTIFICIAL INTELLIGENCE, 311

TRANSLATIONAL MOLECULAR IMAGING, 311

Aortic Valve Disease, 312

REFERENCES, 312

Nuclear cardiology encompasses multiple quantitative imaging techniques with established clinical applications in ischemic heart disease, heart failure, cardiac and vascular inflammation and infection, with emerging applications in valvular heart disease and peripheral arterial disease (PAD). Extensive literature over the last 50 years supports a role for nuclear cardiology imaging to diagnose cardiovascular disease, stratify risk, and guide management. Over the past two decades, novel radiotracers, software improvements, instrumentation advances, and personalized low radiation dose protocols have transformed nuclear cardiology. This chapter reviews the principles of single photon emission computed tomography (SPECT) and positron emission tomography (PET) imaging, stress testing protocols, imaging protocols, and systematic scan interpretation, and methods to reduce radiation dose. We will discuss the diagnostic and prognostic value of nuclear cardiology in the context of case-based patient-centered clinical applications. We conclude with a brief overview of the emerging role of machine learning in nuclear cardiology and summarize some emerging clinical applications.

PRINCIPLES OF IMAGING

The primary nuclear cardiology techniques are SPECT and PET.

Single Photon Emission Computed Tomography Conventional SPECT

Conventional SPECT scanners consist of one or more (most commonly, two) detector heads mounted on a rotating gantry, thereby allowing three-dimensional (3D) SPECT in addition to two-dimensional (2D) planar imaging. Each camera head contains a radiation detector, consisting of a large scintillation crystal coupled to photomultiplier tubes and associated electronics, and a collimator (Fig. 18.1). The scintillation crystal converts energy from each gamma ray (high-energy photon) into many low-energy photons (light), which are converted to an electronic signal using a light sensor and subsequently amplified by an array of photomultiplier tubes. Gamma rays emitted from radiotracers in the patient spread out in all directions such that a 2D image formed on a bare detector would be inevitably blurred. Collimators are sheets of lead or other highly absorbent material mounted on the surface of the detector with a pattern of holes that restricts acceptance of high-energy photons that have traveled a path with a narrow range of angles (most other photons are absorbed) and help provide a clear 2D view. The most commonly used collimator has parallel holes. Although collimators are needed to localize the photons, most are absorbed and only 0.1% of the counts emitted from the patient reach the detector.¹ Conventional SPECT scanners collect planar images at multiple angles around the patient (called projection images) using two heads in a 90- or 180-degree configuration

for cardiac imaging. The American Society of Nuclear Cardiology (ASNC) recommends a 180-degree angular image acquisition, with two heads in a 90-degree configuration, and 60 projection images (30 per detector), 3-degree rotation per stop, 25 to 30 seconds of imaging per stop (13- to 16-minute scan duration), and gated imaging. The images are then reconstructed using a computer algorithm before review.

Because images are derived from multiple planar projections over the scan duration (step and shoot or continuous mode), that is, at any given time data are acquired at only two angular projections, dynamic imaging to quantify absolute radiotracer activity is challenging. In obese patients who cannot fit on the scanner table and for certain imaging applications (such as gated blood pool imaging), images can be acquired in a 2D planar mode (only left anterior oblique, left lateral, and anterior projections). Finally, the quality of SPECT images is determined by the number of counts collected. Some of the photons are attenuated by tissue, with more photon attenuation in obese persons, and they do not reach the detector and contribute to the image. The next two sections discuss novel image reconstruction software and scanner designs that have enhanced image quality.

Novel Image Reconstruction Software

Compared with conventional SPECT reconstruction methods, newer SPECT reconstruction algorithms have substantially enhanced image quality, making possible reduced radiation dose and/or rapid imaging protocols. Previously, analytical reconstruction approaches such as filtered back projection (FBP) were used; these images were often smoothed to reduce statistical noise, resulting in degradation of spatial resolution and image quality. Most current SPECT and PET scanners use iterative approaches such as ordered subset expectation maximization (OSEM). The advantages of these algorithms over FBP are better handling of noise and improved accuracy due to the ability to model the physics of photon attenuation and scatter, and to restore spatial resolution. The resolution of nuclear cardiology images is spatially variant, depending on the distance of the heart from the detector and the collimator geometry. With iterative reconstruction, this distance-dependent image blur can be estimated and corrected in a process called resolution recovery. These novel reconstruction algorithms lead to better spatial resolution and improved accuracy. In addition, improved noise compensation allows for reduced dose and/or scan duration with improved image quality. A significant practical advantage of these novel reconstruction methods is that they can be easily incorporated into older systems, as only software modifications are needed.

Novel SPECT Scanners

Modern SPECT scanners include innovative gantry designs with cardiofocal or 360-degree detector geometry (eFig. 18.1), semiconductor detectors and, in some cases, the potential for quantitative imaging.





Solid-state detectors convert photon energy directly to electrons, eliminating the need for bulky photomultiplier tubes. Importantly, the cardiocentric design allows for an approximately fivefold higher count sensitivity and improved spatial resolution, by nearly twofold. Protocols can thus be personalized into rapid protocols or low radiation dose protocols. Rapid protocols improve test tolerability, minimize patient motion, allow for multiposition imaging, and can provide early and rapid poststress ejection fraction (EF) measurements. With low radiation dose protocols, stress images can be performed first with a <2 mSv dose. Some dedicated cardiac scanners allow imaging in a seated position, further improving test tolerability. Novel detector geometries provide for simultaneous angular sampling over 180 degrees (cardiac scanners) or 360 degrees (novel whole-body scanners). Because all detectors acquire images simultaneously, patient motion can be challenging to detect. On the other hand, if the scan is prematurely terminated for any reason, tomographic SPECT images can still be

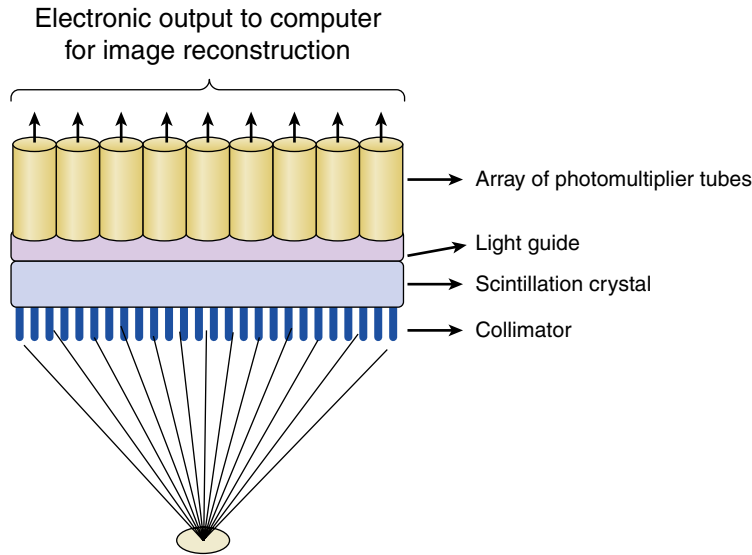


FIGURE 18.1 Principles of conventional SPECT. Conventional SPECT scanners include a collimator (blocks scattered photons and provides a clear view of the imaged object), a scintillation crystal (typically sodium iodide), light sensor (conversion of light into an electronic signal), and an array of photomultiplier tubes (amplification of the electronic signal).

reconstructed with the acquired data; this is not possible with conventional SPECT. A major advantage of the 360-degree geometry scanners and some dedicated cardiac scanners, compared with rotating conventional SPECT scanners, is that complete tomographic data are acquired simultaneously, making dynamic imaging and quantification of myocardial blood flow possible. These novel scanners have greatly expanded the range of cardiac SPECT applications.

Positron Emission Tomography

The fundamental principle of positron tomography is that positron emitting radionuclides (e.g., ¹¹carbon, ¹³nitrogen, ¹⁵oxygen, ¹⁸fluorine) decay by emitting “positively” charged electrons (positrons). Once released from the nucleus, these positrons travel short distances in tissue and annihilate when they encounter a nearby electron. This annihilation releases energy in the form of two high-energy gamma rays or photons that are emitted at 180 degrees from each other. These opposite high-energy photons (511 keV) are captured externally by an array of radiation detector elements (scintillators) in the PET gantry (Fig. 18.2). The most common PET detector materials are bismuth germanate (BGO), gadolinium oxyorthosilicate (GSO), lutetium oxyorthosilicate (LSO), and lutetium yttrium orthosilicate (LYSO).² The electronics of the PET system are arranged to facilitate detection of 511-keV photons arriving at opposite detectors within a narrow temporal window, and rejection of scattered photons arriving outside the preset temporal window (so-called electronic collimation), thereby enhancing the spatial and contrast resolution. Because there is no need for a physical collimator, as in SPECT, the sensitivity of PET is much higher. If one of the two photons is attenuated by tissue and does not reach a detector, the entire event is rejected by the system, amplifying the adverse effects of attenuation on image quality.² Attenuation correction is, therefore, necessary for PET. A radionuclide transmission image or, most commonly, a computed tomography (CT)-based transmission image provides soft tissue densities from which photon attenuation maps are generated and used to correct the inhomogeneities caused by soft tissue attenuation on the PET emission images. Older generation PET scanners operate in a 2D mode using lead septa to separate detector rings; this improves image quality by minimizing detection of cross-slice scattered counts. However, these septa also

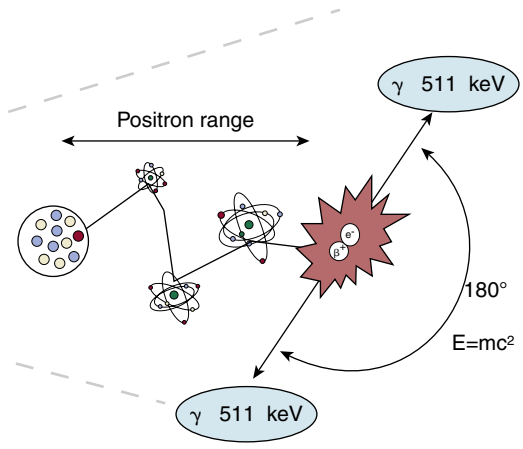
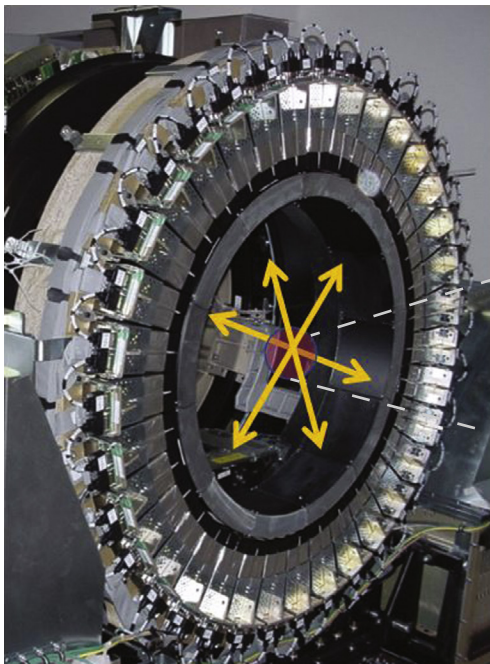


FIGURE 18.2 Principles of PET. The PET scanner consists of a series of rings of detector blocks that are typically integrated with a computed tomography (CT) scanner in the PET/CT gantry. The collision of a positron with a nearby electron produces an annihilation reaction that typically releases two high-energy photons (511 keV) that are emitted at 180 degrees from each other and captured by opposite detectors to form a coincidence line.

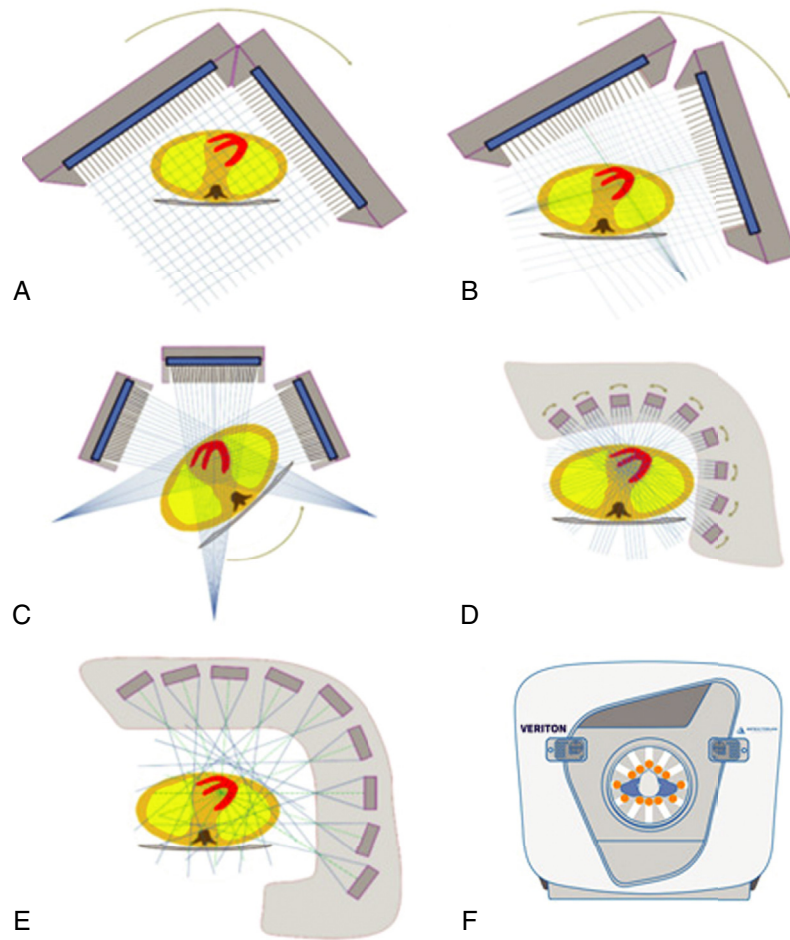


FIGURE 18.1 Novel SPECT scanner designs. **A** and **B**, Conventional scanners included two detector heads mounted on a gantry that rotate around the patient. **C–E**, Novel scanners offer simultaneous tomographic imaging with cardiofocal imaging that improves image resolution and count sensitivity. A novel collimator with converging holes (**B**) can be fitted to a conventional scanner to improve image resolution. **F**, A new-generation whole-body cadmium zinc telluride detector scanner is shown. (From Abbott BG, et al. Contemporary Cardiac SPECT Imaging-Innovations and Best Practices: An Information Statement from the American Society of Nuclear Cardiology. *Circ Cardiovasc Imaging* 2018;11:e000020.)

reduce true count rates, because they limit detection of photon pairs that are coincident to those detected in the same or adjacent rings. Current generation PET scanners are manufactured as 3D scanners without lead septa. Although the lack of collimation increases scatter and reduces effective spatial resolution, the 3D scanner design leads to substantially increased count rates, allowing rapid imaging and low radiotracer dose imaging.² Newer digital PET scanners include solid-state detectors with silicon photomultipliers with very high count rate capabilities that reduce radiotracer dose even more and allow for very rapid imaging. However, PET scanners are not widely available, and perfusion tracers and expertise with PET imaging remains limited. PET offers several advantages as listed in [Table 18.1](#).

Indications for cardiac PET myocardial perfusion imaging (MPI) and myocardial blood flow measurement with PET are listed in [Table 18.2](#).

TABLE 18.1 Advantages of Positron Emission Tomography

High spatial and contrast resolution
Capability for tomographic dynamic imaging with high temporal resolution
Accurate and depth-independent attenuation correction
High count sensitivity, making possible rapid protocols
Low radiation dose protocols (due to short half-life of the PET tracers)
Quantitation of absolute radiotracer concentration in tissue, including myocardial blood flow
CT hybrid imaging for quantification of atherosclerotic burden and localizing hot spot imaging tracers
Availability of a wide array of molecularly targeted clinical and research radiotracers that can image molecular processes in the pico and nano molar concentrations

TABLE 18.2 Indications for Cardiac Positron Emission Tomography Myocardial Perfusion Imaging and Myocardial Blood Flow Measurements

Rest-stress myocardial perfusion PET is a first-line preferred test for patients with known or suspected CAD who meet appropriate criteria for a stress imaging test and are unable to complete a diagnostic-level exercise stress imaging study
Rest-stress myocardial perfusion PET is recommended for patients with suspected active CAD, who meet appropriate use criteria for a stress imaging test, and who also meet one or more of the following criteria:
<ul style="list-style-type: none"> • Prior stress imaging study that is of poor quality, equivocal or inconclusive, affected by attenuation artifact, or discordant with clinical impressions or other diagnostic test results including findings at coronary angiography • Body characteristics that commonly affect image quality such as large breasts, breast implants, obesity, etc. • High-risk patients in whom diagnostic error carries even greater clinical implications, such as chronic kidney disease stages 3, 4, or 5; diabetes mellitus; and high-risk CAD • Young patients with established CAD who are expected to need repeated exposures to radiation associated cardiac procedures • Patients in whom myocardial blood flow quantitation is needed • Patients without known CAD who present with symptoms suspicious for myocardial ischemia • Increased suspicion of multivessel CAD • Suspected heart transplant vasculopathy • Patients with known CAD in whom more specific physiologic assessment is desired

CAD, coronary artery disease.
From Bateman TM, et al. American Society of Nuclear Cardiology and Society of Nuclear Medicine and Molecular Imaging Joint Position Statement on the Clinical Indications for Myocardial Perfusion PET. *J Nucl Cardiol* 2016;23:1227-1231.

Hybrid SPECT/CT, PET/CT, and PET/MR

Hybrid SPECT/CT and PET/CT scanners, in which the gantry integrates a CT scanner with a PET or SPECT scanner, are available. Depending on the type of CT scanner, CT images can be used for attenuation correction, quantification of coronary artery calcium, and/or CT coronary angiography (see [Chapter 20](#)). Attenuation correction CT is a low-dose, noncontrast, ungated free tidal breathing scan of the chest. A calcium score CT scan is a noncontrast, prospectively gated CT scan for dose reduction, acquired during an inspiratory breath-hold. With hybrid scanners, coronary artery calcification can be assessed either on the attenuation correction CT scan or using a dedicated calcium score CT scan. Calcium score, in conjunction with SPECT and PET MPI, plays a major diagnostic role, particularly in the evaluation of patients without prior known coronary artery disease (CAD) and with normal MPI (see section Patient-Centered Clinical Applications).

A coronary CT angiogram (CTA) is a prospectively electrocardiogram (ECG)-gated CT, with iodinated contrast, acquired during an inspiratory breath-hold (see [Chapter 20](#)). Unlike calcium score imaging, PET or SPECT MPI combined with coronary CTA is associated with a high radiation burden; therefore it is not recommended routinely. Sequential imaging (CTA followed by MPI or vice versa) can be helpful in complex cases. Radionuclide imaging has limited anatomic resolution and hybrid CT imaging (without or with iodinated CT contrast) provides localization of the tracer uptake, which is helpful in hot spot imaging (e.g., ^{99m}Tc-pyrophosphate for amyloidosis or 2-deoxy-2-[¹⁸F] fluoro-D-glucose [¹⁸F-FDG] for sarcoidosis or infection imaging).

PET/MR (magnetic resonance) scanners are currently used primarily for research. Attenuation correction is challenging in these scanners, but PET/MR offers the advantages of respiratory motion compensation and simultaneous imaging of dual physiologic processes. Details of PET/MR imaging are beyond the scope of this chapter, and readers are referred to more comprehensive reviews on this topic (see [Chapter 19](#)).

SPECT and PET Image Acquisition

There are four common modes of image acquisition with SPECT or PET: list mode, static, ECG gated, or dynamic. PET scanners and certain advanced SPECT scanners can acquire data in list mode (i.e., information is stored for every detected event). The list mode data can be summed into a single frame and reconstructed as a static image, binned into 8 to 16 cardiac cycle frames to evaluate cardiac function, or binned into time frames and reconstructed into dynamic image series for absolute quantification of radiotracer concentration in tissue (e.g., myocardial blood flow).

ECG-gated images allow assessment of regional wall motion and quantification of left ventricular (LV) volumes and EF [(LV end-diastolic volume – LV end-systolic volume/LV end-diastolic volume)×100]. Compared with echocardiography, gated SPECT or PET provides tomographic information and measurement of LVEF. Ventricular dyssynchrony can also be assessed using specialized software. Typically, a 8- or 16-frame gating is used with MPI (a higher frame gating of 24 or 32 frames is used for gated blood pool imaging).

Dynamic imaging allows tracking of radiotracer transit through the blood vessels and the heart starting with the time of radiotracer injection. These images can be analyzed using compartmental analysis, with an image-derived input function from arterial blood and tissue time activity curves from the myocardium. Myocardial blood flow estimates can be derived by this approach, incorporating corrections for radiotracer extraction characteristics, radiotracer decay, and the effects of limited spatial resolution. This can be performed at rest and during peak pharmacologic stress to compute rest and stress myocardial blood flow, respectively. The ratio of stress to rest myocardial blood flow is termed myocardial flow reserve (MFR). Dynamic imaging for myocardial blood flow quantitation requires pharmacologic stress testing with vasodilators (preferred) or dobutamine. During treadmill exercise stress, radiotracer injection occurs outside the PET gantry. Postexercise myocardial blood flow quantification is not feasible because of the lack of an arterial input function.

Radiotracers and Protocols

Nuclear cardiology uses radionuclide tracers with distinct molecular structures to probe various physiologic processes in the heart and vasculature. This section will mainly focus on clinically recommended radiotracers and standard stress and imaging protocols recommended by the ASNC.

Radiotracers

A wide array of radiotracers has been validated for the evaluation of myocardial blood flow, metabolism, innervation, amyloidosis, and microcalcification (Table 18.3), and several other radiotracers are currently under development.

Myocardial Perfusion Imaging Tracers. An ideal radiotracer for MPI should be extracted by the myocardium at a rate that is linearly related to myocardial blood flow. As shown in Fig. 18.3, most SPECT and PET perfusion radiotracers demonstrate linear extraction at relatively low blood flow rates, as in the resting state, or when there is significant obstructive CAD with a reduction in stress myocardial blood flow. As myocardial blood flow increases with exercise or pharmacologic stress, radiotracer extraction falls off and, consequently, myocardial blood flow is underestimated. Accuracy can be increased by using radiotracers with greater extraction at high flow rates; this is particularly important for the evaluation of nonobstructive CAD, diffuse CAD, or microvascular dysfunction. ^{15}O -water is close to an ideal tracer, as it is freely diffusible and the relationship between radiotracer extraction and blood flow remains linear at high flow rates. However, because it is freely diffusible, myocardial perfusion images are difficult to interpret, requiring special corrections or the use of parametric flow maps. Most software programs for myocardial blood flow quantitation correct for the expected roll off phenomenon at high flow rates; therefore ^{82}Rb and ^{13}N -ammonia, and ^{15}O -water can all be used to quantify myocardial blood flow; the first two are approved by the U.S. Food and Drug Administration (FDA) in the United States.

SPECT MPI Tracers. $^{99\text{m}}\text{Tc}$ -sestamibi, $^{99\text{m}}\text{Tc}$ -tetrofosmin, and ^{201}Tl are FDA-approved SPECT myocardial perfusion tracers. $^{99\text{m}}\text{Tc}$ is produced by a $^{99\text{m}}\text{Tc}$ -molybdenum generator and then compounded into $^{99\text{m}}\text{Tc}$ -sestamibi or $^{99\text{m}}\text{Tc}$ -tetrofosmin. $^{99\text{m}}\text{Tc}$ emits 140-keV gamma rays and has a half-life of 6 hours. After intravenous (IV) injection, $^{99\text{m}}\text{Tc}$ perfusion tracers passively diffuse into cardiomyocytes at rates proportional to blood flow and bind to the mitochondria within the first 60 to 90 seconds after injection. There is no significant redistribution of $^{99\text{m}}\text{Tc}$ perfusion tracers and imaging can be delayed for up to several hours. Because of the 6-hour half-life of $^{99\text{m}}\text{Tc}$, these SPECT perfusion tracers are commercially available as unit doses, increasing their accessibility. They are also suitable for exercise or pharmacologic stress testing.

In contrast, ^{201}Tl is produced by a cyclotron, emits lower energy photons (80 keV), and has a half-life of 73 hours. ^{201}Tl circulates to the heart at a rate proportional to blood flow and enters the cardiomyocytes via the Na^+/K^+ ATPase pump. ^{201}Tl washes out of normally perfused and hypoperfused regions at different rates. Early perfusion

defects on ^{201}Tl images represent reduced blood flow from ischemia or scar. Perfusion defects may resolve over time because of redistribution of ^{201}Tl in ischemic and hibernating regions; therefore poststress ^{201}Tl images are obtained within 10 to 15 minutes after injection. Because of its long half-life and relatively low photon energy, ^{201}Tl imaging is associated with a higher radiation dose. For this reason, it is currently not recommended for perfusion imaging; instead, it is used for viability assessment at sites without access to other viability tests (e.g., PET or cardiac magnetic resonance [CMR] imaging). Because of the high radiation dose, injected doses are low, leading to high levels of statistical noise and limited image quality. The newer solid-state scanners with high sensitivity provide much higher quality ^{201}Tl images and provide good quality gated images.

PET MPI Tracers. ^{82}Rb and ^{13}N -ammonia are FDA-approved PET perfusion tracers, whereas ^{15}O -water and ^{18}F -flurpiridaz are novel tracers that are currently under development.

^{82}Rb is a monovalent cation that enters the cardiomyocyte via the Na^+/K^+ ATPase pump. Because it has a very short half-life (76 seconds), (1) it is produced from a $^{82}\text{Sr}/^{82}\text{Rb}$ generator housed in an infusion cart next to the PET scanner, (2) exercise stress imaging is not feasible, and (3) rapid sequential imaging is possible.

^{13}N -ammonia enters the cardiomyocytes passively where it is converted into ^{13}N -glutamine and trapped in the glutamate pool. Compared with ^{82}Rb , it has a higher extraction fraction and a shorter positron range and is produced by a cyclotron. Because of its short (9.96 minutes) half-life, (1) an on-site cyclotron is required, (2) exercise PET is feasible, and (3) lower injected doses are administered compared with ^{82}Rb . Exercise PET with ^{13}N -ammonia can be logistically challenging. Close coordination is required with the cyclotron for delivery of the tracer, and exercise stress protocols may have to be modified to minimize radiotracer decay during the exercise period. Also, as mentioned earlier, exercise PET does not allow for quantitation of myocardial blood flow, which is an important advantage of PET MPI.

The superior extraction characteristics of PET tracers, compared with SPECT perfusion tracers, makes them more suitable for quantifying myocardial blood flow (see Fig. 18.3). ^{82}Rb and ^{13}N -ammonia have shorter half-lives compared with SPECT perfusion radiotracers, leading to a lower radiation dose for patients and rapid clinic throughput. However, unlike SPECT tracers, these PET perfusion tracers cannot be transported as single unit doses because of the short half-lives. ^{18}F -flurpiridaz is a novel PET perfusion tracer with a half-life of 109 minutes. This will make unit dose radiotracer delivery possible, which will greatly improve access to PET MPI. The extraction characteristics of ^{18}F -flurpiridaz are superior to those of ^{13}N -ammonia and ^{82}Rb and image resolution is superior to that of $^{99\text{m}}\text{Tc}$ -SPECT MPI (see section Translational Molecular Imaging).

Myocardial Metabolic Imaging Tracers. A number of SPECT and PET radiotracers have been developed to study myocardial metabolism.³ SPECT tracers of fatty acid metabolism (^{123}I -IPPA, phenylpentadecanoic acid, ^{123}I -BMIPP, 15-(p-iodophenyl)-3-(R,S)-methyl-pentadecanoic acid) are not approved by the FDA in the United States; therefore

TABLE 18.3 Characteristics of Clinically Used Radiotracers

	MECHANISM OF UPTAKE	EXTRACTION FRACTION	ENERGY	SOURCE
SPECT				
^{201}Tl	Na^+/K^+ ATPase pump	85%	69-81 keV	Cyclotron
$^{99\text{m}}\text{Tc}$ -sestamibi	Mitochondrial uptake	65%	140 keV	Generator
$^{99\text{m}}\text{Tc}$ -tetrofosmin	Mitochondrial uptake	60%	140 keV	Generator
$^{99\text{m}}\text{Tc}$ -PYP, DPD, MDP	Unknown	N/A	140 keV	Generator
^{123}I -meta iodobenzylguanidine (MIBG)	Active uptake via norepinephrine transporter	N/A	159 keV	
PET				
^{13}N -ammonia	Passive diffusion and incorporation into the glutamate pool	75%	511 keV	Cyclotron
^{82}Rb	Na^+/K^+ ATPase pump	55%	511 keV	Generator
^{15}O -water*	Diffusion	100%	511 keV	Cyclotron
^{18}F -flurpiridaz [†]	Mitochondrial complex 1 inhibitor	94%	511 keV	Cyclotron
2-deoxy-2-[^{18}F]fluoro-D-glucose (FDG) [†]	Active uptake via glucose transporters	N/A	511 keV	Cyclotron
^{18}F -sodium fluoride (NaF)	Microcalcification	N/A	511 keV	Cyclotron

*Not approved by the U.S. Food and Drug Administration for use in the United States.

[†]Shipped as unit doses.

DPD, 3,3-diphosphono-1,2-propanodicarboxylic acid; HMDP, hydroxymethylene diphosphonate; PYP, pyrophosphate; $^{99\text{m}}\text{Tc}$, 99m technetium.

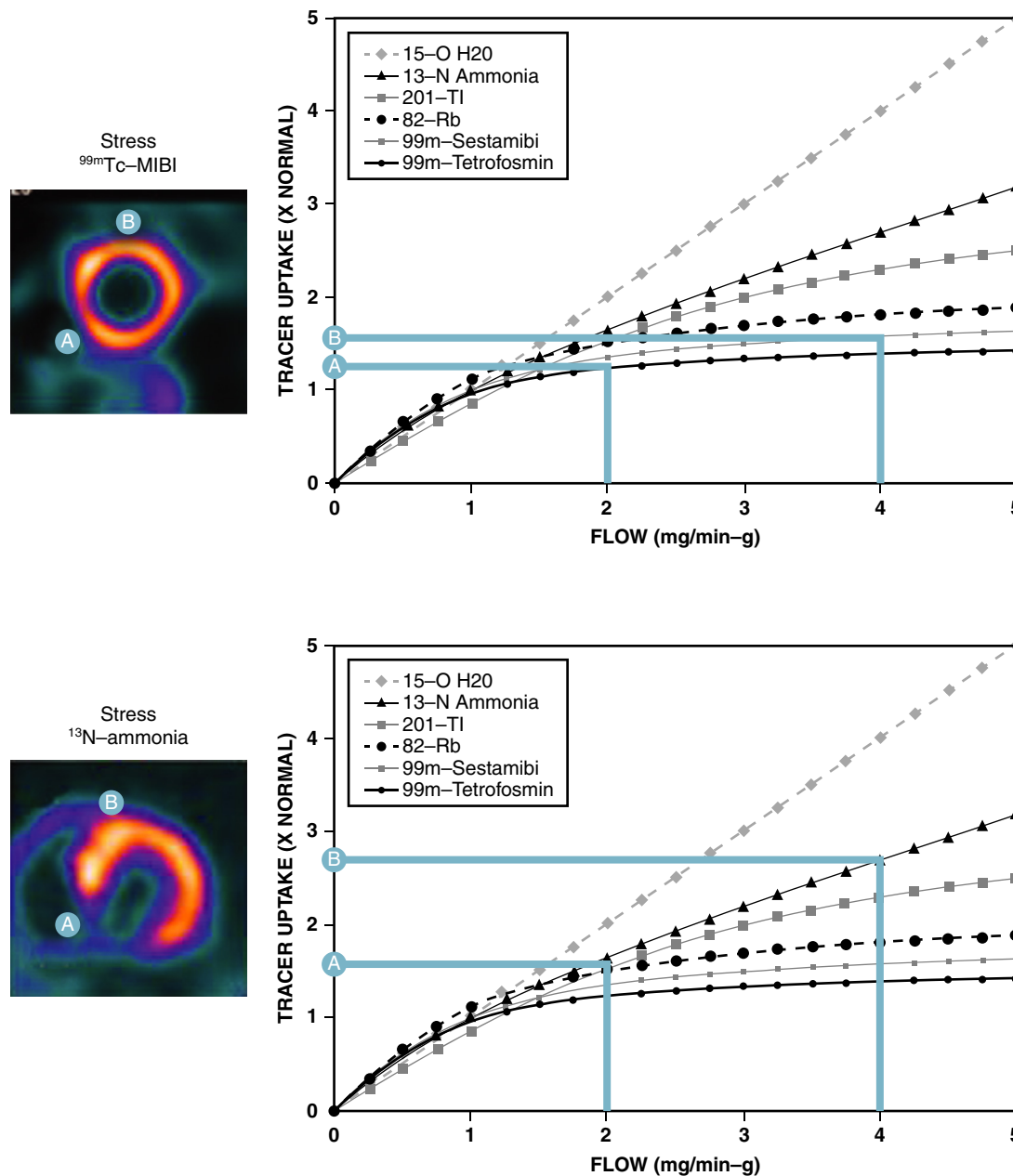


FIGURE 18.3 Relationship between myocardial blood flow, radiotracer uptake, and perfusion defect contrast. The linear scatter plot shows the characteristic roll-off in myocardial retention with increasing myocardial blood flow, which in turn determines perfusion defect contrast, for different radiotracers used in single photon emission computed tomography and positron emission tomography imaging. *Top:* Patient with an approximately 50% coronary stenosis imaged with ^{99m}Tc -sestamibi. The marked roll-off of sestamibi uptake at high flow rates leads to minimal contrast between the diseased coronary territory (point A) and the normal coronary artery (point B) and a relatively normal image. *Bottom:* Improved defect contrast when the same patient is imaged with ^{13}N ammonia, which has a less marked roll-off in tracer retention at high flow rates. (Adapted from Salerno M, Beller GA. Noninvasive assessment of myocardial perfusion. *Circ Cardiovasc Imaging* 2009;2:412-424.)

they are not used in clinical practice. PET tracers have been developed to image glucose metabolism (^{18}F -FDG, ^{11}C -glucose), oxidative metabolism (^{11}C -palmitate, $^{15}\text{O}_2$), fatty acid metabolism (^{11}C -palmitate, ^{18}F -FTHA[14(R,S)-[F-18]Fluoro-6-thia-heptadecanoic acid], FTP[4-thia palmitate], FCPHA[trans-9-F-18-fluoro-3,4-methyleneheptadecanoic acid]), lactic acid metabolism (^{11}C -lactate),³ and myocardial innervation (^{11}C -hydroxyephedrine[HED], ^{18}F -N-[3-bromo-4-(3-fluoro-propoxy)-benzyl]-guanidine [(^{18}F)-LMI1195]). The only clinically available FDA-approved tracer to image myocardial metabolism is ^{18}F -FDG.

^{18}F -FDG is a glucose analog used to image myocardial glucose metabolism. The primary clinical applications of cardiac ^{18}F -FDG PET are for imaging myocardial viability, myocardial and vascular inflammation, and infective endocarditis.² ^{18}F -FDG enters the cardiomyocytes through glucose transporters (GLUT 1 and 4), where it is phosphorylated by the enzyme hexokinase and trapped as ^{18}F -FDG-6-phosphate. Unlike glucose-6-phosphate, ^{18}F -FDG-6-phosphate cannot be metabolized. Normal myocytes are metabolic omnivores that can use glucose, fatty acids, or lactic acid based on substrate availability, neurohormonal

milieu, and cardiac work.³ Insulin, ischemia, and hypoxia induce translocation of glucose transporters to the plasma membrane and increase myocyte glucose uptake. Ischemic and hypoxic cells overexpress GLUTs and preferentially use glucose for their metabolic needs, independent of the substrate or insulin availability. Malignant cells and inflammatory cells are also characterized by significantly increased glucose uptake by an insulin-independent mechanism.⁴ Myocardial metabolism can be forced to switch to using glucose or fatty acids by dietary manipulation. Dietary preparation to switch myocardial metabolism to glucose or fatty acids forms the basis for the use ^{18}F -FDG to image myocardial viability (glucose load with IV insulin) and cardiovascular inflammatory conditions (low-carbohydrate, high-fat diet followed by prolonged fasting) such as sarcoidosis, infective endocarditis, and vasculitis.

Physiologic Basis for Stress Testing

The heart extracts oxygen nearly maximally at rest (60% to 80%).⁵ With exercise stress (or dobutamine infusion) there is a severalfold increase

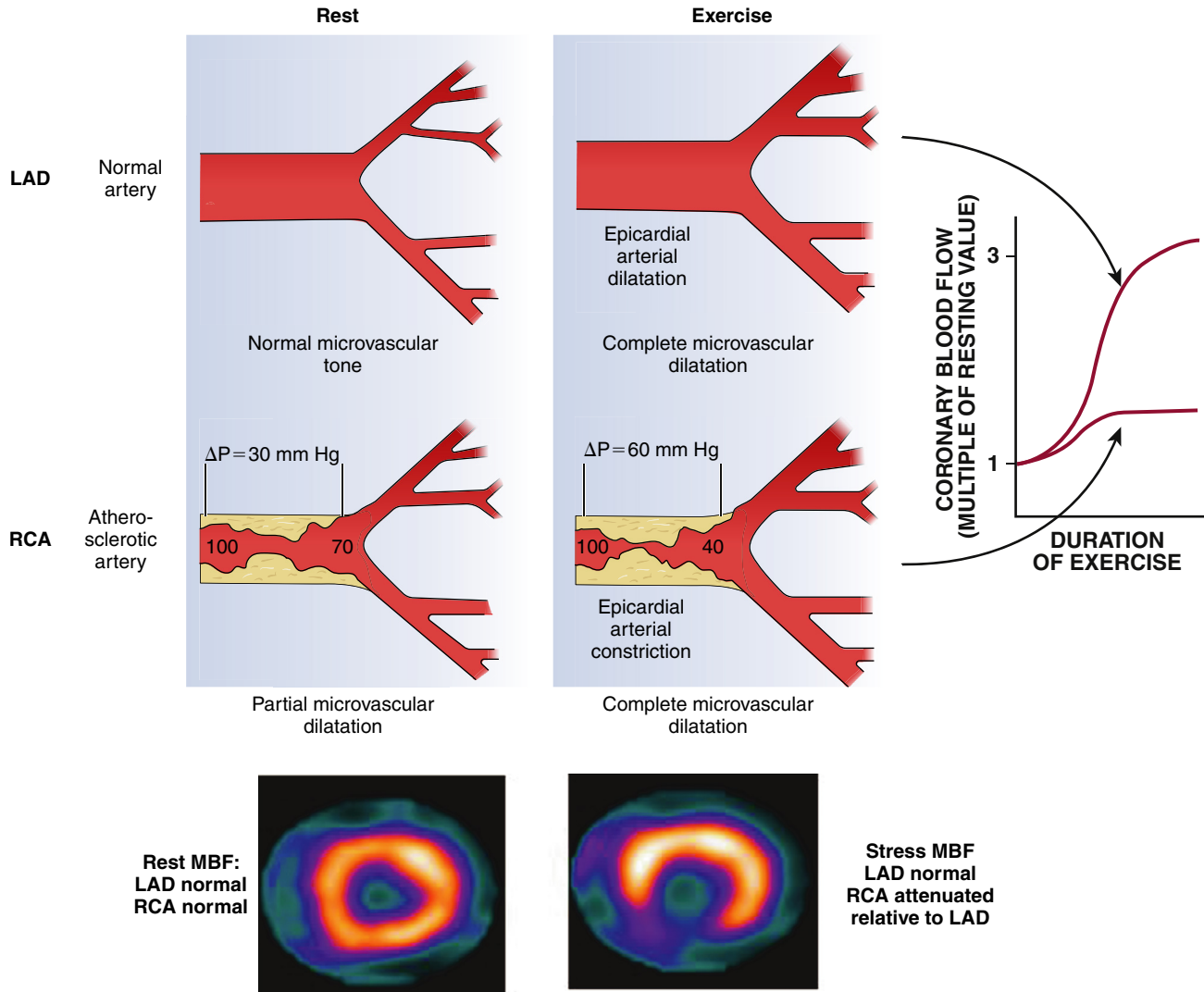


FIGURE 18.4 Physiologic basis of myocardial perfusion imaging. Schematic of two coronary arteries (left anterior descending [LAD], nondiseased, and right coronary artery [RCA], diseased). In the normal LAD artery, exercise stress causes vasodilation of the epicardial and microvascular bed increasing myocardial blood flow two- to fourfold compared to rest. However, the diseased RCA shows blunted coronary vasodilation in response to exercise. This difference in myocardial perfusion between diseased and nondiseased coronary arteries forms the basis for stress perfusion imaging. (Adapted from Wilson RF. Assessing the severity of coronary-artery stenoses. *N Engl J Med* 1996;334:1735-1737.)

in oxygen demand from high heart rate, contractility, and ventricular work that is met physiologically by increased blood supply from metabolic vasodilation. If the myocardial oxygen demand with exercise exceeds supply in any coronary territory, exercise-induced ischemia is provoked.

Normal coronary arteries have a coronary blood flow at rest of 0.7 to 1 mL/min, which can increase three- to fivefold during maximal vasodilation.⁵ Coronary blood flow remains constant over a wide range of coronary perfusion pressures through dynamic changes in tone in arterioles and other resistance vessels,⁵ and it only falls in the presence of very severe upstream coronary stenosis (>90% luminal narrowing; see [Chapter 36](#)). However, augmentation of myocardial blood flow in response to exercise/vasodilator stress is progressively blunted with increasing severity of upstream coronary stenosis ([Fig. 18.4](#)) and forms the basis for the use of stress radionuclide MPI for detection of obstructive CAD. These changes in myocardial perfusion represent the earliest event in the ischemic cascade, which ultimately leads to changes in myocardial metabolism, mechanical function, ischemic ECG changes, and angina ([Fig. 18.5](#)).

In contrast to exercise stress, vasodilator stress does not increase oxygen demand; the diseased and nondiseased territories manifest differential hyperemic responses due to differences in resting microvascular dilation. In myocardial territories supplied by coronary arteries with critical stenosis (>90%), where the microvasculature is maximally vasodilated at rest, vasodilation of the epicardial coronaries by

vasodilator stress agents can redistribute flow away from the subendocardium causing coronary steal,⁵ which can often manifest as ischemic ST depression during vasodilator stress testing. Finally, if there is severe multivessel obstructive CAD and coronary blood flow is reduced in all vascular territories, this can result in an apparently normal appearing relative myocardial perfusion image with no perfusion defects, also known as balanced ischemia. As discussed later in the chapter, integration of data from myocardial perfusion images with clinical, ECG, and hemodynamic response to exercise stress, and calcium score (when available), or myocardial blood flow (with quantitative PET MPI) may raise the suspicion of balanced ischemia. If balanced ischemia is suspected, further testing with coronary angiography (invasive for patients with high-risk stress features or symptoms, or coronary CTA for patients without high-risk features).

Stress Testing Protocols

Exercise stress, vasodilator stress, and dobutamine stress have been shown to have equally high diagnostic accuracy to identify obstructive epicardial CAD. Exercise is most commonly used. If not feasible or contraindicated, vasodilator agents are used. If they are not feasible or contraindicated, dobutamine/atropine stress is used with radionuclide MPI.

Exercise Stress

Stress testing using exercise stress with treadmill or bicycle is safe and is the preferred mode of stress in conjunction with radionuclide MPI.

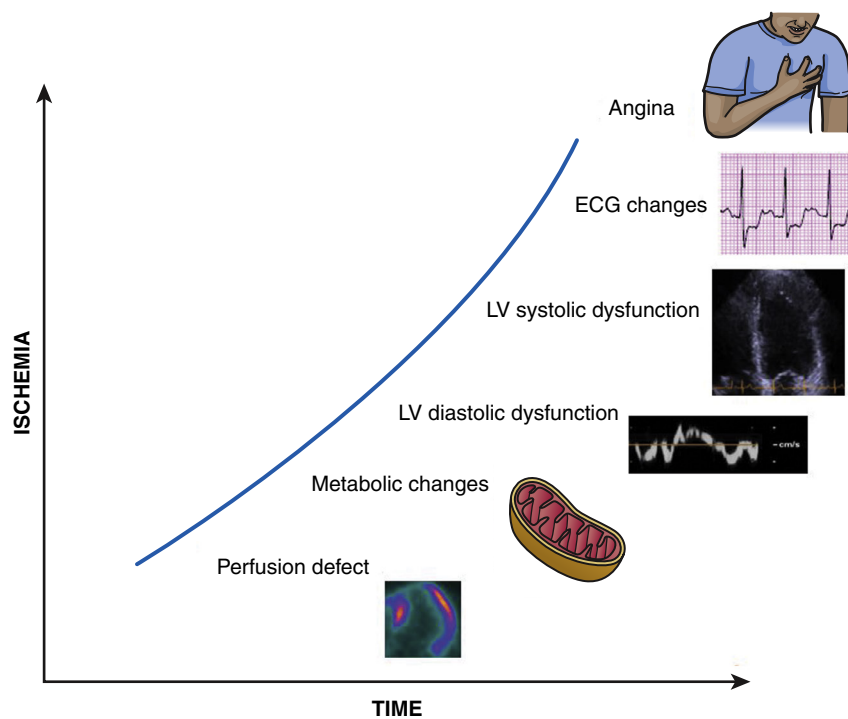


FIGURE 18.5 Ischemic cascade. Reduced regional myocardial perfusion is the initial stage in myocardial ischemia, setting the stage for mismatch between oxygen supply and demand. This leads to cellular metabolic changes, left ventricular diastolic dysfunction, systolic dysfunction, electrocardiogram (ECG) changes, and finally, angina. Typically, stress tests coupled with imaging myocardial perfusion are more sensitive than those that rely on detection of abnormalities in regional wall motion or ECG changes. (The image depicting metabolic changes is from Huss JM, Kelly DP. Mitochondrial energy metabolism in heart failure: a question of balance. *J Clin Invest* 2005;547-555.)

A standard Bruce treadmill exercise is the most widely used protocol. See [Chapter 15](#) for more details on contraindications, protocols, indications for premature termination of exercise, and treatment of complications. Exercise stress is preferred as it is physiologic, providing information on symptoms, functional capacity, and hemodynamic and ECG changes with stress. However, submaximal exercise decreases test sensitivity to detect ischemia and should be avoided. Pharmacologic stress testing provides an excellent alternative if exercise stress is not feasible (orthopedic or other limitations), contraindicated (recent acute coronary syndrome [ACS], or recent deep vein thrombosis, very large aortic aneurysm, etc.), or if patients are unable to exercise maximally. Maximal exercise is defined as ability to achieve an exercise heart rate of at least 85% of age-predicted maximal heart rate (220-age). To evaluate anginal symptoms on maximal medical therapy in patients with known prior CAD, a symptom-limited stress test irrespective of heart rate is often adequate if a reasonable workload of at least 5 metabolic equivalents (METs) is achieved. To evaluate anginal symptoms in patients without documented prior CAD, maximal heart rate response is desirable with exercise stress. If not, the radiotracer is not administered, and stress test is converted to a vasodilator stress. In those instances, regadenoson, a non-weight-based fixed dose stress agent is well suited for administration on the treadmill or soon after termination of exercise.

Pharmacologic Stress

Pharmacologic stress testing is the preferred stress modality for radiotracer MPI (SPECT and PET) in patients who are unable to exercise adequately, and for evaluation of residual ischemia in patients with recent ACS/myocardial infarction (MI) (see section Patient-Centered Clinical Applications).

Adenosine, dipyridamole, and regadenoson are the three most commonly used vasodilator stress agents. Adenosine binds to four types of adenosine receptors. Binding to A_{2A} receptors causes coronary vasodilation, whereas binding to the A_1 , A_{2B} , and A_3 receptors causes side effects of heart block, wheezing, and peripheral vasodilation, respectively.⁶ Dipyridamole causes coronary vasodilation by increasing endogenous adenosine levels. Regadenoson is a specific A_{2A} receptor agonist that

was developed to avoid the side effects of the nonspecific vasodilators. Vasodilator agents are contraindicated in patients with active wheezing, high-grade atrioventricular (AV) block without a functioning pacemaker, systolic blood pressure (BP) <90 mm Hg, and any contraindications for stress testing (acute MI, unstable angina, aortic dissection, acute pulmonary embolism). A few reports indicated that regadenoson stress testing is associated with seizures; thus it is contraindicated in patients with a history of seizures that are not well controlled or in those with structural brain injury (ischemic or hemorrhagic stroke or brain tumors). In those patients, a short-acting vasodilator like adenosine or dobutamine can be used.

Vasodilator agents provoke maximal hyperemia and thus are well suited for tests relying on perfusion imaging. As shown in [Fig. 18.6](#), adenosine (140 mcg/kg/min) and dipyridamole (0.56 mg/kg) are weight-based infusions administered over 4 minutes, whereas regadenoson is a fixed-dose rapid IV bolus over 10 seconds (0.4 mg/5 mL prefilled solution administered as a rapid bolus over 10 seconds).⁶ Vasodilator stress agents often cause symptoms of hyperemia in about 50% of patients including an urge to breathe deeply, chest tightness, headache, flushing, a 10 to 20 beat increase in heart rate, and a 10-mm Hg decrease in systolic BP. These side effects occur acutely with adenosine but are typically short-lived (due to the 3-second half-life of adenosine) and terminate when the infusion is completed. Exercise, including swinging the legs

on the side of the bed, hand grip exercise, or low-level treadmill exercise, improves symptoms and reduces heart block, which is common during adenosine infusion. Unlike exercise, which shunts blood to the exercising muscles, vasodilator agents cause splanchnic hyperemia and intense radiotracer uptake in the liver that may scatter into the inferior wall of the left ventricle; addition of low-level treadmill exercise has been shown to improve heart to liver ratio.⁶ Methylxanthines are competitive agonists of the adenosine receptors and can reverse the vasodilatory effects of adenosine, dipyridamole, and regadenoson. For this reason, they need to be held for at least 12 hours before vasodilator stress (see section Imaging Protocols). IV aminophylline (1 to 2 mg/kg slow push over 1 to 2 minutes) is used as an antidote for side effects of vasodilator stress agents. Vasodilator stress has been shown to be safe for evaluation of myocardial ischemia within 24 to 48 hours after presentation with ACS or uncomplicated MI. When vasodilators are contraindicated or cannot be used because of caffeine intake, dobutamine stress testing is used.

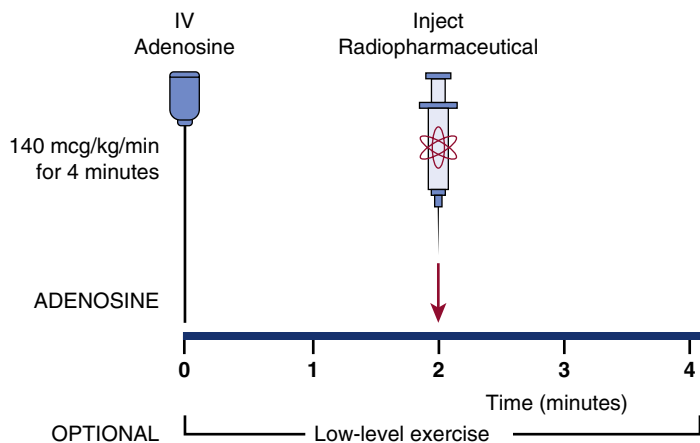
Dobutamine is administered as a weight-based graded infusion starting at 10 mcg/kg/min and escalating every 3 minutes by 10 mcg/kg/min to a maximum of 40 mcg/kg/min. The infusion is terminated 1 minute after injection of the radiotracer. If target heart rate is not achieved, atropine is administered as 0.5 mg IV followed by increments of 0.25 mg IV to a maximum of 2 mg IV (see [Chapter 16](#)). Dobutamine-atropine testing is less well tolerated compared with vasodilator agents and nearly 80% of the patients experience side effects from dobutamine. Dobutamine plus atropine stress testing with maximal heart rate response has been shown to increase myocardial blood flow equivalently to vasodilator stress. Atropine is contraindicated in patients with angle closure glaucoma and prostatism. For more details about indications and contraindications for stress agents, readers are referred to the ASNC stress protocols and tracers document.⁶

Imaging Protocols

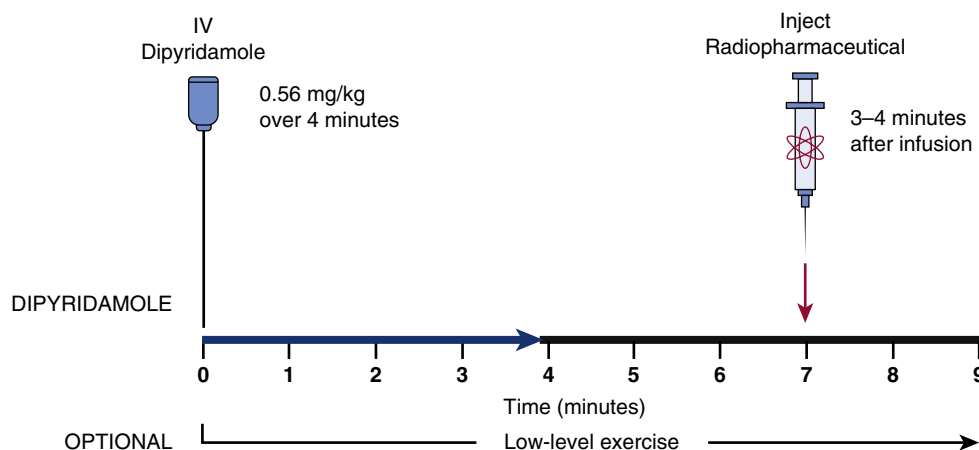
General Principles

Given the number of scanners, software, and radiotracer choices, and clinical questions, many possible protocols can be used for nuclear

A. Adenosine protocol



B. Dipyridamole protocol



C. Regadenoson protocol

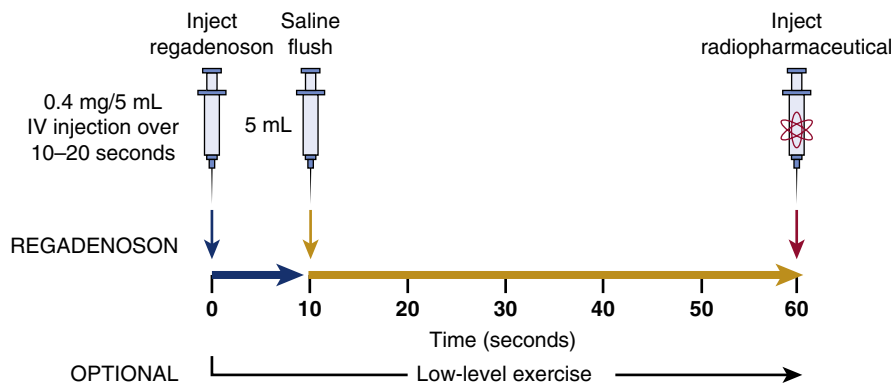


FIGURE 18.6 Pharmacologic stress protocols. Adenosine (A) and dipyridamole (B) are weight-based infusions administered over 4 minutes, whereas regadenoson (C) is a non-weight-based slow bolus injection administered over 10 to 20 seconds. Each of these pharmacologic stressors can be combined with low-level exercise.

PREPARATION FOR NUCLEAR CARDIOLOGY TESTING

Stress Testing

Patients are typically prepared with a 4 to 6 hour fast before a stress test and asked to abstain from smoking for 6 hours prior. Caffeine intake (including caffeine-containing medications) should be withheld for 12 hours, and theophylline-containing medications and oral dipyridamole are withheld for 48 hours before vasodilator testing. Patients with known CAD are generally tested on their anti-ischemic therapy. Patients without known CAD are ideally tested by withholding their beta blockers and antianginal medications for 12 hours before testing when feasible. Patients on dialysis are typically scheduled for their test on the day after dialysis. For more details of preparation readers are referred to ASNC/Society of Nuclear Medicine and Molecular Imaging (SNMMI) SPECT MPI guidelines.¹

¹⁸F-FDG for Viability Testing

Patients are prepared by a 6-hour fast. On arrival, fingerstick glucose level is checked and they are given an oral glucose drink. Forty-five minutes later fingerstick glucose is checked again and IV regular insulin is administered to drive down the blood glucose level to <150 mg/dL before administration of ¹⁸F-FDG. For more details of preparation readers are referred to ASNC imaging guidelines/SNMMI procedure standard for PET nuclear cardiology procedures.²

¹⁸F-FDG for Inflammation/Infection

Patients are prepared by using a high-fat, low to zero carbohydrate diet for at least two large meals 24 hours before the test followed by overnight fast (8 to 12 hour fast). For more details of preparation readers are referred to ASNC/SNMMI expert consensus recommendations.⁷

Amyloidosis Imaging and Gated Blood Pool Scans

No specific dietary preparation is necessary for gated blood pool scanning⁸ or for amyloidosis imaging with ^{99m}Tc-pyrophosphate, 3,3-diphosphono-1,2-propanodicarboxylic acid (DPD), or hydroxymethylene diphosphonate (HMDP) imaging.

SPECT Protocols

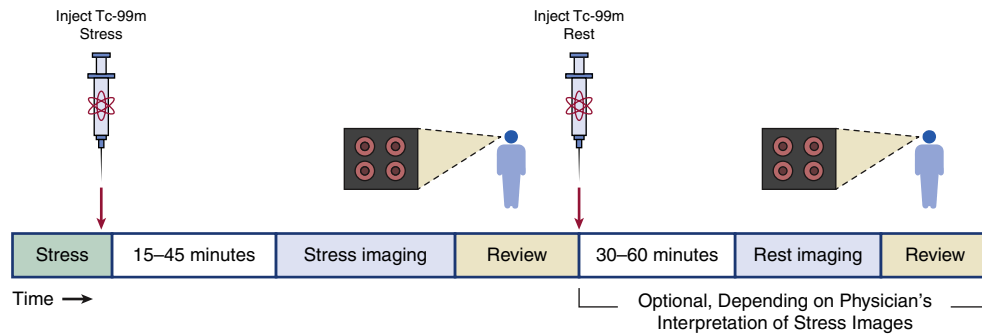
Myocardial Perfusion Imaging

With SPECT MPI the imaging protocol can be personalized to the patient and the clinical question. ^{99m}Tc-radiotracers with gated SPECT imaging is recommended. When available, advanced hardware (cadmium zinc telluride [CZT] SPECT scanners, novel collimators, attenuation correction) and advanced reconstruction methods (advanced iterative reconstruction and resolution recovery with noise reduction)

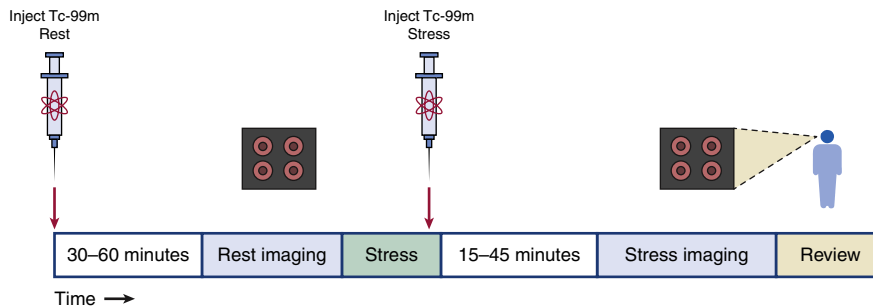
cardiology studies. Imaging protocols are optimally planned before the patient arrives for the test.¹ The optimal protocol is one that provides the best image quality with the lowest radiation dose and in the most expeditious manner.

Stress first and single-day rest followed by stress MPI are the mostly widely used protocols (Fig. 18.7A–B). Two-day protocols with stress first followed by rest on another day if stress MPI is abnormal are used in patients with large body habitus (see Fig. 18.7C).

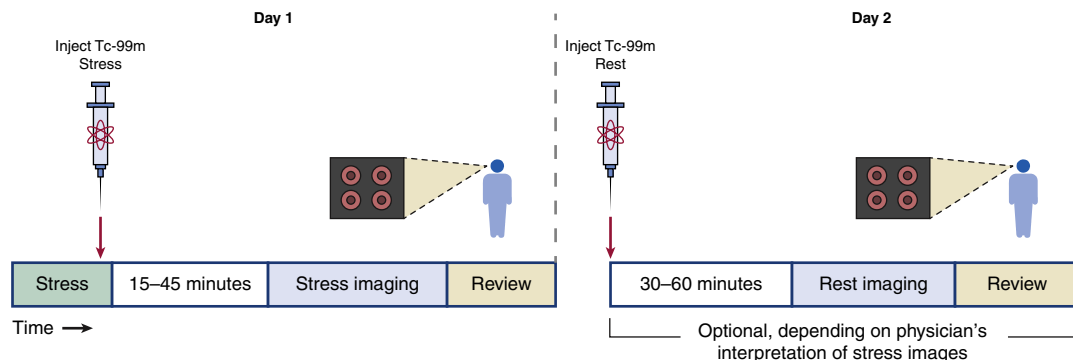
A. Stress-first single-day protocol



B. Rest-first single-day protocol



C. Stress-first two-day protocol



D. ^{99m}Tc -PYP/DPD/HMDP SPECT/CT protocol



FIGURE 18.7 SPECT imaging protocols. A–C, Recommended protocols for myocardial perfusion imaging. Two-day protocol is typically used for large patients or for young patients for low radiation dose studies. D, Recommended protocol for imaging cardiac amyloidosis. A dose of 15 to 20 mCi of ^{99m}Tc -PYP/DPD/HMDP is administered; after a 2- to 3-hour delay, planar and SPECT images are obtained. If available, SPECT/CT imaging is recommended to better delineate blood pool from myocardial retention.

In a stress-first protocol, stress MPI is performed first and only followed by rest imaging when stress images are abnormal. This protocol is preferred for patients without prior CAD because it is most efficient and associated with the lowest radiation dose to the patient. Stress-first MPI requires careful patient selection, review of the stress images as soon as they are completed, and a definitive scan interpretation

as normal. Advances in machine learning algorithms will soon guide the imaging teams on which patients to safely avoid rest imaging and improve the workflow for stress-first MPI. Also, this protocol is most effective with attenuation correction and advanced scanners. If stress-first MPI is performed using conventional scanners, multiposition imaging (supine/prone or upright/supine) and/or novel reconstruction

methods may help mitigate artifacts and minimize the need for additional rest MPI.¹ Most patients referred for SPECT MPI are candidates for stress-first imaging, except for patients with documented prior MI, those needing viability assessment, or those presenting with ACS who may benefit from rest and stress imaging. A normal stress-first imaging has been proven to have excellent prognostic value and portends very low likelihood of major adverse cardiac events (MACE).¹

For single-day ^{99m}Tc-rest-first MPI, the low rest radiotracer dose (4 to 8 mCi) is typically followed by a larger stress radiotracer dose (12 to 25 mCi, approximately three times the initial dose) to overcome the shine through of the first injection.¹ This is not necessary for two-day protocols where an equal amount of radioactivity is used, with stress imaging performed first, so that rest is only performed if needed (i.e., stress is not normal). Two-day protocols provide the lowest possible radiation dose and optimal image quality because there is no shine through of rest radiotracer activity.

SPECT and PET perfusion tracers are administered intravenously and extracted by cardiomyocytes within 60 to 90 seconds after injection. The images reflect myocardial perfusion at the time of radiotracer injection (rest or peak stress). Therefore it is important to maintain maximal stress (exercise or vasodilator) for at least 1 minute after injection of the radiotracer. In contrast, the ECG-gated images reflect myocardial function, EF and volumes at the time of the scan acquisition. SPECT MPI scans are typically acquired 15 to 45 minutes after stress radiotracer injection. Hence, most patients with reversible perfusion defects do not demonstrate regional wall motion abnormalities on the gated SPECT studies, unless ischemia is severe leading to postschemic stunning. In contrast, PET MPI-gated images are obtained immediately after completion of vasodilator stress and during peak dobutamine infusion. A lack of increase in LVEF with vasodilator stress or a decrease in LVEF post vasodilator stress with ⁸²rubidium PET has been shown to be a

marker of significant obstructive multivessel CAD (see section Patient-Centered Clinical Applications).²

Transthyretin Cardiac Amyloidosis Imaging

Transthyretin cardiac amyloidosis (ATTR-CA) can be imaged using 10 to 20 mCi ^{99m}Tc-PYP, ^{99m}Tc-DPD, ^{99m}Tc-HMDP (see section Infiltrative Cardiomyopathy: Amyloidosis), and planar and SPECT (SPECT/CT if available) imaging 2 to 3 hours after injection of the radiotracer (see Fig. 18.7D).⁸

PET Protocols

Myocardial Perfusion Imaging

For PET,² a single-day rest and stress MPI is performed with ⁸²rubidium or ¹³N-ammonia (Fig. 18.8A). With most advanced scanners, images are acquired in a list mode and reconstructed into static, gated, and dynamic images. With hybrid PET/CT MPI a dedicated noncontrast gated cardiac CT can be obtained for calculation of a coronary artery calcium score. The low-dose free-breathing CT obtained for attenuation correction can also be reviewed to assess semiquantitatively the presence and extent of coronary calcification. Although this is specific, it may be insensitive for detection of milder degrees of coronary artery calcification.

¹⁸F-FDG Metabolic Imaging Protocols

For viability imaging, glucose/insulin preparation is necessary. Then, ¹⁸F-FDG (5 to 10 mCi) is administered intravenously and cardiac PET/CT images are acquired 60 minutes later (see Fig. 18.8B).² For cardiac sarcoidosis (see Fig. 18.8C), infection, or vasculitis imaging (see Fig. 18.8D), patients undergo the high-fat/low-carbohydrate dietary preparation. Cardiac and partial or full-body PET/CT images are acquired 90 minutes after IV injection of ¹⁸F-FDG. For viability imaging and for sarcoidosis imaging rest MPI is performed before

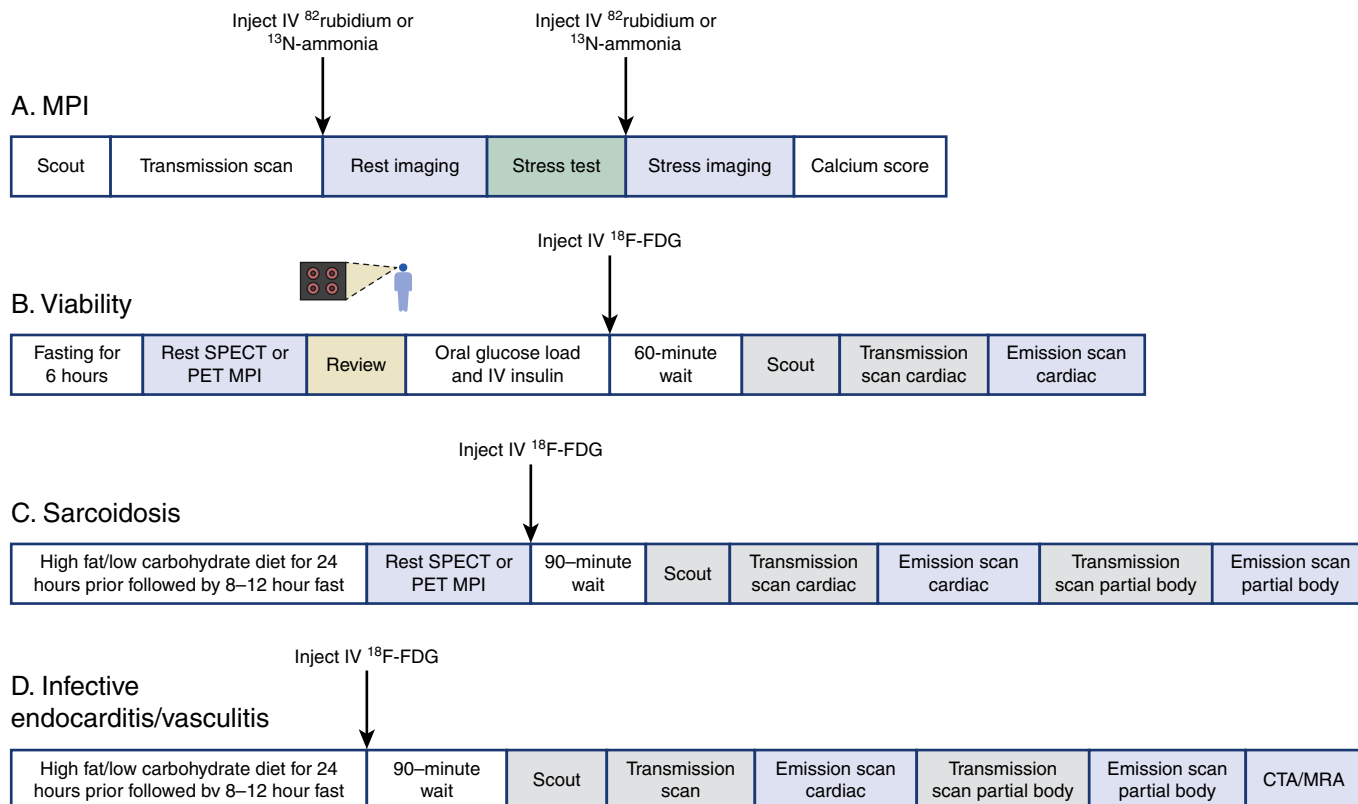


FIGURE 18.8 PET/CT imaging protocols. **A**, Myocardial perfusion imaging (MPI) protocols include (1) a scout scan to position the heart in the field of view; (2) nongated, low-dose CT transmission scan for attenuation correction; and (3) emission scan. MPI is typically performed in association with pharmacologic stress. However, exercise PET MPI is possible with ¹³N ammonia because of its longer physical half-life. In patients without known coronary artery disease, a gated CT scan to measure coronary artery calcium score can be added. **B–D**, ¹⁸F-FDG PET/CT protocols for myocardial viability, sarcoidosis, and infective endocarditis/vasculitis assessment. Specific dietary preparation is required for each of these ¹⁸F-FDG protocols as discussed in the text and in American Society of Nuclear Cardiology guidelines. Myocardial perfusion imaging is required for the evaluation of myocardial viability and cardiac sarcoidosis. Limited whole-body (chest, abdomen, and pelvis) ¹⁸F-FDG imaging is recommended for sarcoidosis, whereas whole-body (scalp to toes) imaging is recommended for infective endocarditis and vasculitis. CTA, CT angiography useful in cases of infective endocarditis; IV, intravenous; MRA, magnetic resonance angiography useful in cases of aortitis and vasculitis.

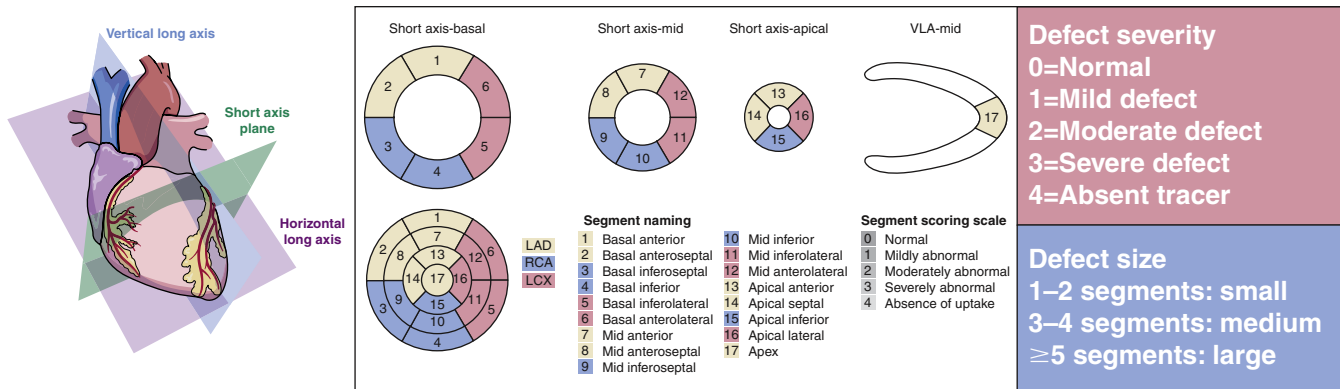


FIGURE 18.9 Myocardial segmentation model. A 17-segment heart model is recommended for segmental evaluation of myocardial perfusion and metabolic imaging. For semiquantitative scan interpretation, myocardial perfusion in each segment is scored from normal to absent tracer uptake and defect size estimated from small to large, as shown in the figure. Short-axis, vertical long-axis, and horizontal long-axis images are in a plane parallel to the mitral valve, the septum, and the inferior wall, respectively. (From Dorbala S, et al. Single photon emission computed tomography (SPECT) myocardial perfusion imaging guidelines: instrumentation, acquisition, processing, and interpretation. *J Nucl Cardiol* 2018;25:1784-1846.)

Interpretation	Normal	Attenuation artifact	Scar	Ischemia
Stress				
Rest				
Perfusion	No defects	Fixed defects	Fixed defects	Reversible defect
Wall motion	Normal	Normal	Abnormal	Normal or abnormal

FIGURE 18.10 Interpretation of myocardial perfusion images. Patterns of regional myocardial perfusion and corresponding regional wall motion associated with scans showing normal myocardial perfusion, attenuation artifact, scar, and ischemia.

the ^{18}F -FDG scan. A coronary CTA, and a vascular CTA or MR angiogram (MRA), is also added for endocarditis and vasculitis protocols, respectively. Please review ASNC guidelines for more protocol details.^{2,7}

SYSTEMATIC INTERPRETATION OF IMAGES

A systematic review of images will improve diagnostic accuracy of scan interpretation and intra/interreader variability.¹

Image Quality

Following image acquisition, each image is checked for quality and appropriate measures taken to mitigate any artifacts before the patient leaves. The projection images are viewed sequentially in a cine loop format to identify patient motion on conventional SPECT. Vertical motion is easier to identify on the rotating projection images and the sinogram may provide a clue to horizontal motion. Motion is more challenging to identify on novel multidetector SPECT (semiconductor detector scanners) and PET scanners because of simultaneous acquisition of projection images. Identification of distortion or blurriness on reconstructed images may provide some clues to motion artifact. Identification of motion on cardiac PET images is also possible by a review of the cine loop display of the multiframe dynamic images. Misregistration of the transmission and emission images is checked in a fusion screen.

Image Display

The perfusion images are interpreted using cardiac projection images of short-axis, vertical-long axis, and horizontal-long axis images. The rest and stress images are viewed simultaneously in alternate rows. Adequate alignment of rest and stress slices is required.

Image Review and Interpretation

Scan interpretation starts with a visual evaluation of rest, stress images for LV size, right ventricular (RV) size, and tracer uptake. Any transient changes in size of the left ventricle or RV tracer uptake from rest to stress are noted.

Perfusion Imaging Interpretation. The perfusion images are reviewed visually and semiquantitatively. Interpretation is performed in a segmental fashion using a 17-segment heart model (Fig. 18.9) and a 0 to 4 scale (where each of the 17 segments are scored using 0 = normal, 1 = mild, 2 = moderate, 3 = severe, and 4 = absent tracer uptake). The sum of the stress scores, rest scores, and their difference is termed summed stress score (SSS), summed rest score (SRS), and summed difference score (SDS), respectively. These visual scores are often converted into percentage myocardium abnormal [(SSS/68) × 100], ischemic [(SDS/68) × 100] or scarred [(SRS/68) × 100]. Well-validated commercially available software programs provide semiautomatic estimates of perfusion defect size, extent, and severity (in terms of percentage myocardium abnormal, ischemic, or scarred).

Fig. 18.10 illustrates the common patterns of stress and rest myocardial perfusion images including normal, fixed defect, and reversible defect. Common normal variants in MPI include apical thinning (a fixed perfusion defect in the apical inferior wall or septum with normal wall motion) on SPECT or PET/MPI and a fixed basal lateral perfusion defect with normal wall motion on ^{13}N -ammonia PET/CT. The differential diagnosis of a fixed perfusion defect includes artifact (if wall motion is normal) or real defect (if wall motion is abnormal). Real fixed perfusion defects can be further evaluated for myocardial viability using radionuclide methods, CMR, or low-dose dobutamine echocardiography (see Chapters 16 and 19). High-risk features of MPI are listed in Table 18.4.

ECG-Gated Image Interpretation. The gated images are reviewed for regional wall motion, wall thickening, and calculation of LV volumes and EF. Dyssynchrony can also be evaluated using specialized software. **PET/SPECT Dynamic Image Interpretation.** For cardiac PET MPI, absolute myocardial blood flow images are checked for quality and motion. Motion correction is applied if necessary. An image-derived input function is placed in the left atrium or ascending aorta and positioned to capture the peak blood pool activity. The time activity curves

are checked for an adequate tight bolus of radiotracer (sharp peak of the input function). When low-dose/high-dose ^{13}N -ammonia studies are performed, the second images are corrected for residual activity from the first injection.⁹ Myocardial blood flow is displayed in segmental or vascular distribution.

PET Viability Imaging Interpretation. Fig. 18.11 illustrates the common patterns of MPI and ^{18}F -FDG viability imaging including perfusion-metabolism mismatch, perfusion-metabolism match, and perfusion-metabolism partial match. Segmental radiotracer uptake on rest perfusion polar maps can also be used to guide viability assessment. Resting counts are normalized to peak counts and expressed as percentage of peak activity (counts in the pixels with highest uptake considered

100%, and all other pixel values compared relative to that maximal uptake). Myocardial segments with >60% peak activity of perfusion tracer are considered viable, those with <40% peak activity are considered nonviable, and those with 40% to 60% of peak activity are further evaluated for myocardial viability.

PET Imaging of Infiltrative and Inflammatory Processes. Fig. 18.12 shows the common patterns of MPI and ^{18}F -FDG imaging in cardiac sarcoidosis. Hot-spot images (sarcoidosis, amyloidosis, and infective endocarditis) are quantified using target to background ratio (myocardium to rib uptake in amyloidosis and myocardium to blood activity in sarcoidosis), standardized uptake value (SUV), volume of myocardial pixel above a threshold SUV mean value, and other advanced metrics.

TABLE 18.4 High-Risk Features

Myocardial Perfusion Imaging	
Large single or multiterritorial fixed and/or reversible myocardial perfusion defects involving >15% of the LV mass	
Transient ischemic dilation of the left ventricle	
Stress-induced myocardial stunning with a drop in LVEF poststress	
Transient RV tracer uptake	
Increased pulmonary tracer uptake	
Stress Test	
Significant (>3 mm) ST-segment depression	
Prolonged ST-segment depression	
ST depression at low workload	
Multilead ST depression	
ST-segment elevation (>1 mm)	
Hypotension (>10 mm Hg) with exercise	
Sustained ventricular tachycardia	

LVEF, Left ventricular ejection fraction; RV, right ventricular.

Interpretation	Hibernation	Scar	Nontransmural scar
Perfusion			
Glucose metabolism			
Perfusion	Defect	Defect	Defect
Wall motion	Abnormal	Abnormal	Normal/Abnormal
^{18}F -FDG uptake	Increased	Absent	Partial uptake
Pattern	Mismatch	Match	Partial mismatch

FIGURE 18.11 Patterns of myocardial perfusion and ^{18}F -FDG in viability imaging. Patterns of regional myocardial perfusion, metabolism, and corresponding regional wall motion associated with scans showing viable and nonviable myocardium. The most common perfusion-metabolism patterns are mismatch (perfusion defect with preserved ^{18}F -FDG uptake, representing hibernating myocardium), match (perfusion defect with concordantly reduced ^{18}F -FDG uptake, representing myocardial scar), and partial match (nontransmural perfusion defect with concordantly reduced ^{18}F -FDG uptake, representing nontransmural scar). Occasionally, a reversed mismatch (normal perfusion but reduced ^{18}F -FDG uptake) can be seen in association with myocardial stunning, left bundle branch block, or both.

Photon Attenuation and Attenuation Correction

In patients with excess soft tissue, the photons emitted by the heart may be attenuated (stopped by soft tissue) or scattered before they reach the detectors and cause artifactual perfusion defects. Attenuation artifacts are more prominent in obese patients, in patients with large chest size, and in those who are unable to raise their left arm for MPI. Anterior wall attenuation in women from overlying breast tissue (Fig. 18.13A) and inferior wall attenuation in men from diaphragmatic muscle are common sources of attenuation artifacts.

Attenuation artifacts are mitigated by multiposition imaging, ECG-gated SPECT imaging, or radionuclide or CT-based transmission imaging for attenuation correction.¹ Multiposition SPECT imaging (supine/prone and upright/supine) may improve attenuation artifacts, particularly inferior wall artifacts, while true defects remain unchanged. ECG-gated SPECT imaging showing normal wall motion despite a fixed perfusion defect is another way to discern attenuation artifacts. Attenuation- and scatter-corrected SPECT improves the specificity and normalcy of MPI.¹ Most attenuation artifacts typically result in fixed defects, but variable attenuation may result in pseudo-reversible perfusion defects, which can be challenging to detect and attenuation correction is optimal in those instances.

Measurement of photon attenuation and correction using radionuclide or CT transmission imaging is the most direct way to correct for attenuation artifacts. Attenuation correction is depth independent and more robust with PET compared with SPECT imaging (see Fig. 18.13B).¹

Older generation SPECT and PET scanners used a transmission scan based on a rotating line source of a radionuclide such as Gd-153 (gamma rays with energies of 97 and 103 keV). This image takes about 3 to 4 minutes or longer based on the life of the line source. Current generation SPECT and PET scanners most commonly use a CT-based transmission imaging (a low-dose, free tidal breathing, noncontrast CT) for attenuation correction.¹⁰ High-resolution chest CT images are transformed into a low-resolution attenuation map of the chest based on density of bone, soft tissue, or air. The transmission images are obtained sequentially before or after the emission images; hence accurate alignment of the transmission and emission images is important for accurate attenuation correction. It is particularly important to ensure adequate coregistration of the emission and CT to avoid misregistration artifacts that typically result in regional perfusion defects from incorrect attenuation correction of the myocardial counts caused by overlap with lung tissue (Fig. 18.14).² If the emission image overlies a metallic object, such as implantable cardiac defibrillator (ICD) leads, the emission image is overcorrected resulting in artifactual hot spots that can interfere with interpretation of inflammation or infection images (see section Patient-Centered Clinical Applications).

REDUCING RADIATION DOSE

Radiation risks from diagnostic nuclear cardiology imaging are small and challenging to estimate as the effects are stochastic with a potential unknown risk of cancer several decades after exposure (extrapolated from atom-bomb survivor studies).¹¹ A large body of evidence accumulating over the last 50 years strongly supports the power

Interpretation	Normal	Nonspecific	Focal myocardial inflammation	Fibrosis
Perfusion				
¹⁸ F-FDG				
Perfusion	Normal	Normal	Normal	Defect
¹⁸ F-FDG uptake	None	Diffuse	Focal uptake	Focal uptake

FIGURE 18.12 Patterns of myocardial perfusion and ¹⁸F-FDG images in cardiac sarcoidosis. In patients undergoing evaluation for cardiac sarcoidosis, ¹⁸F-FDG images are typically interpreted in conjunction with perfusion images. Normal perfusion with no myocardial ¹⁸F-FDG uptake is normal and diffuse ¹⁸F-FDG uptake is nonspecific. Normal or abnormal perfusion with focal ¹⁸F-FDG uptake is abnormal and indicates focal myocardial inflammation. Myocardial perfusion defect with no myocardial ¹⁸F-FDG uptake indicates myocardial fibrosis (*last panel* shows intense blood pool activity without myocardial ¹⁸F-FDG uptake).

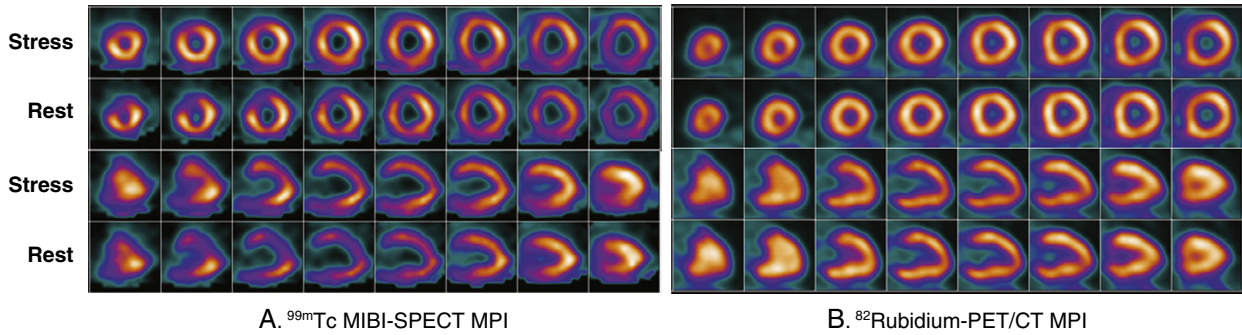


FIGURE 18.13 Breast attenuation artifact. ^{99m}Tc-sestamibi SPECT MPI (A) and ⁸²rubidium positron emission tomography (PET)/computed tomography (CT) MPI (B) of a 59-year-old woman with a body mass index of 31 kg/m² are shown. SPECT images show a medium-sized perfusion defect of moderate intensity in the mid and apical anterior wall that was fixed. Gated SPECT images (not shown) demonstrated diffuse global left ventricular hypokinesis and an ejection fraction of 35%. A cardiac PET was ordered because of concern for anterior wall attenuation artifact versus nontransmural scar. ⁸²Rubidium PET MPI was normal confirming attenuation artifact on SPECT MPI. In this and subsequent figures, short-axis images (*rows 1 and 2*) are shown from apex to base (left to right). Vertical long-axis images (*rows 3 and 4*) are shown from the septum to the lateral wall and horizontal long-axis images (not shown in this figure) are shown from inferior to anterior walls. MPI, Myocardial perfusion imaging.

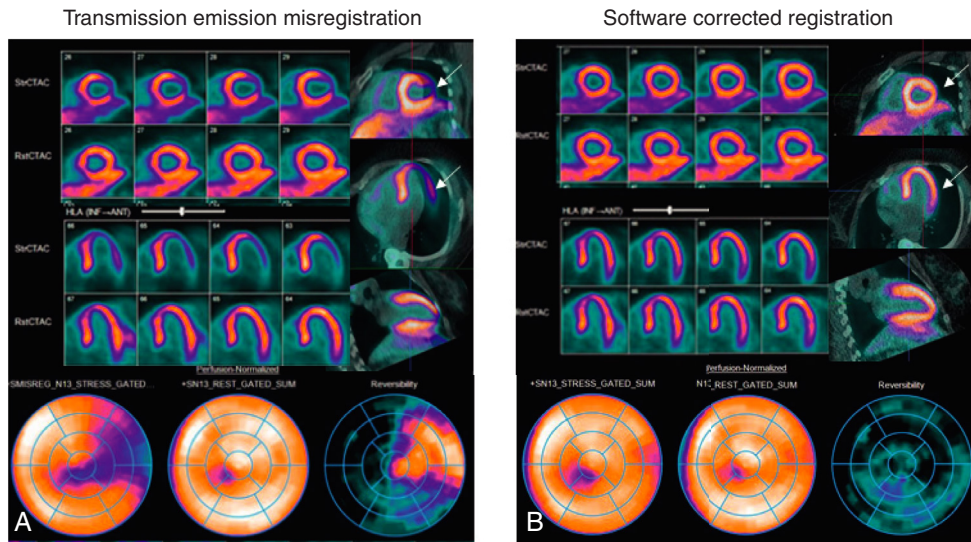


FIGURE 18.14 Misregistration artifact on hybrid PET/CT imaging. A, Stress and rest ¹³N-ammonia PET/CT images and corresponding polar maps show a medium-sized and severe perfusion defect in the anterolateral wall that is reversible. A review of the stress transmission and emission fused images show misalignment of the CT and perfusion images with the lateral wall on the PET images overlying the lung field on the CT (*white arrows*). B, Proper realignment of the perfusion and CT images and new reconstruction of the PET images resulted in a normal study.



of nuclear cardiology testing in the diagnosis, management, and risk assessment of patients with heart diseases. Hence any theoretical long-term effects of radiation from the use of radiotracers must be carefully weighed against the established short-term benefits from this test. There are several strategies for dose reduction (eTable 18.1). These include ensuring appropriate use of the test, use of weight-based radiotracer dosing, avoiding dual isotope and thallium protocols for MPI, and employing stress-first protocols, novel scanners, and processing software to allow for lower injected dose, and cardiac PET, particularly with 3D PET. Novel scanner technologies (CZT SPECT) and weight-based tracer dosing have cut radiation dose by more than half while maintaining or even improving image quality. PET MPI is associated with a substantially lower radiation dose compared with SPECT MPI (eFig. 18.2). But a recent worldwide survey¹² has identified marked variability in the use of these radiation dose reduction practices across countries. Effective radiation dose reduction efforts must begin before the test (by ensuring the test is appropriate for the clinical question), continue during the test (by use of advanced protocols, technology, and lowest possible radiation dose for high-quality imaging), and after the test (clear reporting of test results will minimize layered testing and reduce radiation dose).¹¹ Following the principles of justification of the test and optimization of imaging will ensure that the risks of ionizing radiation, if any, will far outweigh its benefits. Indeed, stress-only imaging can be performed with <1.7 mSv for CZT SPECT and <1 mSv for PET (see eFig. 18.2).¹¹ Radiation dose for common nuclear cardiology studies can be calculated using the SNMMI radiation dose tool (see <http://www.snmmi.org/clinicalpractice/dosetool.aspx?itemnumber=1>).

PATIENT-CENTERED CLINICAL APPLICATIONS

Ischemic Heart Disease

Principles of Perfusion Imaging

The basic principle of radionuclide MPI for detecting CAD is based on the ability of a radiotracer to identify a transient regional perfusion deficit in a myocardial region subtended by a coronary artery with a flow-limiting stenosis. A reversible myocardial perfusion defect

is indicative of ischemia, whereas a fixed perfusion defect generally reflects scarred myocardium from prior MI (see Fig. 18.10). Generally, myocardial perfusion defects during stress develop downstream to a epicardial stenosis with $\geq 50\%$ to 70% luminal narrowing and become progressively more severe with increasing degree of stenosis. It is noteworthy that coronary stenosis of intermediate severity (e.g., 50% to 90%) is associated with significant variability in the resulting maximal myocardial blood flow, which in turns affects the presence and/or severity of regional perfusion defects. For any degree of intermediate luminal stenosis, the observed physiologic variability is multifactorial and includes geometric factors of coronary lesions not accounted for by a simple measure of minimal luminal diameter or percentage of stenosis (see Chapter 36). These factors include shape, eccentricity, and length, which are known to modulate coronary resistance; collateral blood flow; and the presence of diffuse coronary atherosclerosis and microvascular dysfunction. All these factors account for the frequent disagreements between angiographically defined CAD and its associated physiologic severity by radionuclide perfusion imaging.

Suspected Stable Coronary Artery Disease

Patients with New-Onset Chest Pain

Radionuclide MPI is appropriate in symptomatic patients with suspected CAD (Fig. 18.15). Although in younger patients coronary CT angiography may be an excellent choice to screen for CAD, it is probably not ideal in older patients who are more likely to show coronary artery calcifications, especially in patients with cardiometabolic risk factors. The diagnostic accuracy of SPECT MPI for detecting obstructive CAD as defined by invasive coronary angiography was examined in a recent large meta-analysis including 86 studies (10,870 patients).¹³ The pooled sensitivity was 87% and the specificity was 78% with similar accuracy for exercise and pharmacologic stress. However, one needs to keep in mind that the reported accuracies of noninvasive testing for radionuclide MPI (and other modalities) are limited by the referral biases intrinsic to the design of most studies in this area, especially partial verification bias that refers to selective referral to the reference standard (catheterization) based on the results of the test being studied. That is, very few patients with normal noninvasive tests will be

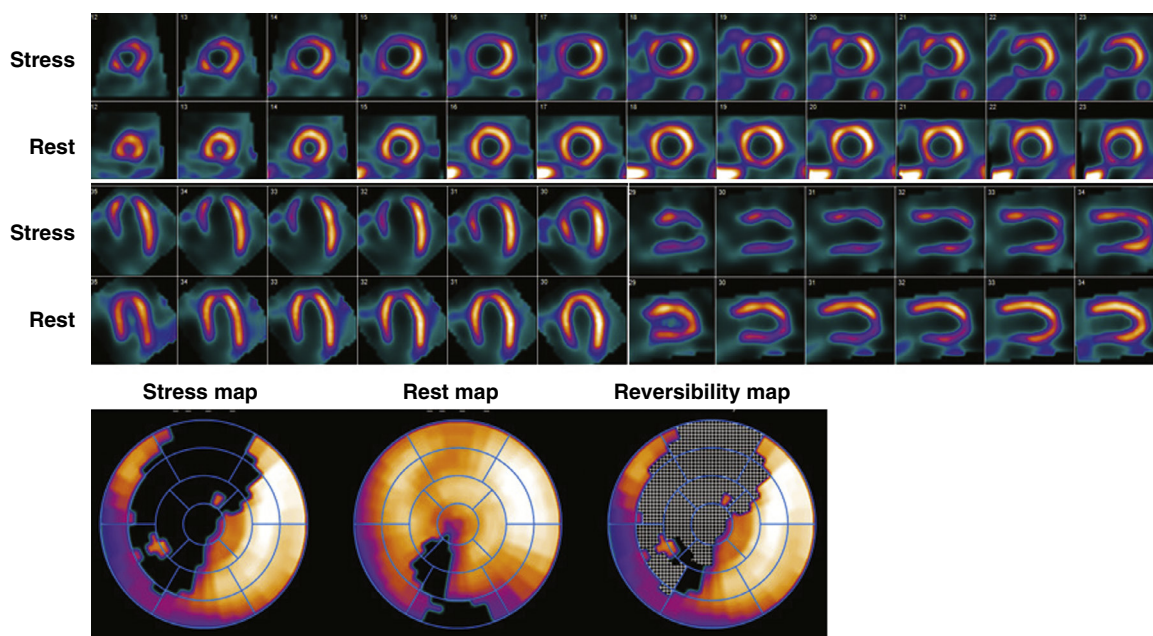


FIGURE 18.15 High-risk myocardial perfusion SPECT study. Exercise-stress and rest ^{99m}Tc-MIBI myocardial perfusion imaging of an 80-year-old man presenting with atypical chest pain and dyspnea. Exercise was terminated because of chest pain, with associated decrease in blood pressure and 3-mm downsloping ST-segment depression in the inferolateral leads. Images demonstrate transient left ventricular (LV) dilatation and a large and severe perfusion defect throughout the anterior, anteroseptal, and apical LV segments and the LV apex, showing complete reversibility. In addition, there was a medium-sized perfusion defect of severe intensity in the mid and basal inferior and inferoseptal walls, showing moderate reversibility. Polar maps confirmed these findings. There was also a decrease in LV ejection fraction after exercise. These findings are highly predictive of high-risk coronary artery disease, which was confirmed on coronary angiography.

ETABLE 18.1 Strategies for Radiation Dose Reduction in Nuclear Cardiology

- Ensure appropriate use of the test
- Use weight-based radiotracer dose
- Use lower dose of radiotracer with novel scanners or novel software reconstruction
- Use stress-first and stress-only protocols
- Use two-day MPI protocols
- Use cardiac PET, particularly with 3D PET
- Avoid dual isotope and thallium protocols for myocardial perfusion imaging

MPI, myocardial perfusion imaging; PET, positron emission tomography.

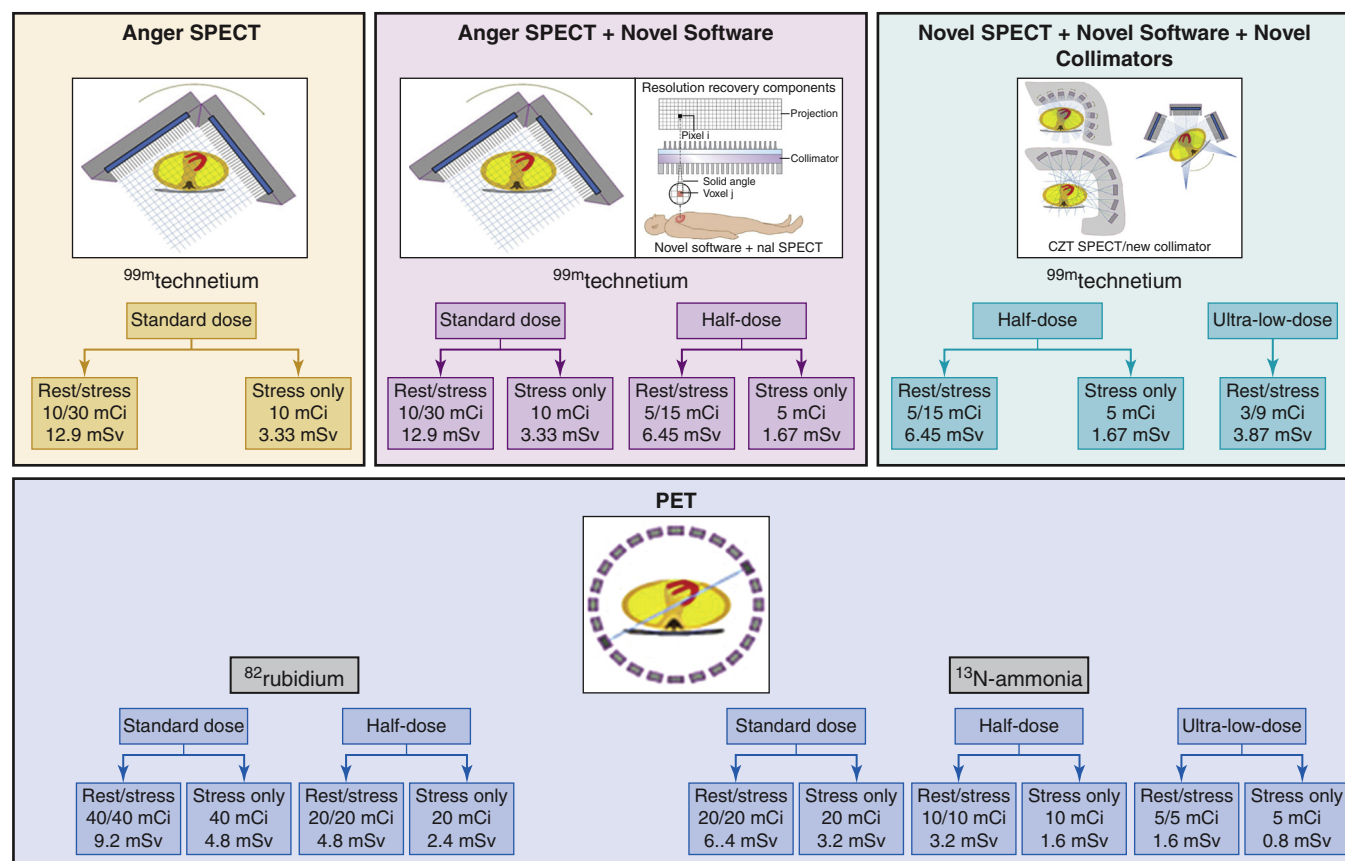


FIGURE 18.2 Options to reduce radiation dose from MPI. Different ways to reduce radiation dose for myocardial perfusion imaging with Anger single photon emission computed tomography (SPECT), novel software, novel SPECT, or positron emission tomography.

referred to catheterization, whereas many more with abnormal tests will be referred for coronary angiography, resulting in relatively fewer true or false-negatives and more true- or false-positives, yielding an increase in sensitivity and a marked reduction in specificity.

Fig. 18.16 underscores that despite its widespread use and acceptance, a recognized limitation of semiquantitative visual assessment of radionuclide myocardial perfusion images with SPECT and PET often uncovers only coronary territories supplied by coronary arteries with the most severe stenosis. Consequently, it is relatively insensitive to accurately delineate the extent of obstructive angiographic CAD, especially in the setting of multivessel CAD. As illustrated in this example, quantification of myocardial blood flow (in mL/min/g) and MFR (calculated as the ratio of maximum hyperemic myocardial blood flow over that at rest) showed that myocardial ischemia was far more extensive than predicted by the visual extent of perfusion abnormalities. The severely reduced MFR corresponded with the high-risk angiographic findings.

A number of studies have demonstrated a relationship between myocardial blood flow and flow reserve and percentage diameter stenosis on angiography; that is, there is a progressive reduction in myocardial blood flow and flow reserve with increasing severity of angiographic stenosis (eFig. 18.3). These observations have served as the basis for the clinical use of quantitative myocardial blood flow to improve identification of obstructive CAD and, especially, to exclude the presence of severe angiographic multivessel CAD.

Recent meta-analyses,^{14,15} a prospective European multicenter study (Evaluation of Integrated CAD Imaging in Ischemic Heart Disease [EVINCI]),¹⁶ and a prospective comparative effectiveness study (Prospective Comparison of Cardiac PET/CT, SPECT/CT Perfusion Imaging and CT Coronary Angiography With Invasive Coronary Angiography

[PACIFIC])¹⁷ support the notion that PET MPI is one of the most accurate noninvasive techniques for detecting flow-limiting CAD.¹⁷ As discussed earlier, one unique advantage of PET over SPECT is that it allows routine quantification of myocardial blood flow and MFR. These quantitative measures of myocardial perfusion improve the sensitivity and negative predictive value of PET for ruling out high-risk angiographic CAD. Indeed, an MFR >2.0 is associated with a >97% negative predictive value for ruling out high-risk angiographic CAD.

Risk Stratification with Radionuclide Myocardial Perfusion Imaging

Radionuclide MPI provides robust prognostic assessments of patients with suspected stable CAD, which has been documented for over four decades and forms the basis of its widespread use and clinical utility. The power of radionuclide MPI (including SPECT and PET) for risk stratification is based on the fact that major determinants of prognosis in patients with CAD are readily available from gated MPI. These include the amount of myocardial scar, the extent and severity of stress-induced ischemia, degree of LV dilatation, and reduced LVEF. Optimal risk stratification is based on the concept that the risk associated with a normal study is sufficiently low that referral to revascularization will not further improve patient outcomes; hence catheterization is an unlikely option after testing. Conversely, patients with abnormal stress imaging results are at greater risk of adverse events and, thus, are potential candidates for intervention, and the magnitude of their risk is related to the extent and severity of the imaging abnormalities.

A normal or low-risk rest/stress radionuclide MPI with SPECT or PET was associated with an annual risk of MACE of 0.85% and 0.4%, respectively.¹⁸ The low risk associated with normal SPECT MPI has

recently been extended to the radiation-sparing, stress-only radionuclide MPI protocols and to PET MPI as well.^{10,18,19} However, the risk associated with a normal radionuclide MPI has not necessarily been low (<1%) in higher risk cohorts (e.g., diabetes, chronic kidney impairment, elderly). The reasons for the observed increased adverse event rate in higher risk cohorts despite a visually normal radionuclide MPI are likely multifactorial. On one hand, coexisting comorbidities including hypertension, obesity, and others increase clinical risk even in the absence of obstructive CAD. On the other hand, and notwithstanding the clinical utility of SPECT MPI, it is a somewhat insensitive test to uncover diffuse obstructive and nonobstructive atherosclerosis and/or coronary microvascular dysfunction (CMD) associated with myocardial ischemia and increased risk of adverse events. Consequently, absolute quantification of myocardial blood flow and flow reserve by PET (an integrated marker of epicardial stenosis, diffuse atherosclerosis, and microvascular dysfunction) is a definite advantage in higher-risk patients. In such patients, a relatively preserved MFR identifies truly low-risk individuals among high-risk patients.²⁰ For example, patients with diabetes without known CAD but abnormal MFR had a cardiac mortality risk similar to that in nondiabetics with known

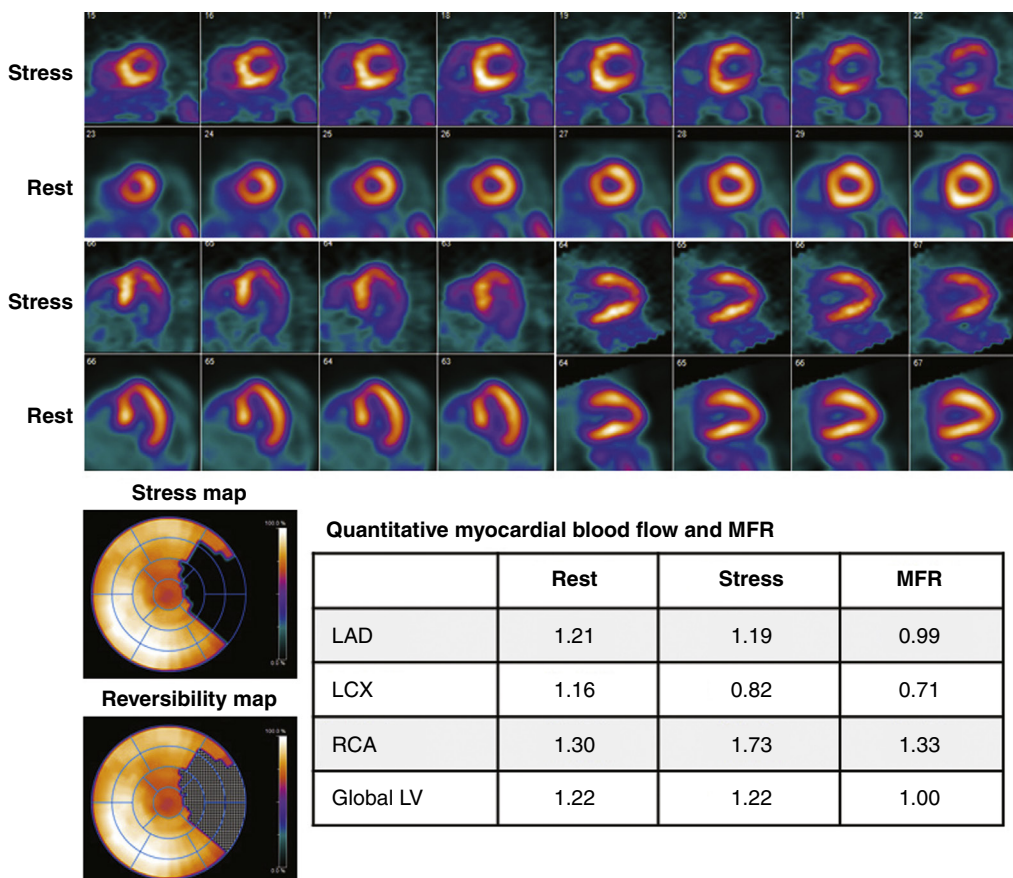
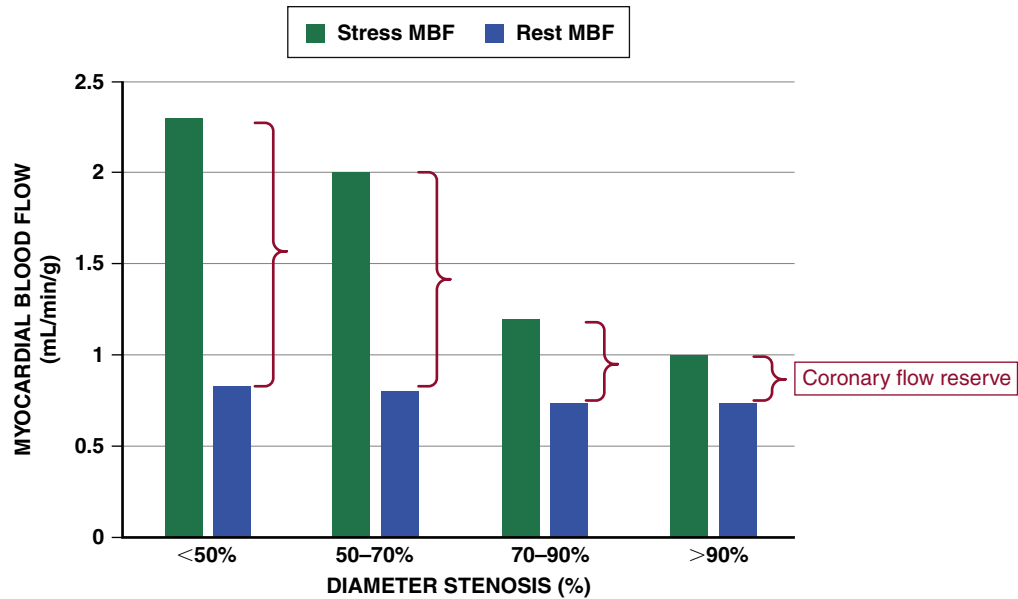


FIGURE 18.16 Quantification of myocardial blood flow and multivessel obstructive CAD. Rest and vasodilator-stress ⁸²rubidium position emission tomography scan of an 85-year-old woman presenting with exertional dyspnea. Stress images demonstrate a medium-sized perfusion defect of severe intensity throughout the lateral wall showing complete reversibility, consistent with single-vessel left circumflex (LCX) ischemia. However, the quantitative myocardial blood flow and myocardial flow reserve data show a severely blunted hyperemic flow response to vasodilator stress and reduced flow reserve in all coronary territories. The noncontrast computed tomography scan showed severe coronary artery calcification of the left main, left anterior descending (LAD), and LCX arteries (images not shown). Follow-up coronary angiography showed severe left main and LCX disease. LV, left ventricle; RCA, right coronary artery.



EFIGURE 18.3 Relationship between myocardial blood flow and flow reserve and angiographic severity of coronary stenosis. There is a progressive reduction in myocardial blood flow and flow reserve with increasing severity of angiographic stenosis. *MBF*, myocardial blood flow.



CAD. Conversely, diabetic individuals without overt CAD with relatively preserved MFR had an annual risk of <1% that was comparable to subjects without diabetes or CAD (eFig. 18.4). Similar findings have been shown in patients with chronic kidney disease.²¹

The risk associated with an abnormal radionuclide MPI study is not only greater than that after a normal MPI but increases as a function of the extent and severity of perfusion abnormalities (Fig. 18.17). This concept is applicable to both SPECT and PET MPI, vasodilator and exercise stress testing, and virtually all patient groups. The prognostic information provided by the results of radionuclide MPI is incremental to that provided by demographics and medical history data and that from exercise stress testing. Most importantly, the postscan risk increases with the degree of perfusion and LV functional abnormalities present on the radionuclide MPI. Importantly, the presence of LV dilatation and/or reduced LVEF further increases clinical risk across all levels of myocardial perfusion abnormalities. Finally, fixed perfusion defects (and the presence of often associated LV dilatation and reduced LV function) are associated with a greater risk of cardiac death, whereas reversible or ischemic defects are more closely associated with the occurrence of nonfatal MI. The constellation of extensive myocardial scar (fixed defects), LV remodeling, and reduced EF represents the highest risk subgroup.

As discussed previously, the quantitative regional and global myocardial blood flow and MFR information obtained with PET MPI provide incremental information that is useful in risk stratification. Indeed, for any amount of ischemic and/or scarred myocardium, a severely reduced global MFR is associated with a higher risk of death than in the setting of relatively preserved MFR (Fig. 18.18). The increased risk of adverse events in patients with reduced MFR (<2.0) also applies to patients with visually normal radionuclide MPI. In the majority of these patients, the reduced MFR reflects a combination of diffuse nonobstructive atherosclerosis and CMD and is found frequently in symptomatic men and women without overt obstructive CAD (51% and 54%, respectively). Importantly, the noninvasive PET measure of MFR improves risk reclassification, especially among high-risk cohorts (e.g., patients with diabetes, non-ST elevation MI [NSTEMI], chronic renal impairment, and high coronary calcium scores). Thus the ability to quantify MFR allows a level of risk assessment well beyond that achieved thus far using semiquantitative

analysis of regional perfusion defects, with the potential to incorporate measures of endothelial function and vascular health status into routine patient evaluations.

Symptomatic Patients Without Angiographic Obstructive Coronary Artery Disease

CMD is quite common in symptomatic patients with risk factors (Fig. 18.19) and the relative frequency and severity of CMD is similar in women and men (eFig. 18.5), but numerically there is a larger number of women with CMD than men. When present, symptomatic patients with CMD have a worse prognosis than asymptomatic patients. Because it is a diffuse process, conventional exercise stress testing and stress imaging tests, such as with echocardiography or SPECT imaging, lack sensitivity and specificity for detecting CMD and thus have a relatively limited role in its diagnosis. Because the coronary microcirculation is beyond the resolution of invasive or noninvasive coronary angiography, direct interrogation of coronary microvascular function is necessary to establish the diagnosis of CMD. There are several noninvasive and invasive approaches for this evaluation, each with advantages and limitations, and quantitative PET imaging is considered the most accurate and reproducible noninvasive technique. Reduction of stress myocardial blood flow and MFR reflects the combined effects of altered coronary fluid dynamics caused by diffuse atherosclerosis and microcirculatory dysfunction. Diffuse nonobstructive atherosclerosis in the epicardial coronary arteries is a common finding in symptomatic patients with CMD and can be identified using coronary artery calcium scoring (Fig. 18.19). The combined effects of extensive nonobstructive atherosclerosis and CMD increases the clinical risk compared to the risks associated with either one alone.²² This consideration highlights the important complementary role of delineating atherosclerotic burden with a noncontrast coronary artery calcium score or contrast CTA in addition to MPI.

Evaluation Before Organ Transplantation

Pretransplant patients are part of a special population and optimal strategies for detection of CAD in these patients are yet to be defined. However, there is general agreement that it may be reasonable to consider noninvasive testing in patients with multiple risk factors for CAD. The choice of the ideal test remains controversial and there is high

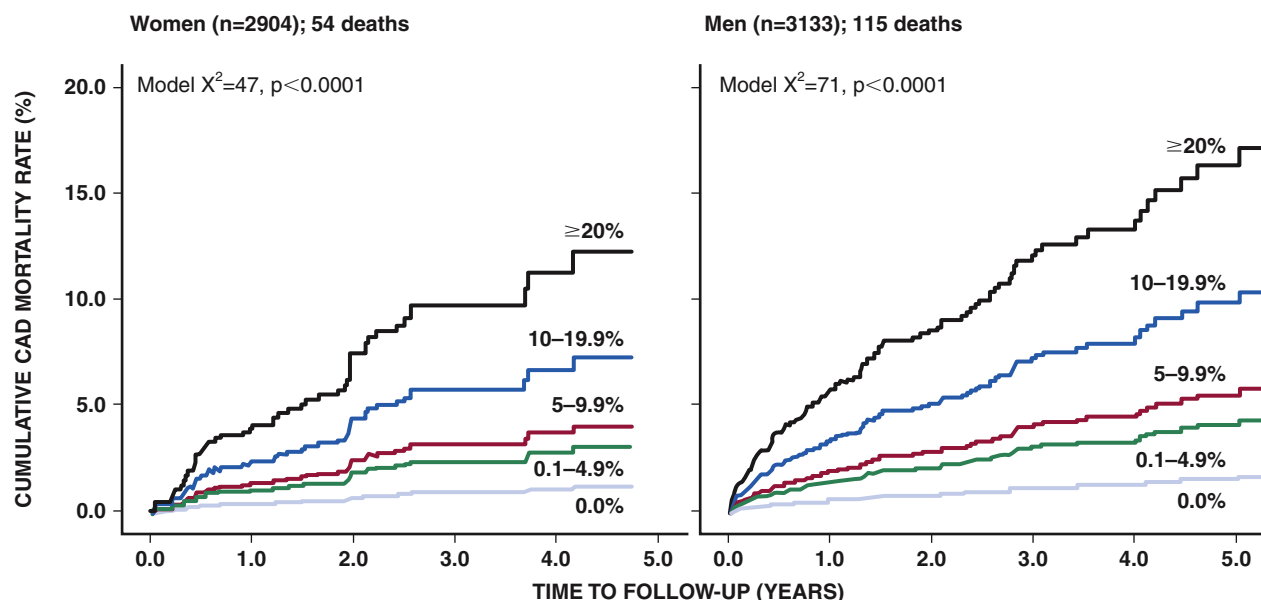


FIGURE 18.17 Annualized coronary artery disease mortality stratified by magnitude of perfusion abnormality. Multicenter data in 7061 patients at four institutions show a progressive increase in cardiac mortality with increasing extent of perfusion abnormality on position emission tomography, based on percentage of left ventricular myocardium, in both women (left) and men (right). (From Kay J, et al. Influence of sex on risk stratification with stress myocardial perfusion Rb-82 positron emission tomography: Results from the PET (Positron Emission Tomography) Prognosis Multicenter Registry. *J Am Coll Cardiol* 2013;62:1866-1876.)

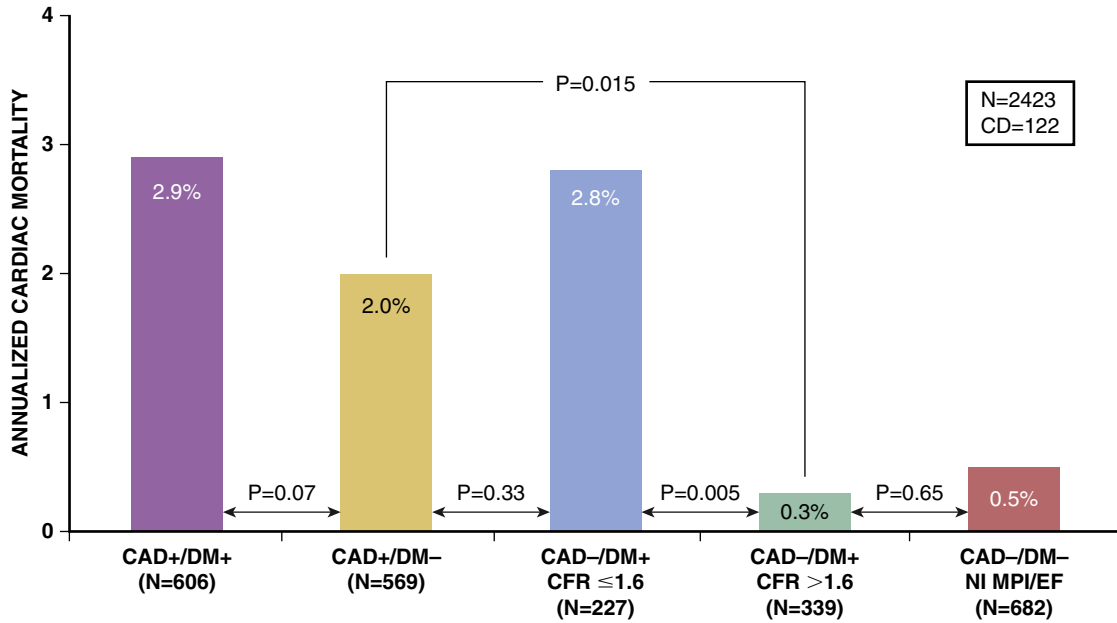


FIGURE 18.4 Annualized cardiac mortality stratified by the presence or absence of diabetes (DM), coronary artery disease (CAD), and microvascular dysfunction. Patients with diabetes without known CAD but abnormal coronary flow reserve (CFR) (blue bar) had a cardiac mortality risk similar to that in nondiabetics with known CAD (gold bar). Conversely, diabetic patients without overt CAD with relatively preserved CFR (green bar) had an annual risk of <1% that was comparable to subjects without diabetes or CAD (red bar). Data are adjusted for Duke treadmill score, ischemia+scar, resting ejection fraction, and early revascularization. CD, cardiac death; EF, ejection fraction; MPI, myocardial perfusion imaging (From Murthy VL, et al. Coronary vascular dysfunction and prognosis in patients with chronic kidney disease. JACC Cardiovas Imaging 2012;5:1025-1034.)

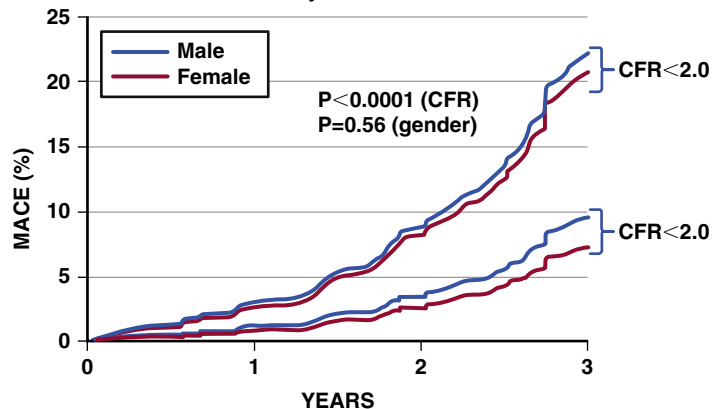
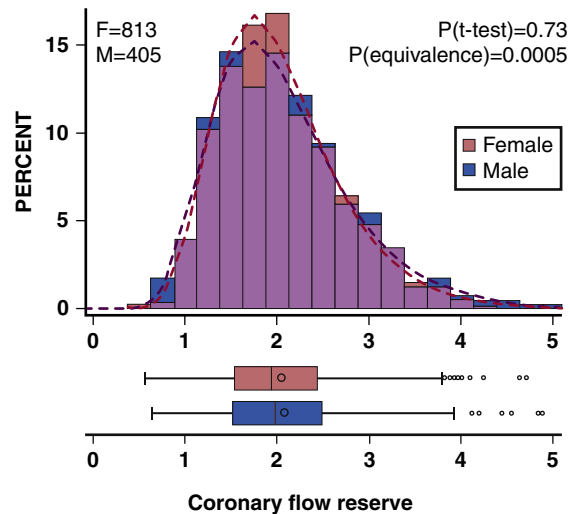
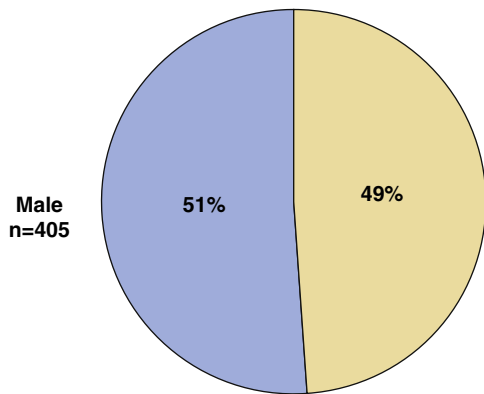
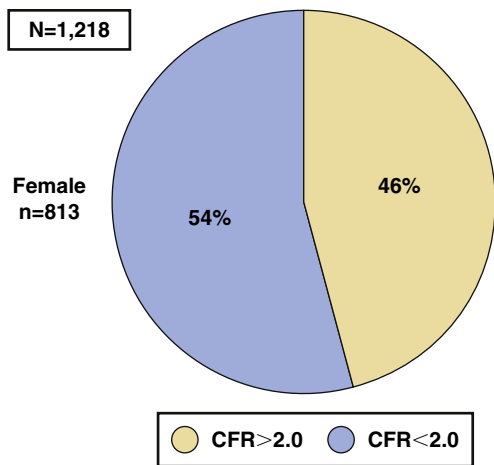


FIGURE 18.5 Coronary microvascular dysfunction (CMD) in women and men. CMD, as assessed by a reduced coronary flow reserve (CFR), affects more than 50% of men and women presenting with ischemic symptoms. The severity of CMD is similar in men and women. When present, CMD is a marker of increased clinical risk. (From Murthy VL, et al. Effects of sex on coronary microvascular dysfunction and cardiac outcomes. Circulation 2014;129:2518-2527.)

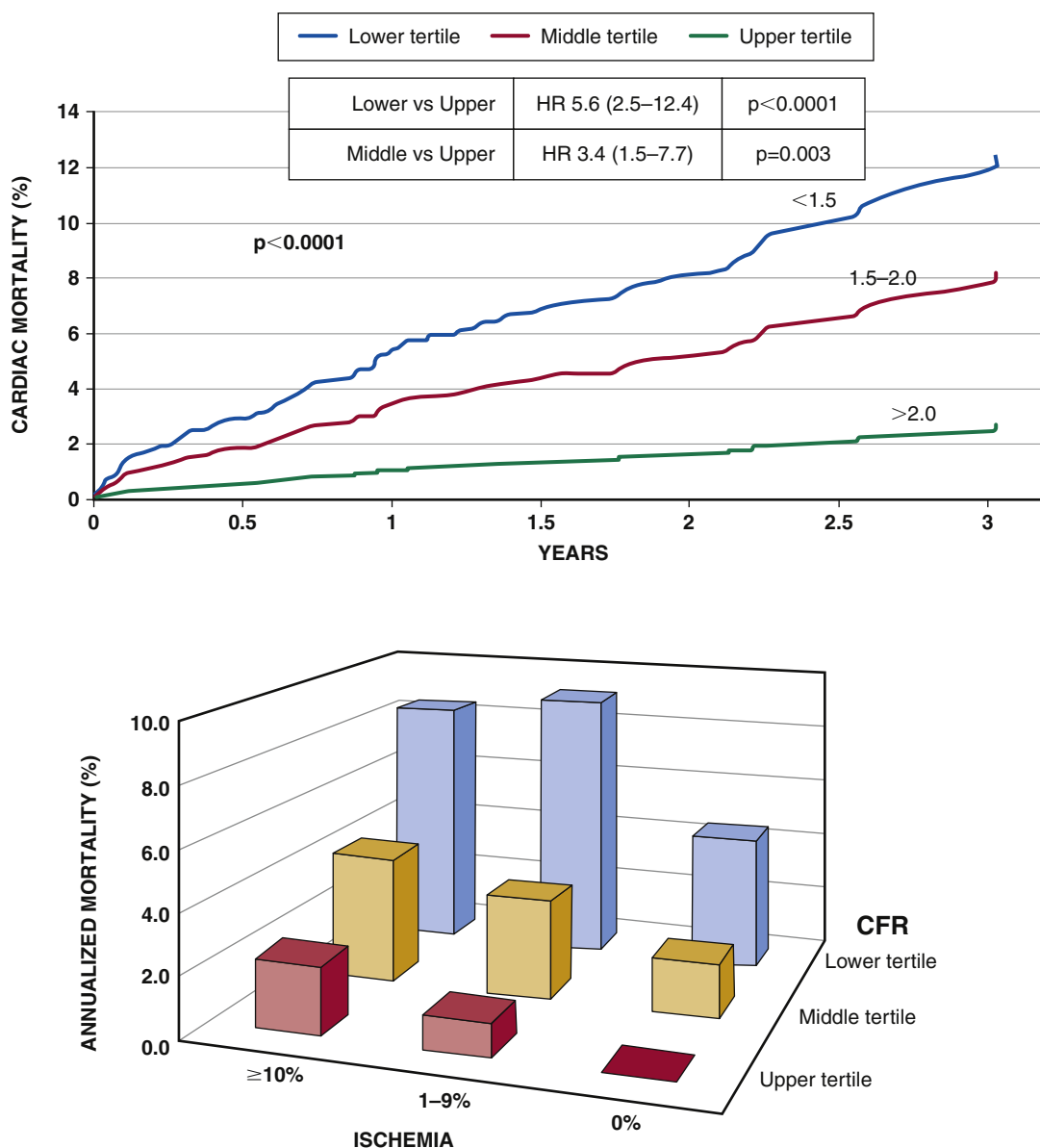


FIGURE 18.18 Risk stratification with myocardial flow reserve by PET MPI. *Top*, Probability of cardiac mortality in 2783 patients by tertiles of coronary flow reserve (CFR) with the highest risk corresponding to patients with the lowest tertile of CFR (<1.5). *Bottom*, Bar graph shows that annualized cardiac mortality is consistently higher for patients in the lowest CFR tertile across all levels of myocardial perfusion abnormalities. (From Murthy VL, et al. Improved cardiac risk assessment with noninvasive measures of coronary flow reserve. *Circulation* 2011;124:2215-2224.)

regional variability depending on availability and local expertise. Coronary CTA may be reasonable in young patients undergoing evaluation for organ transplantation because they are unlikely to show extensive coronary calcifications. However, noninvasive stress imaging may be more appropriate for patients over the age of 55, especially those with chronic kidney disease who are more likely to show coronary calcifications. Although exercise stress testing is preferred if the patient is likely to achieve an adequate cardiac workload, many patients require pharmacologic stress testing because of reduced functional capacity. There is a wealth of data on the diagnostic and prognostic utility of radionuclide MPI in renal transplant patients. A number of studies have shown that abnormal MPI is associated with both short- and long-term adverse cardiac events in patients with chronic kidney disease including renal transplant patients, and that a normal MPI study has a high negative predictive value. PET perfusion imaging offers the advantage of flow quantification, which provides incremental prognostic information beyond that of conventional perfusion imaging in patients on hemodialysis evaluated for renal transplantation.²³ Similar data have been reported for patients undergoing evaluation for liver transplantation. In summary, given

the limited number of organs available for transplantation, surgeons and transplant teams are generally inclined to ensure that transplant recipients are free of severe CAD and have the best chance of meaningful event-free survival after transplantation.

Suspected Acute Coronary Syndrome Patients with Nondiagnostic Electrocardiogram and Troponin Elevation

Normal radionuclide perfusion imaging in patients with low-level cardiac troponin elevation without typical symptoms or ECG changes and intermediate risk (TIMI risk score <5) is associated with very low short-term cardiac mortality. Conversely, an abnormal perfusion study identifies patients at significantly higher clinical risk. In such patients, the magnitude of stress-induced ischemia quantified by perfusion imaging helps guide the subsequent need of referral to cardiac catheterization and revascularization (see [Chapter 39](#)). In a prior large study of patients with ST-segment elevation MI (STEMI) and NSTEMI undergoing adenosine SPECT MPI, patients with low-risk scans (small defects with no or mild ischemia) had significantly lower risk than those with high-risk scans (large defects with significant residual ischemia) (rate

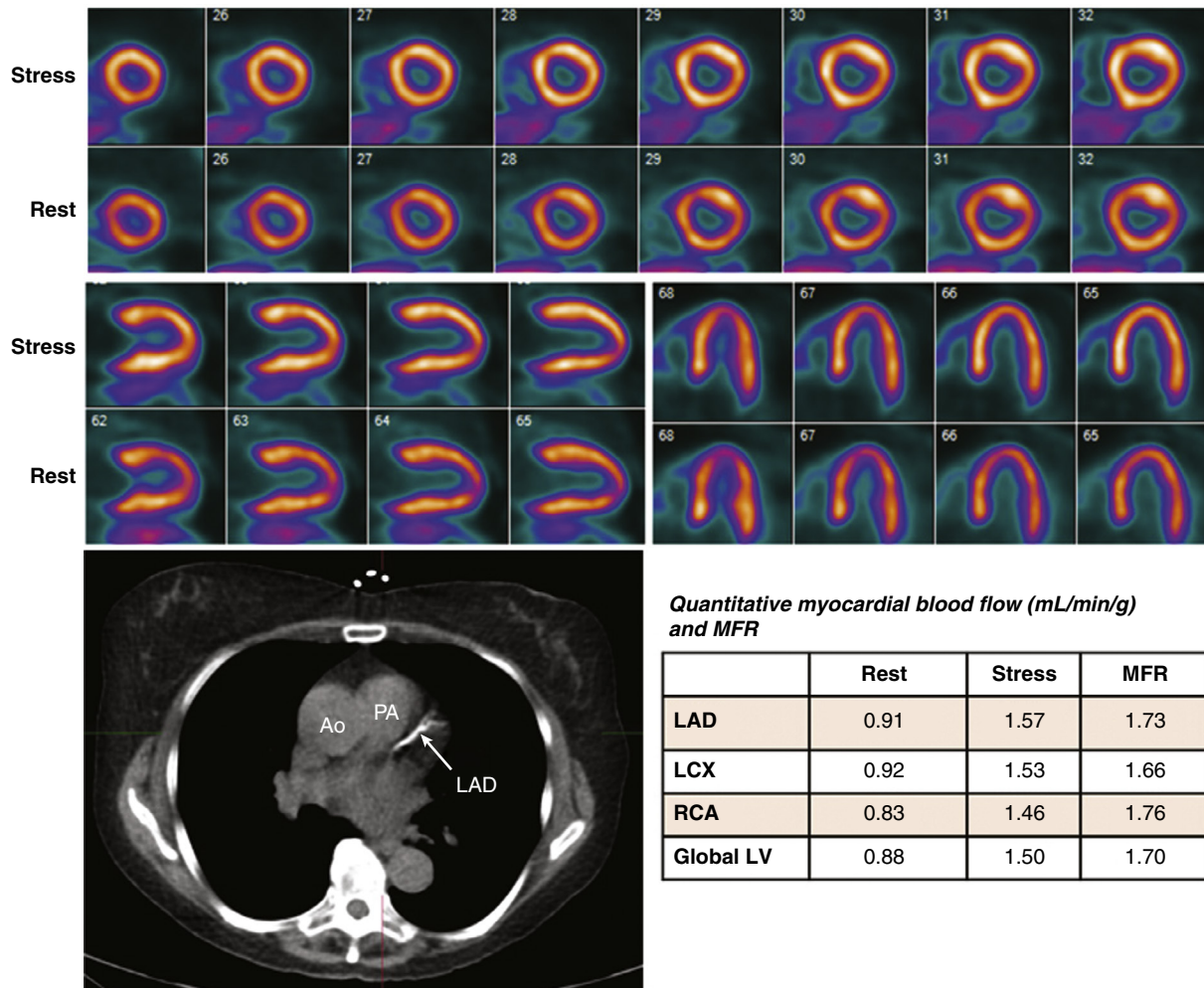


FIGURE 18.19 Evaluation of coronary microvascular dysfunction. Cardiac PET/CT images of a 76-year-old woman with dyslipidemia, hypertension, and nonobstructive angiographic coronary artery disease who presented with atypical chest pain and dyspnea. Vasodilator-stress and rest ^{13}N ammonia PET images demonstrate visually normal myocardial perfusion. The ECG gated images demonstrated a rest left ventricular (LV) ejection fraction of 71% that increased to 73% during stress with normal LV volumes (not shown). The CT transmission scan showed severe coronary artery calcification (lower left). Quantitative stress myocardial blood flow and myocardial flow reserve was moderately reduced in all coronary territories and globally. The abnormal quantitative findings are consistent with myocardial ischemia from nonobstructive atherosclerosis and coronary microvascular dysfunction. Ao, Aorta; LAD, left anterior descending artery; LCX, left circumflex artery; PA, pulmonary artery; RCA, right coronary artery.

of death 5.4%, 14%, and 18.6% and rate of MI 1.8%, 9.2%, and 11.6% for low-risk, intermediate-risk, and high-risk findings, respectively).²⁴

The pathophysiology of minimally elevated levels of serum cardiac troponin in the absence of an ACS is heterogeneous. In one study, impaired global MFR in the absence of obstructive CAD as measured by PET was independently associated with troponin elevation, suggesting an association between chronic microvascular ischemia and myocardial injury, especially among patients with diffuse atherosclerosis.²⁵ More importantly, this quantitative imaging marker provides prognostic information incremental to other clinical markers of risk (Fig. 18.20).²⁵ Therefore, in intermediate-high risk patients with low-level elevation of cardiac troponin, quantitative stress PET perfusion imaging may offer an advantage compared with SPECT and may be preferable if available.

Patients with Known Stable Coronary Artery Disease

Radionuclide MPI is commonly used to facilitate diagnosis and management in patients with known CAD, including those with prior MI and revascularization with recurrent symptoms, worsening LV function, and/or arrhythmias. In these patients, diagnosis and quantification of myocardial ischemia is important for risk stratification and, especially, for guiding the potential need of revascularization (see Chapter 40).

Patients with Prior PCI and Recurrent Symptoms

Radionuclide MPI is appropriate for diagnosis of ischemia and risk stratification among patients with prior revascularization presenting

with new-onset or worsening symptoms of angina or anginal equivalents such as dyspnea. In patients with prior percutaneous coronary intervention (PCI) or coronary artery bypass surgery (CABG), radionuclide MPI provides localization and quantification of myocardial ischemia that helps with risk prediction and management decisions regarding the potential need for targeted revascularization (Fig. 18.21). In these patients, exercise stress is ideal and should be performed when feasible because it provides important prognostic information and helps reproduce exertional symptoms. However, it is important to avoid submaximal exercise as this reduces the sensitivity of the test for detection of myocardial ischemia. In such cases, conversion to vasodilator stress helps avoid nondiagnostic tests. Among patients with known CAD, both PET and SPECT MPI offer high sensitivity. However, PET has higher specificity compared with SPECT, and consequently higher diagnostic accuracy. The addition of quantitative myocardial blood flow information is useful in patients with prior PCI but less so in those with prior CABG, as they have extensive disease in the native vessels, which can lead to a blunted flow response to vasodilator-stress despite patent grafts.

Patients with Recent Myocardial Infarction Evaluated for Potential Staged PCI

Stress radionuclide imaging is appropriate and commonly used to quantify the magnitude of residual stress-induced ischemia after MI, which aids in diagnosis, localization of ischemia, and risk stratification as discussed previously. The assessment of functional significance of

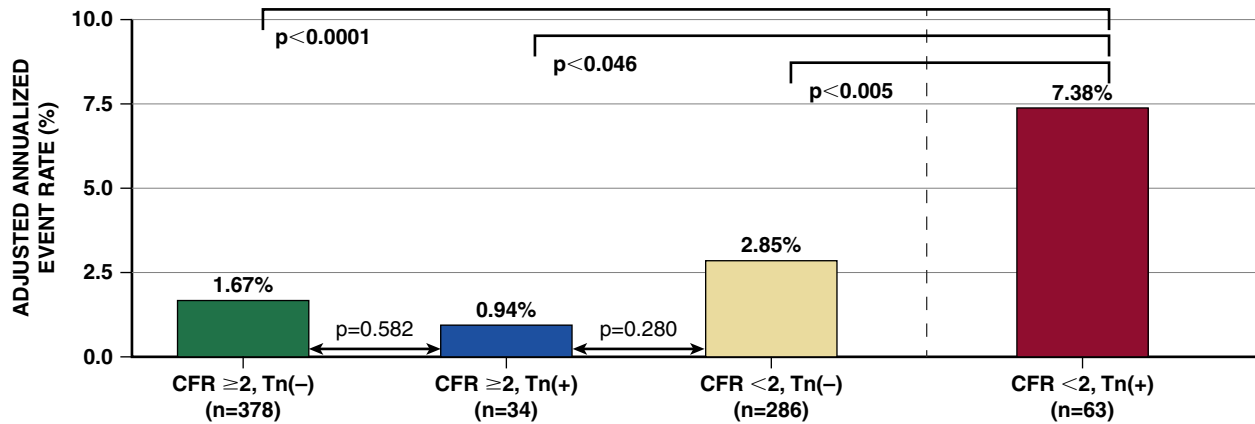


FIGURE 18.20 Incremental risk stratification by quantitative PET in patients with non-ST elevation myocardial infarction. Patients with positive troponin (Tn+) and impaired coronary flow reserve (CFR) (red bar) have a higher annualized event rate compared with those with a positive Tn but preserved CFR (blue bar). (From Taqueti VR, et al. Interaction of impaired coronary flow reserve and cardiomyocyte injury on adverse cardiovascular outcomes in patients without overt coronary artery disease. *Circulation* 2015;131:528-535.)

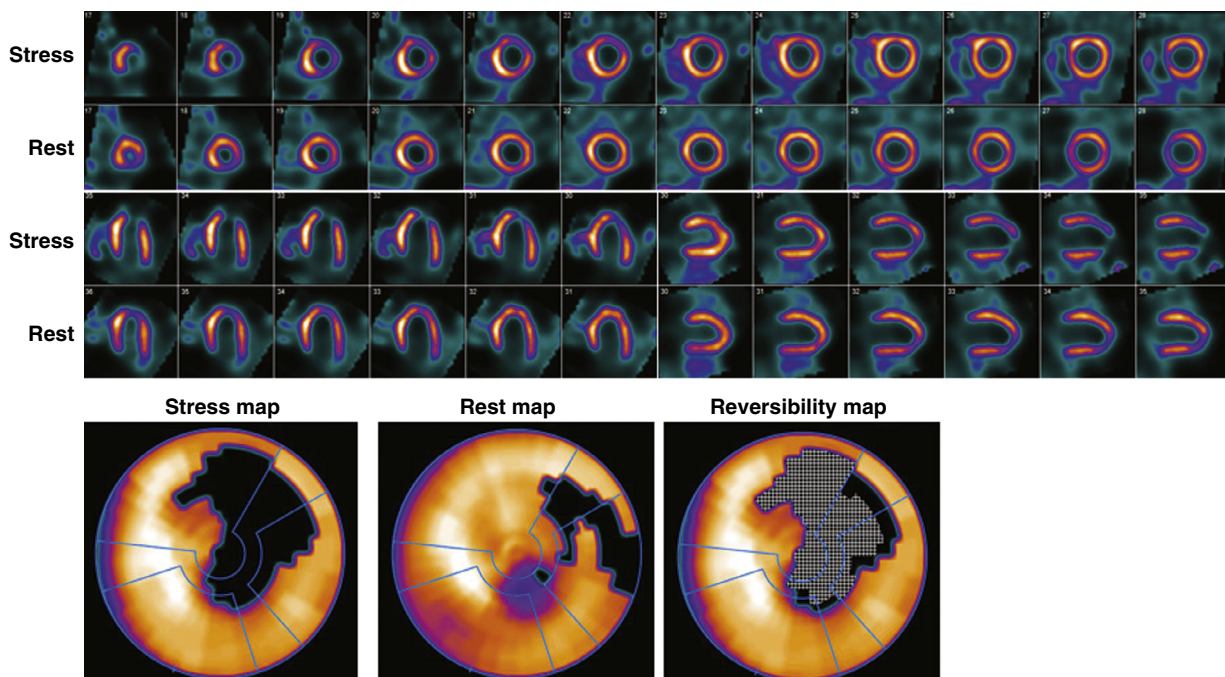


FIGURE 18.21 SPECT MPI in a patient with prior PCI and recurrent symptoms. Vasodilator-stress and rest ^{99m}Tc -sestamibi SPECT MPI of a 58-year-old woman who underwent PCI of the left circumflex (LCX) and left anterior descending (LAD) coronary arteries 3 years ago, now presenting with atypical angina and dyspnea. During vasodilator stress, there was 1-mm downsloping ST-segment depression in the inferolateral leads, which resolved 5 minutes into recovery. Myocardial perfusion images and associated polar maps demonstrate a large perfusion defect of severe intensity in the mid and apical anterior and anterolateral walls with significant but not complete reversibility. Follow-up coronary angiography demonstrated a long segment of severe diffuse disease in the mid-distal LAD including a diagonal branch, and a 50% proximal LCX lesion with total occlusion of the first marginal branch.

residual stenosis requires a maximal stress test. As maximal exercise testing is relatively contraindicated in the immediate post MI setting, a vasodilator stress is commonly used.

Patients with Prior Myocardial Infarction and Ventricular Arrhythmias

Myocardial ischemia is a cause of sustained ventricular arrhythmias/ventricular fibrillation and observational studies have shown that revascularization in addition to arrhythmia management affords improved survival compared with arrhythmia management alone.²⁶ Consequently, investigation of stress-induced ischemia is common in these patients (Fig. 18.22). In addition to ischemia assessment, either SPECT or PET imaging can effectively quantify the extent of myocardial scar and provide effective arrhythmic risk stratification in patients with ischemic and nonischemic cardiomyopathy. For

example, in a study of 439 patients with LVEF $\leq 35\%$ (65% ischemic cardiomyopathy, 35% nonischemic) undergoing rest/stress PET MPI, patients without myocardial scar demonstrated a significantly lower annualized rate of major arrhythmic events (i.e., sudden cardiac arrest [SCA], resuscitated SCA, or appropriate ICD therapy for ventricular tachyarrhythmia) compared with those with any scar (2.1% vs 8.4% per year).²⁷ Importantly, myocardial scar was an independent predictor of major arrhythmic events, whereas other perfusion PET variables including ischemic burden, the presence of nontransmural scar/hibernation, peri-infarct ischemia, and MFR were not. These studies highlight the excellent prognostic value conferred by low scar burden detected by standard radionuclide perfusion imaging, and its ability to further identify a low-risk subgroup, among patients traditionally perceived to be at a high risk of lethal arrhythmic events.

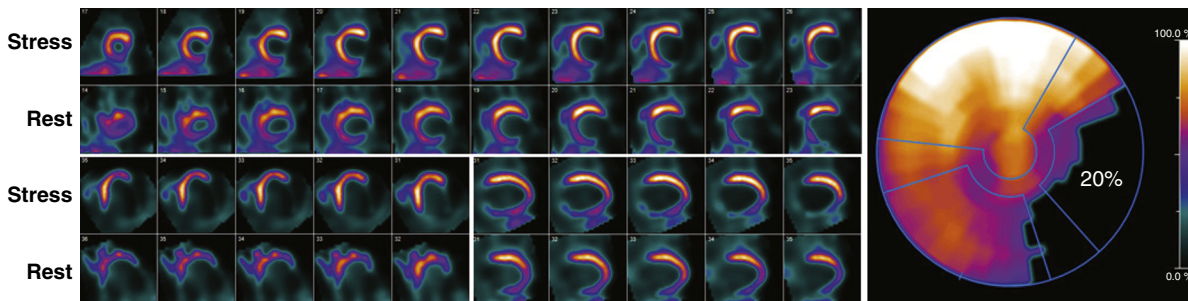


FIGURE 18.22 SPECT MPI in a patient with ventricular arrhythmias. Vasodilator-stress and rest ^{99m}Tc -sestamibi SPECT MPI of a 60-year-old woman with sustained monomorphic ventricular tachycardia 3 years following a large lateral wall myocardial infarction complicated by papillary muscle rupture with cardiogenic shock and need for mitral valve replacement. The myocardial perfusion images demonstrate a mildly dilated left ventricle and a large perfusion defect of severe intensity throughout the inferior and inferolateral and basal anterolateral walls, which was irreversible. Her ECG-gated images demonstrated a left ventricular ejection fraction of 40%.

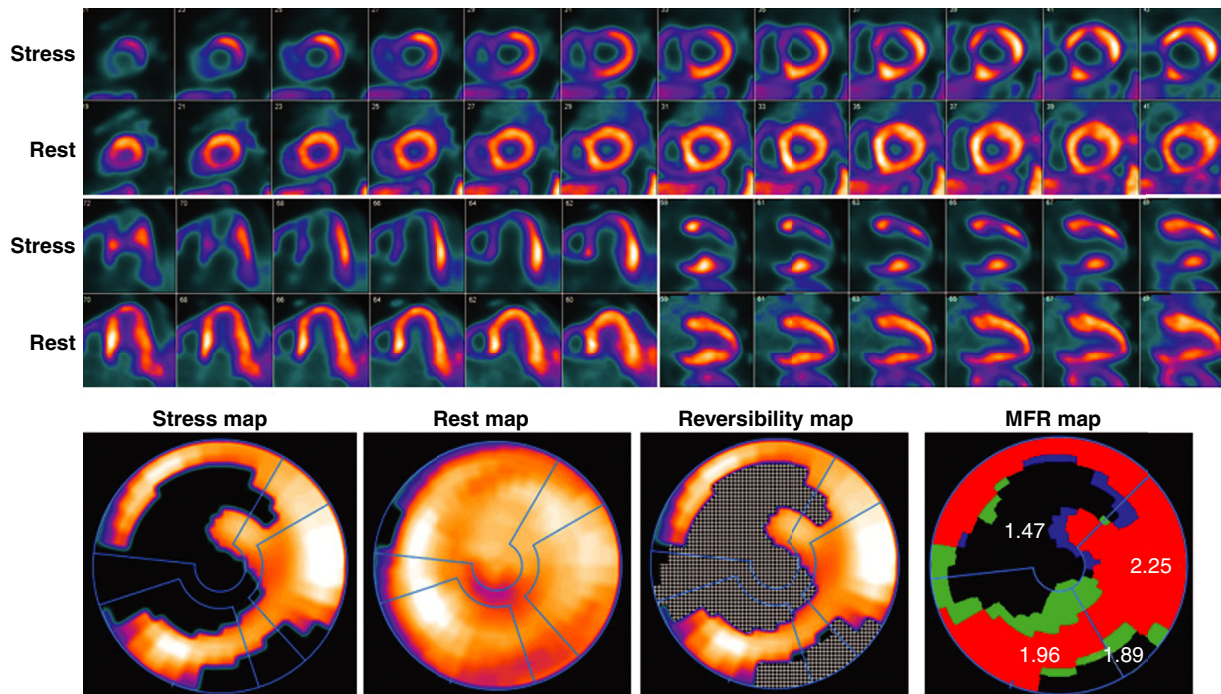


FIGURE 18.23 Quantitative PET in a patient with chronic total coronary occlusion. Vasodilator-stress and rest ^{13}N ammonia PET MPI of a 64-year-old man with known chronic total occlusion (CTO) of the LAD coronary artery who presented with nonanginal chest pain and exertional dyspnea. PET images demonstrate transient left ventricular (LV) dilatation with stress and a large perfusion defect of severe intensity throughout the anteroseptal and anterior walls and LV apex, showing complete reversibility. There is a small but severe perfusion defect involving the basal inferolateral wall, also showing complete reversibility. The ECG-gated images demonstrated a transient increase in the LV end-systolic volume during stress with a decrease in LV ejection fraction from 58% at rest to 51% during stress associated with severe hypokinesis of the anterior and anteroseptal walls, apical LV segments, and LV apex, all consistent with postischemic stunning. The study shows complete viability of the LAD territory with evidence of severe stress-induced ischemia, and a small area of moderate stress-induced ischemia in the inferolateral wall. Myocardial flow reserve is severely reduced in the territory of LAD CTO and relatively preserved in the right coronary artery and left circumflex territories. The patient underwent successful percutaneous coronary intervention of the LAD CTO.

Patients with Chronic Total Coronary Artery Occlusion

Coronary chronic total occlusions (CTOs) are quite common among patients undergoing coronary angiography with a prevalence rate estimated between 18% and 52%. The rapid expansion of dedicated equipment and techniques along with improved operator experience has led to a rapid growth in the number of patients with refractory symptoms despite optimal guideline-directed medical therapy (GDMT) being considered for CTO PCI, in addition to more traditional referral to CABG (see [Chapter 41](#)). In experienced centers, CTO PCI may substantially reduce myocardial ischemia and improve quality of life. In such patients, demonstration of significant myocardial ischemia and viability within the territory supplied by a coronary vessel with a CTO is generally accepted as a useful approach to help inform the risk versus benefit of CTO PCI. Radionuclide perfusion imaging is well suited for this task as it is able to provide more detailed quantitative assessments of ischemia than other noninvasive techniques (e.g., stress echocardiography). One additional advantage of PET imaging is its ability to provide quantitative blood flow and flow reserve data, which helps refine the interrogation of physiologic

significance in non-CTO vessels and inform the extent of revascularization ([Fig. 18.23](#)).

Patients with Cardiac Allograft Vasculopathy. Cardiac allograft transplantation has transformed the lives of patients with advanced heart failure. However, cardiac allograft vasculopathy remains a leading cause of mortality and retransplantation in these individuals (see [Chapter 60](#)). Because of myocardial denervation, silent ischemia is common. Annual surveillance with invasive angiography, endomyocardial biopsy, and imaging is routine in these patients. Transplant vasculopathy develops as diffuse disease that may not result in discrete perfusion defects on MPI ([Fig. 18.24](#)). Emerging data from multiple centers have provided evidence that cardiac PET-measured myocardial blood flow is a sensitive tool with high diagnostic value to identify cardiac allograft vasculopathy ([Fig. 18.25A](#)). Moreover, patients with PET-defined vasculopathy are at significantly higher risk of mortality (see [Fig. 18.25B](#)). Indeed, in patients with serial PET assessments, patients with a decline in myocardial blood flow had worse prognosis.

Patients with Coronary Artery Disease Associated with Complex Congenital Heart Disease. Highly successful surgical

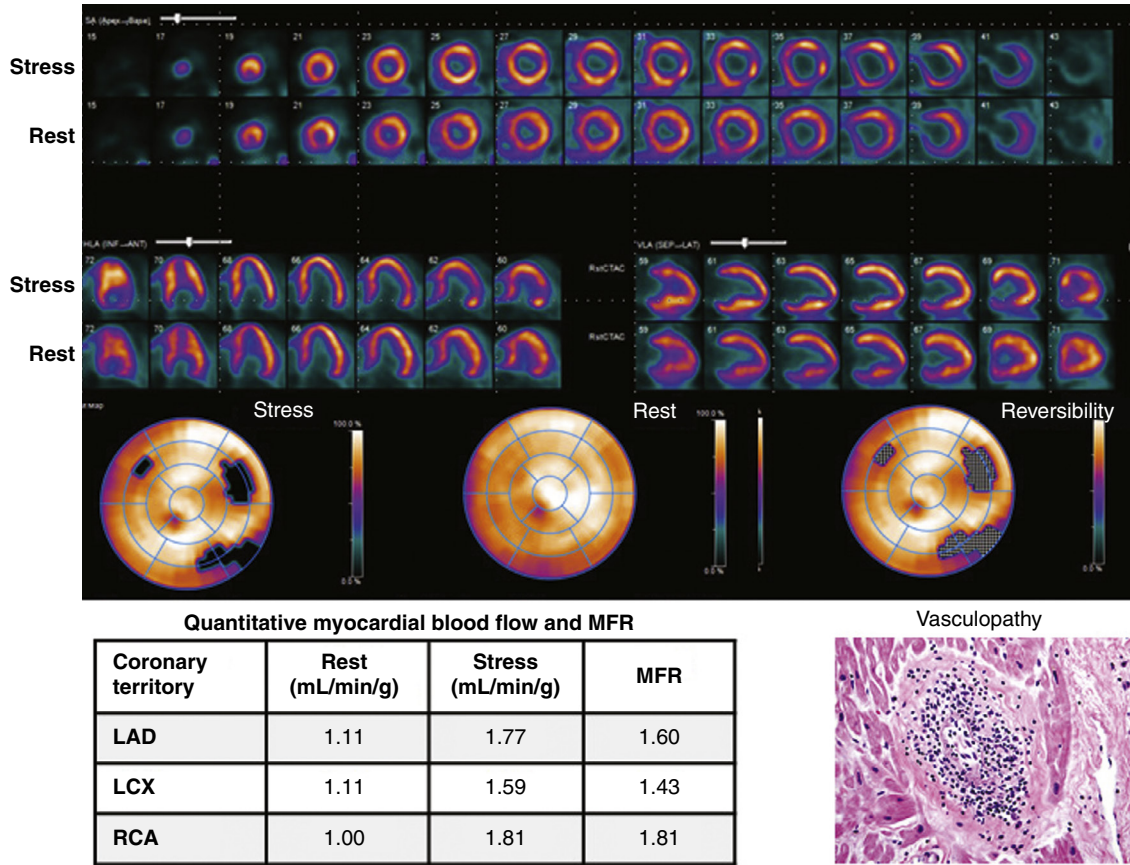


FIGURE 18.24 Quantitative PET imaging in a patient with prior cardiac transplantation. Vasodilator stress and rest ¹³N-ammonia PET images of a 54-year-old woman with cardiac transplantation 3 years earlier who presented with syncope. Myocardial perfusion images show a dilated left ventricle with a medium-sized region of moderate stress-induced ischemia in the mid to basal inferolateral and anterolateral walls. Her left ventricular ejection fraction (LVEF) was 44%. Myocardial blood flow was elevated at rest (>1.0 mL/min/g) in all three vascular territories (common in patients with cardiac transplant) and her stress myocardial blood flow and flow reserve were reduced in all three coronary territories but worse in the left circumflex distribution. The reduced LVEF and abnormal quantitative blood flow are consistent with severe coronary allograft vasculopathy. She underwent a percutaneous coronary intervention to the left circumflex and right coronary arteries, but unfortunately, died 8 weeks later. Autopsy confirmed severe cardiac allograft vasculopathy (bottom right).

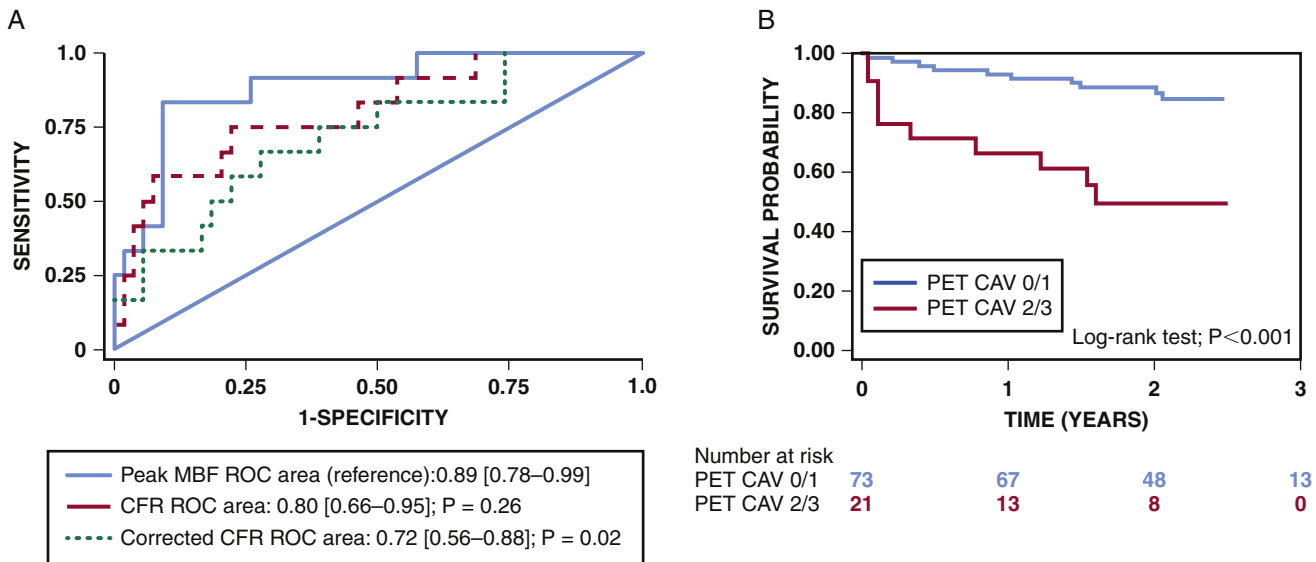


FIGURE 18.25 Diagnostic and prognostic value of quantitative PET after cardiac transplantation. **A**, In a study of 94 patients with prior cardiac transplantation and cardiac PET myocardial perfusion imaging, peak stress myocardial blood flow (MBF) showed the highest accuracy in identifying grade 2 or 3 cardiac allograft vasculopathy (CAV) as defined by the International Society for Heart and Lung Transplantation classification. **B**, In the same study, PET CAV grade 2/3 predicted worse event-free survival. (PET CAV grade 2/3 is defined as multivessel perfusion defects or single-vessel perfusion defect with peak stress MBF <1.7 mL/min/g, or no perfusion defects but peak stress MBF <1.7 and ejection fraction ≤45%.) (From Bravo PE, et al. Diagnostic and prognostic value of myocardial blood flow quantification as non-invasive indicator of cardiac allograft vasculopathy. Eur Heart J 2018;39:316-323.)



interventions and advances in medical therapy have substantially increased the life expectancy of patients with complex congenital heart disease (see [Chapter 82](#)). Atherogenic risk factors increase the risk for ischemic heart disease in adult survivors with complex congenital heart disease. Additionally, these patients are at risk of ischemia due to congenital coronary abnormalities, surgical reimplantation of coronary arteries, mechanical obstruction of coronary arteries caused by compression from abnormal cardiac structures or implanted devices, and atherosclerosis. Finally, device and prosthetic material infections are increasing in this population and ^{18}F -FDG PET/CT may play a role.

Echocardiography is the usual first test for the evaluation of ischemia in these patients. However, stress echocardiography can be challenging to interpret particularly in those with complex congenital heart disease. CMR is also often used to study anatomy, but stress CMR is limited to pharmacologic stress, which is not suitable to provoke ischemia in compressive physiologies. Radionuclide MPI, particularly SPECT with novel scanners or PET, is performed with very low radiation doses. Exercise stress is preferable in these patients and is feasible with SPECT and with ^{13}N -ammonia PET ([Fig. 18.26](#)). Pharmacologic PET with flow quantitation can play a role in the evaluation of patients with atherosclerotic coronary artery stenosis including familial hypercholesterolemia and Kawasaki disease. Patients with transposition of great arteries (arterial switch and systemic right ventricle), anomalous left coronary artery from pulmonary artery, Fontan surgery, cyanotic heart disease, and Kawasaki disease have been shown to have significantly reduced peak stress myocardial blood flow and flow reserve. Radionuclide imaging is also playing an increasing role in the evaluation of device and prosthetic material infection in these complex patients.

Interpretation of the images can be challenging as the current software is not optimized for review of MPI in complex anatomies. When evaluating complex congenital heart disease patients with radionuclide imaging it is important to evaluate perfusion to the systemic ventricle. Knowledge of prior surgical repairs and patches improves specificity of interpretation, and hybrid SPECT/CT and PET/CT help in the interpretation. Because of the high burden of lifetime procedures and related radiation dose, protocols should be personalized to minimize radiation dose.²⁸ Stress-first imaging, novel scanners, two-day protocols, and cardiac PET are some methods used to reduce radiation dose.

Heart Failure and Cardiomyopathies

Patients with Newly Diagnosed Left Ventricular Systolic Dysfunction

An important question in patients presenting with newly diagnosed LV systolic dysfunction is whether significant obstructive CAD is present and likely represents the underlying cause of heart failure. This question can be addressed by invasive coronary angiography or noninvasive imaging including coronary CTA or radionuclide MPI. Both the American and European practice guidelines recommend a diagnostic strategy largely based on symptoms and clinical presentation, patient history, and the likelihood that revascularization may be necessary. There is general agreement that patients with heart failure, severe LV dysfunction, and severe angina should be referred to coronary angiography provided the patient is otherwise suitable for revascularization. However, the initial diagnostic approach for patients without angina or history of MI, or those with prior MI but no angina, is less clear. The latter two categories of patients probably make up the majority of heart failure patients. In patients without angina or a prior history of MI, coronary CTA may be an attractive option, especially in younger patients who are less likely to show coronary calcifications. Another reasonable option includes radionuclide MPI, which may be preferred in older patients with chronic kidney disease. Previous studies have shown that a completely normal radionuclide MPI study is associated with a very high negative predictive value to rule out significant CAD as the likely etiology of heart failure. If available, PET MPI may be preferred as it allows quantification of myocardial blood flow and MFR. The absence of perfusion defects involving a typical coronary artery territory and normal MFR would support a diagnosis of nonischemic cardiomyopathy ([Fig. 18.27](#)). In patients

without angina but a history of MI, radionuclide MPI helps define the extent of scarred and viable myocardium and the magnitude of residual stress-induced ischemia, which in turn helps inform patient management ([Fig. 18.28](#)).

Patients with Ischemic Cardiomyopathy and Heart Failure

LVEF is a well-established and powerful predictor of poor outcome after MI, especially when associated with heart failure. In selected patients, high-risk revascularization appears to afford long-term survival benefit.²⁹ However, selection of patients with severe LV dysfunction for high-risk revascularization remains controversial. Noninvasive imaging can help determine the presence and severity of myocardial ischemia and viability and, consequently, can help identify patients who may benefit from revascularization.

Pathophysiology of Ischemic Left Ventricular Dysfunction

For many years, chronic LV dysfunction at rest in patients with CAD was thought to represent previous MI and, thus, irreversible damage. However, it is now clear that myocardium that has been subjected to acute or chronic ischemia may remain viable and demonstrate regional and global LV dysfunction that can be improved with revascularization. Such reversible contractile dysfunction may be caused by myocardial stunning or hibernation (see [Chapter 36](#)).

Myocardial stunning is a reversible state of regional contractile dysfunction that can occur after restoration of coronary blood flow following a brief episode of ischemia despite the absence of myocardial necrosis. In humans, stunned myocardium can be demonstrated in patients undergoing reperfusion therapy for acute MI, following attacks of unstable angina, and in some patients with exercise-induced ischemia. Although commonly regarded as an acute phenomenon, stunned myocardium may also occur in patients with chronic coronary stenoses who experience recurrent episodes of ischemia (symptomatic or asymptomatic) in the same territory. The latter mechanism is probably the most common form of stunning in patients with chronic LV dysfunction caused by CAD. Myocardial stunning is considered a form of reperfusion injury, in which reintroduction of oxygen after a period of ischemia induces a transient calcium overload that damages the contractile apparatus. The posts ischemic contractile abnormality is fully reversible provided that recurrent ischemia (followed by stunning) does not occur and sufficient time is allowed for the myocardium to recover.

Myocardial hibernation refers to a state of persistent LV dysfunction associated with chronically reduced blood flow but preserved viability. This chronic downregulation in contractile function at rest is thought to represent a protective mechanism in which the heart reduces its oxygen requirements to ensure myocyte survival. However, this protective mechanism can result in a considerable amount of myocardium that is rendered hypocontractile, thus, it may contribute to overall LV dysfunction.

It is generally accepted that stunning and hibernation represent a continuum of severity that depends on the critical interplay between the severity of angiographic CAD, associated reduction in MFR, and severity of myocardial ischemia. Initially, the presence of a flow-limiting coronary artery stenosis leads to a reduction in coronary vasodilator reserve with preserved resting coronary blood flow. The reduced flow reserve in turn results in episodes of ischemia during periods of increased oxygen demand. Ultimately, these transient, recurrent episodes of ischemia lead to a state of persistent LV dysfunction (so-called repetitive stunning). As the severity of coronary stenosis increases, coronary vasodilator reserve becomes critically reduced and resting coronary blood flow eventually falls. The presence of resting hypoperfusion marks the transition from “repetitive” stunning to hibernation. The varying degree of flow deficit underlying these two conditions likely explains the distinct morphologic changes present in stunned and hibernating myocytes. This precarious balance between perfusion and viability in hibernating myocardium cannot be maintained indefinitely, and myocardial necrosis ultimately occurs if blood flow is not restored.

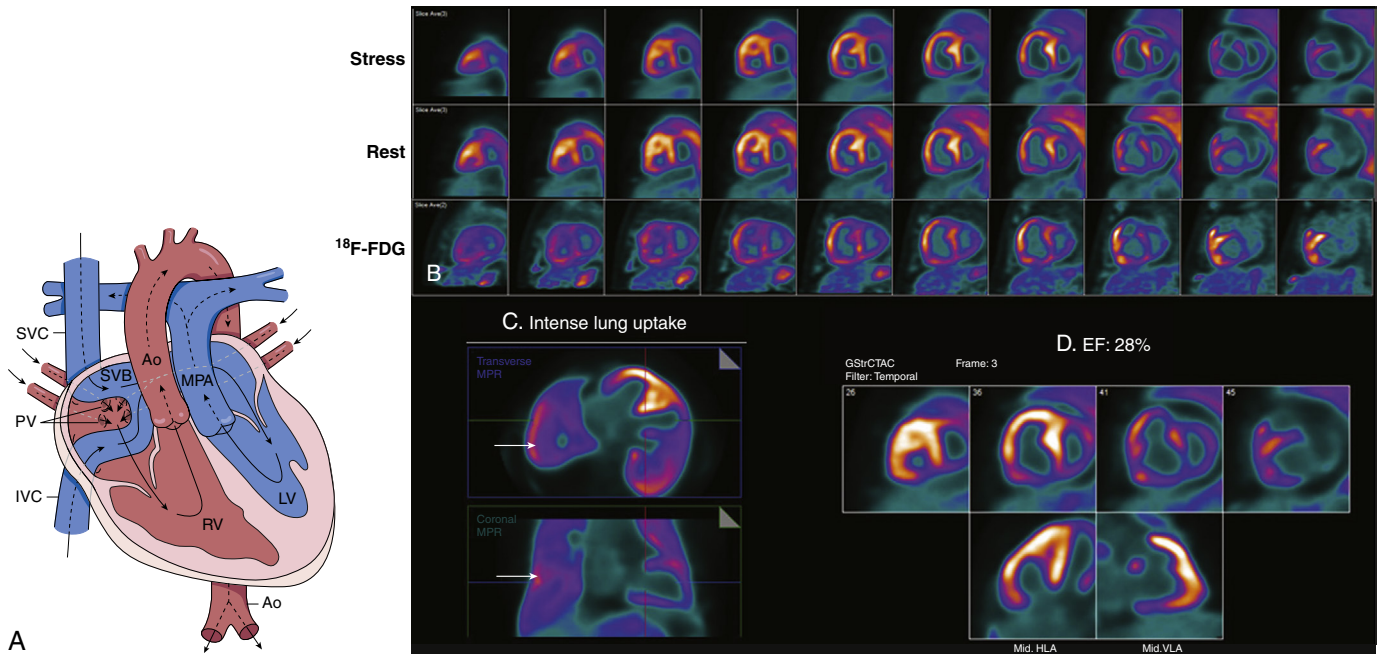


FIGURE 18.26 Cardiac PET scan in an adult patient with congenital heart disease. Vasodilator stress and rest ^{13}N -ammonia and ^{18}F -FDG PET images of a 48-year-old man with D-transposition of great arteries with prior atrial switch operation (Mustard repair) (A), with prior inferior myocardial infarction and residual systemic right ventricular systolic dysfunction, presenting with dyspnea and progressive heart failure. B, PET images demonstrate an anteriorly positioned and dilated systemic right ventricle associated with moderately increased lung uptake (C) (arrows). The subpulmonic left ventricle showed little radiotracer uptake, as expected. There was a medium-sized and severe perfusion defect in the inferior wall of the systemic right ventricle with a partial mismatch on the ^{18}F -FDG images. D, The gated images showed global hypokinesis of the systemic right ventricle with akinesis of the inferior segments. These findings were consistent with a small area of viable but hibernating myocardium in the right coronary artery (RCA) territory. He underwent a repeat coronary angiography, which demonstrated a patent RCA. PV, pulmonary veins; Ao, aorta; MPA, main pulmonary artery; SVC, superior venacava; IVC, inferior vena cava; RV, right ventricle; LV, left ventricle; SVB, systemic venous baffle.

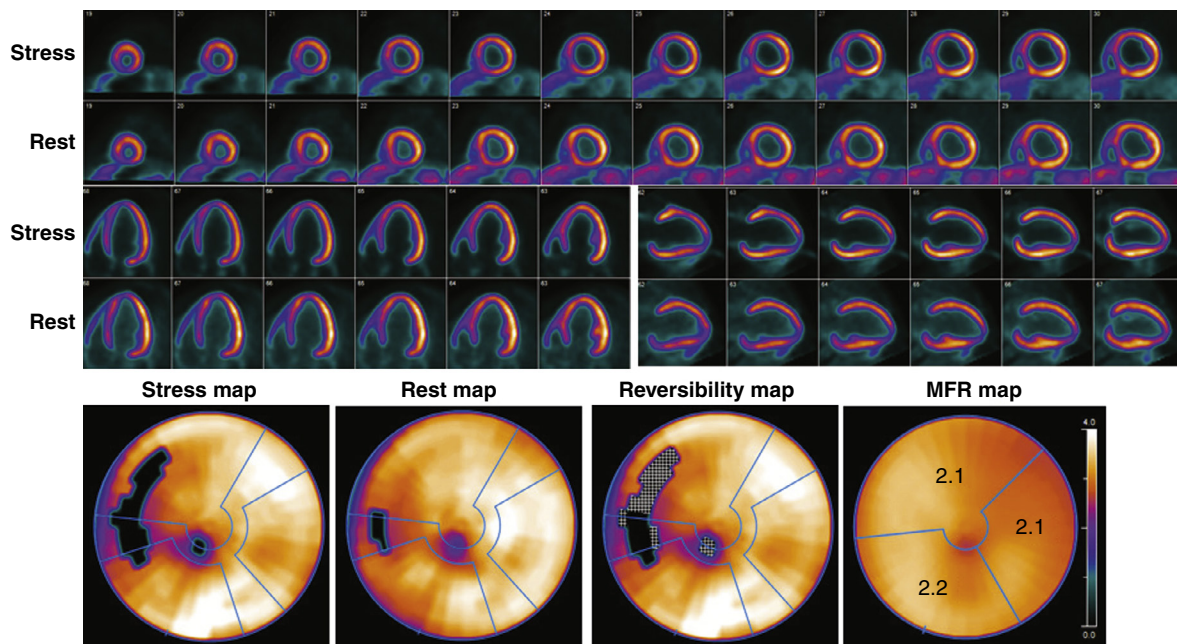
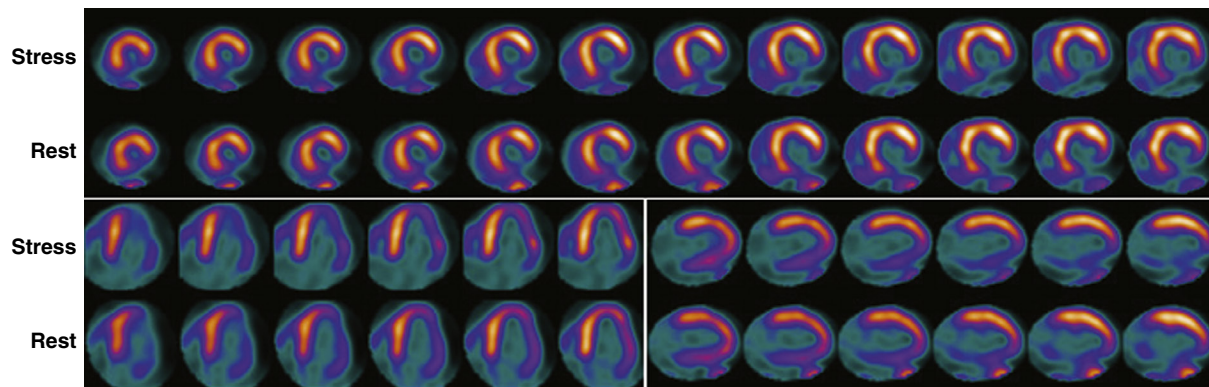


FIGURE 18.27 Myocardial perfusion imaging in a patient with cardiomyopathy. Vasodilator stress and rest ^{13}N -ammonia PET images of a 74-year-old woman with hypertension, diabetes, and chronic kidney dysfunction who presented with new-onset exertional dyspnea. The ECG showed left bundle branch block (LBBB). PET MPI shows a severely dilated left ventricle and a small septal perfusion defect showing apparent reversibility, likely secondary to LBBB. The ECG-gated images demonstrated an ejection fraction of 15% that rose to 20% during peak stress, and evidence of septal dyssynchrony. Myocardial flow reserve was preserved in all coronary territories. These findings are consistent with a nonischemic cardiomyopathy, which was subsequently confirmed on coronary angiography LBBB, left bundle branch block.

Radionuclide Imaging Approaches to Assess Myocardial Ischemia and Viability

The evaluation of patients with severe LV dysfunction and angiographic CAD often requires the combination of stress testing to quantify the extent of myocardium at risk and metabolic imaging to distinguish viable from nonviable myocardium (Fig. 18.29).

SPECT MPI can be used to assess the extent and severity of myocardial ischemia using exercise or pharmacologic stress in combination with $^{99\text{m}}\text{Tc}$ -labeled radiotracers or ^{201}Tl , as described earlier in this chapter. For viability assessment, attenuation-corrected SPECT MPI is preferable. One advantage of ^{201}Tl is that it provides a more accurate assessment of viable myocardium, especially in the setting



Quantitative myocardial blood flow and MFR

Coronary territory	Rest (mL/min/g)	Stress (mL/min/g)	MFR
LAD	0.83	0.89	1.07
LCX	0.86	1.01	1.17
RCA	0.64	0.66	1.03

FIGURE 18.28 Quantitative myocardial perfusion imaging in a patient with ischemic cardiomyopathy. Vasodilator-stress and rest ¹³N-ammonia PET images of a patient with prior myocardial infarction (MI) who presented with worsening heart failure. His left ventricular ejection fraction was estimated at 30%. Myocardial perfusion images MPI demonstrate a large and severe perfusion defect throughout the inferior and inferolateral walls, which was irreversible and consistent with prior MI. However, the quantitative myocardial blood flow and flow reserve (MFR) data show blunted augmentation of flow during stress, resulting in a severe reduction in MFR in all three vascular territories. Coronary angiography demonstrated severe multivessel obstructive coronary artery disease. LAD, left anterior descending artery; LCX, left circumflex artery; RCA, right coronary artery.

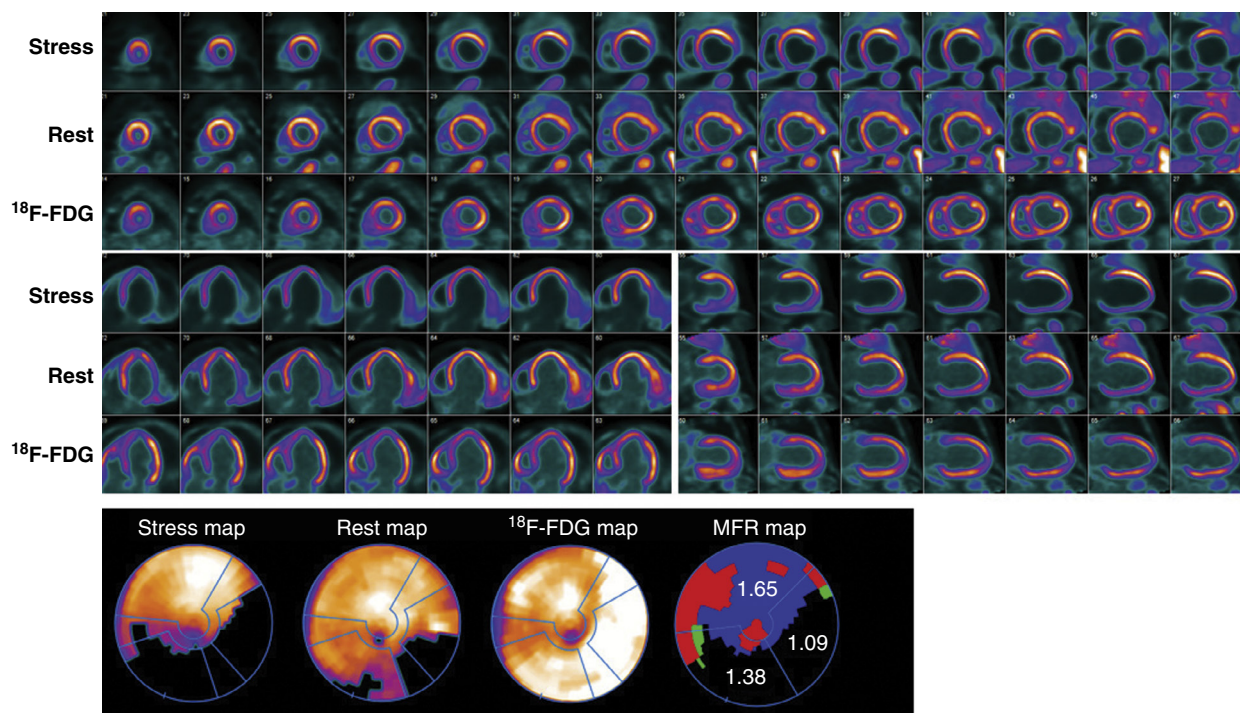


FIGURE 18.29 Assessment of myocardial ischemia and viability in a patient with ischemic cardiomyopathy. Vasodilator stress and rest ¹³N-ammonia and ¹⁸F-FDG PET images of a 70-year-old man with progressive dyspnea, hypotension, and new severe biventricular systolic dysfunction with elevated natriuretic peptides. Coronary angiography demonstrated multivessel coronary artery disease with left circumflex (LCX) chronic total occlusion (filled by left-to-left collaterals), serial severe right coronary artery (RCA) lesions (80% to 90%), and moderate left anterior descending (LAD) stenosis (40% to 50%) in the proximal mid segments. PET images demonstrate severe left ventricular (LV) dilatation and mild right ventricular (RV) dilatation with increased RV uptake of ¹⁸F-FDG, consistent with pulmonary hypertension. Stress perfusion images show a large and severe perfusion defect throughout the inferoseptal, inferior, and inferolateral walls, with moderate reversibility. The ¹⁸F-FDG images demonstrate normal glucose uptake in all hypoperfused LV segments (perfusion-¹⁸Fmetabolism mismatch). Quantitative PET confirmed severely reduced flow reserve (MFR) in the LCX and RCA territories, consistent with the severe stress perfusion defects. In addition, MFR was also moderately reduced in the LAD territory. The ECG-gated images demonstrated a rest LV ejection fraction (LVEF) of 14% and end-systolic volume index (ESVI) of 158 mL/m². Poststress LVEF was 17% with ESVI 155 mL/m². The findings are consistent with extensive areas of mixed stress-induced ischemia and hibernating myocardium throughout the LCX and RCA territories, and a flow-limiting stenosis in the LAD territory. The patient underwent successful three-vessel coronary artery bypass graft surgery.

of severe resting hypoperfusion. A common approach to improve detection of hibernating myocardium is the use of nitrates to improve collateral flow at rest and enhance radiotracer uptake in areas of severe hypoperfusion.

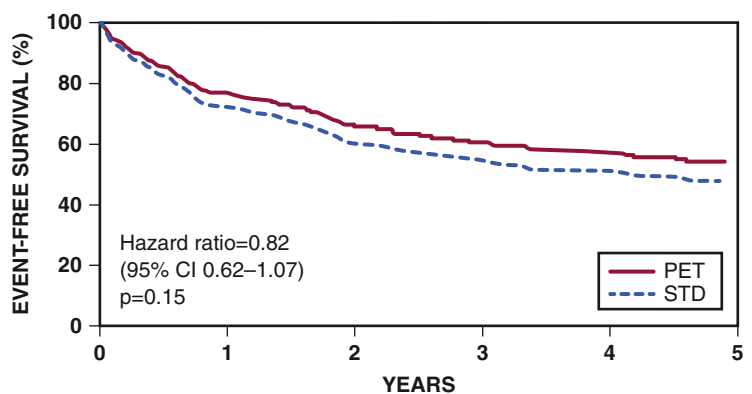
PET imaging provides a more comprehensive approach for the evaluation of patients with ischemic cardiomyopathy and its use for this application is growing worldwide. As was discussed earlier, the advantages of PET include its more accurate quantitative assessment of ischemia and the use of ^{18}F -FDG to assess myocardial metabolism and myocardial viability. The use of metabolic ^{18}F -FDG imaging for viability assessment requires careful patient preparation before imaging. For a detailed step-by-step description of the available methods for patient preparation before ^{18}F -FDG imaging, the reader should review the Guidelines for PET Imaging published by the ASNC.²

Myocardial Viability Imaging to Guide Revascularization in Patients with Ischemic Heart Failure

Several studies using different PET approaches have shown that the gain in global LVEF after revascularization is related to the magnitude of ischemic and/or viable myocardium assessed preoperatively. These data demonstrate that clinically meaningful changes in global LV function can be expected after revascularization only in patients with relatively large areas of hibernating and/or stunned myocardium (~20% of the LV mass). Similar to other noninvasive imaging modalities, the extent of nonviable or scarred myocardium by ^{18}F -FDG PET correlates inversely with changes in LVEF after revascularization.

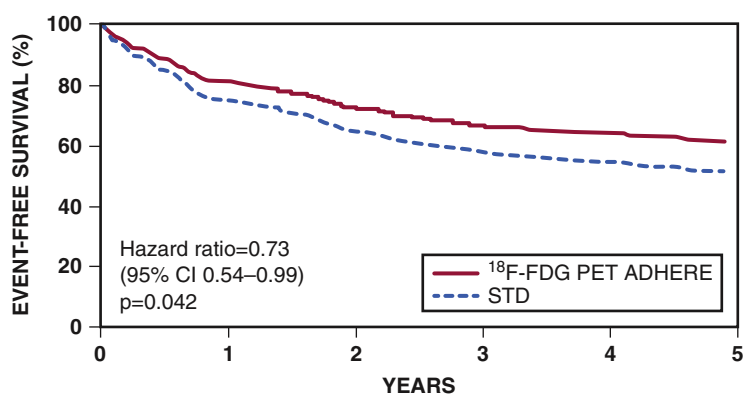
Consistent data from single-center, observational studies demonstrate that the presence of ischemic, viable myocardium among patients with severe LV dysfunction identifies patients at higher clinical risk, and that prompt revascularization in selected patients is associated with improved LV function, symptoms, and survival compared with medical therapy alone. The PARR-2 clinical trial, in which patients were randomized to PET-guided management versus standard clinical care, however, did not demonstrate an overall benefit of PET; it did show in a post hoc analysis that image-guided decisions regarding revascularization were associated with improved clinical outcomes following revascularization if treatment decisions adhere to imaging recommendations³⁰ (Fig. 18.30).

Nonetheless, the main criticism of those older studies is that they were retrospective and medical therapy did not reflect current accepted management of heart failure nor was it standardized in any way. The results of the Surgical Treatment of Ischemic Heart Failure (STICH) trial, especially its ancillary viability substudy, have challenged all prior data as they failed to demonstrate a significant interaction between ischemia or viability information, revascularization, and improved survival compared with optimal medical therapy²⁹ (Fig. 18.31). This casts significant uncertainty whether noninvasive characterization of ischemia, viability, and scar can actually provide useful information to guide management decisions. This issue is currently undergoing intense debate in the medical community. As we begin to incorporate the results of the STICH trial into clinical practice, it is important to consider the strengths and weaknesses of the STICH substudies.



No. at risk

PET	197	132	103	86	75	67
STD	195	124	92	76	69	58



No. at risk

^{18}F -FDG PET ADHERE	138	98	80	66	58	52
STD	195	124	93	76	69	58

FIGURE 18.30 PET-guided revascularization in ischemic cardiomyopathy. *Top*, Event-free survival in patients randomized to a PET-guided approach versus standard care (STD) in the PARR-2 study. There was no difference in survival between the standard arm and the PET-guided arm. *Bottom*, In post hoc analysis, PET-guided management showed improved survival compared with standard care among patients in whom management decisions adhered to the PET recommendation (i.e., revascularization for hibernating myocardium; medical therapy alone for scar). (From McArdle B, et al. Long-term follow-up of outcomes with F-18-fluorodeoxyglucose positron emission tomography imaging-assisted management of patients with severe left ventricular dysfunction secondary to coronary disease. *Circ Cardiovasc Imaging* 2016;9:e004331.)

The STICH viability³¹ and ischemia substudies are the largest reports to date relating myocardial viability and ischemia to clinical outcomes of patients with CAD and LV dysfunction associated with heart failure. They are also the first to assess these relationships prospectively among patients who were all eligible for CABG as well as optimal medical management alone. As mentioned previously, medical therapy in the STICH trial was standardized and followed published guidelines that were current during the course of the trial (angiotensin converting enzyme inhibitors or angiotensin receptor blockers, beta blockers, statins, and aspirin). However, these studies also have important limitations. First, viability data were only available in half of the STICH population, which is likely to introduce some selection bias. In fact, patients in the STICH viability study had higher prevalence of prior MI, lower frequency of limiting angina symptoms, lower LVEF, and more advanced LV remodeling compared with those who did not receive viability imaging before randomization. Second, the definition of viability in the STICH substudy was quite broad resulting in 81% of the total study population considered as having “viability” by study criteria. This number is a great deal higher than that seen in other studies using similar methodologies for viability assessment. Third, neither PET nor CMR was used to evaluate ischemia or viability. On the other hand, medical therapy did not include newer agents that might further improve outcome of medically treated patients, such as sacubitril-valsartan and sodium-glucose cotransporter-2 inhibitors (see Chapter 50). An important additional consideration to

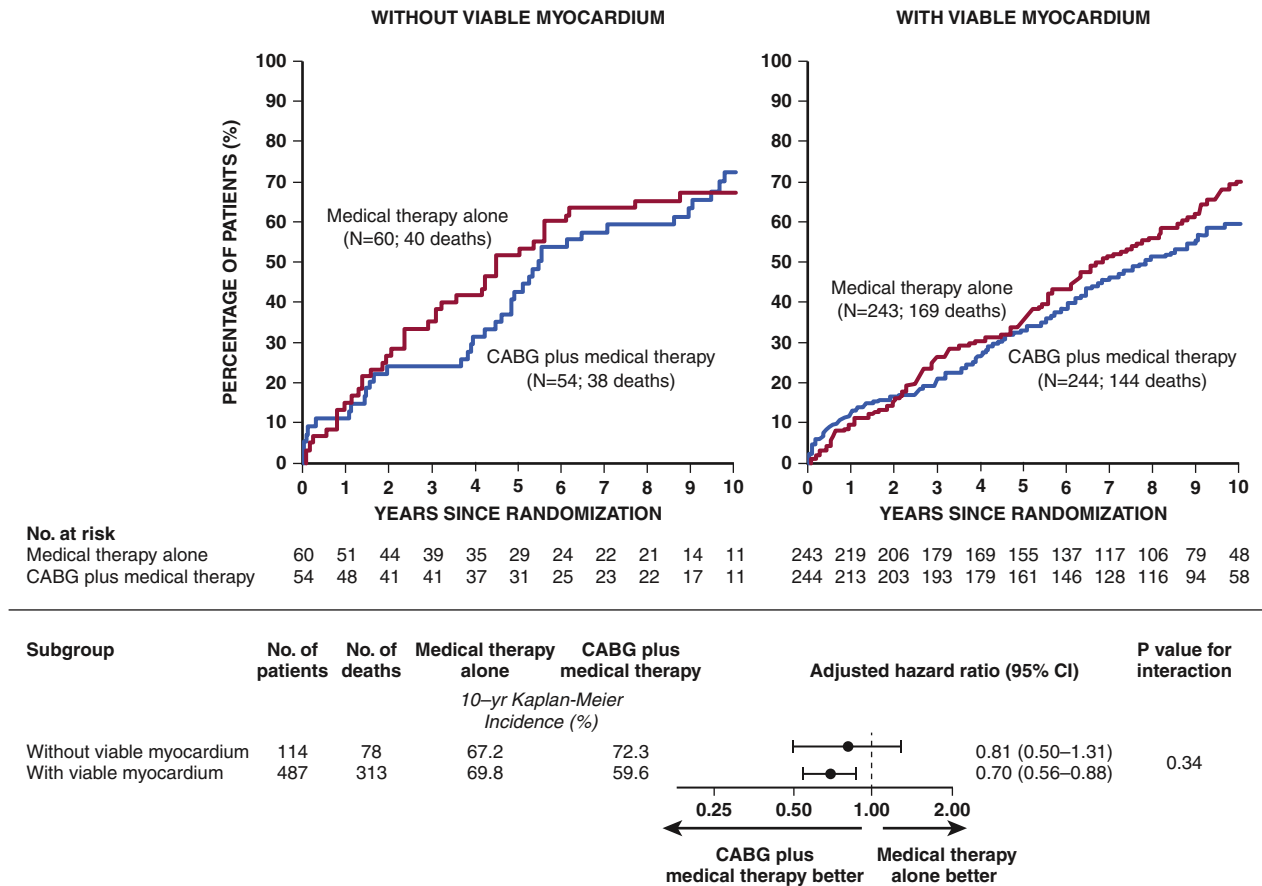


FIGURE 18.31 Role of viability imaging in the STICH study. Survival probability in patients without (left) and with (right) myocardial viability by treatment assignment in the long-term follow-up of the STICH patients included in the viability substudy. *Bottom*, Results of a Cox proportional-hazards model that tested for the interaction between myocardial viability and treatment with adjustment for baseline covariates, which was not significant. CABG, Coronary artery bypass graft surgery. (From Panza JA, et al. Myocardial viability and long-term outcomes in ischemic cardiomyopathy. *N Engl J Med* 2019;381:739-748.)

understand the generalizability of the STICH substudies is that patients in the main trial in general, and those in the viability and ischemia studies in particular, had end-stage LV remodeling. Indeed, the mean LV end-diastolic volume index was >120 mL/m², and LV end-systolic volume index approached 100 mL/m². This degree of advanced LV remodeling has generally been associated with poor outcomes regardless of the presence of ischemia or viability and treatment applied. In summary, the STICH trial and its imaging substudies suggest that among patients with heart failure and end-stage LV remodeling, identification of moderate ischemia or viability is not associated with a significant survival advantage from revascularization. Although the benefits of optimal medical therapy in patients with ischemic cardiomyopathy are undeniable, we cannot and should not generalize the STICH findings to all patients with heart failure and severe systolic dysfunction, especially those with a lesser degree of LV remodeling, as these patients were not studied in the STICH trial. As data from randomized clinical trials in such patients are limited, careful integration of clinical, anatomic, and functional information regarding ischemia and viability from noninvasive imaging is necessary to individualize difficult management decisions based on the best available evidence and sound clinical judgment.

Neuronal Imaging to Identify Patients at Risk for Sudden Cardiac Death. There is experimental and clinical evidence supporting the concept that sympathetic activation plays an important role as a potential trigger of ventricular arrhythmias after MI. Indeed, MI and ischemia can lead to sympathetic denervation in both the infarct and peri-infarct zone. Viable but denervated myocardial regions show supersensitive shortening of effective refractory period in response to the infusion of norepinephrine and are more vulnerable to ventricular arrhythmias. This suggests that direct imaging of cardiac sympathetic innervation may have an important clinical role in risk stratification of patients after MI.

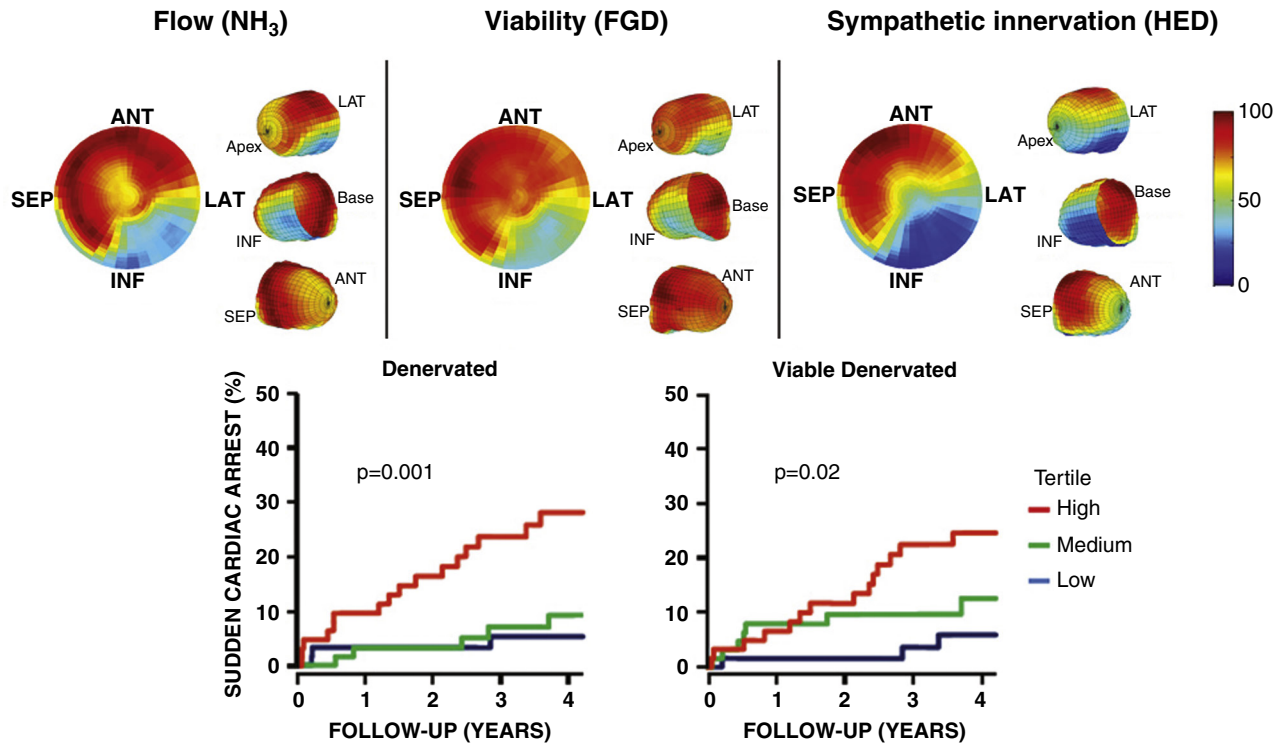
For radionuclide imaging, tracer analogues to the sympathetic neurotransmitter norepinephrine (NE), the parasympathetic mediator

acetylcholine (ACh), and postsynaptic adrenergic receptors have been used to visualize and quantify autonomic innervation and receptor density and function. Most of the clinical evidence regarding the potential applications of neuronal imaging in heart failure has been obtained with NE analogue ¹²³I-meta-iodobenzylguanidine (MIBG), currently the only FDA-approved imaging tracer for this application. PET radiotracers have also been used including ¹¹C-meta-hydroxyephedrine (¹¹C-HED).

AdreView Myocardial Imaging for Risk Evaluation in Heart Failure (ADMIRE-HF), the largest study to date, included 961 patients with class II–III heart failure and LVEF ≤35% who were initially followed over a median of 17 months for the occurrence of worsening HF class, cardiac death, and life-threatening ventricular arrhythmias defined as a spontaneous sustained (>30 seconds) ventricular tachyarrhythmia, a resuscitated cardiac arrest, or an appropriate ICD discharge (anti-tachycardic pacing or defibrillation).³² The principal finding of this study was that patients with a quantitative heart to mediastinum ratio (HMR) of ¹²³I-MIBG <1.6 had a higher rate of adverse events than those with HMR ≥1.6 (37% vs. 15%) (Figs. 18.32 and 18.33).³² Importantly, patients with an HMR ≥1.6 had a mortality rate below 1%.

The Prediction of Arrhythmic Events with Positron Emission Tomography (PAREPET) study tested the hypothesis that the extent of inhomogeneity in myocardial sympathetic innervation and/or hibernating myocardium increased the risk of arrhythmic death independent of LV function in patients with ischemic cardiomyopathy (LVEF ≤35%).³³ The study included 204 patients who were eligible for primary prevention ICDs. Myocardial sympathetic denervation was quantified with ¹¹C-HED and PET imaging. The primary endpoint was SCA defined as arrhythmic death or ICD discharge for ventricular fibrillation or ventricular tachycardia >240 beats/min. Compared with patients in the lowest tertile of cardiac sympathetic denervation assessed by HED PET, those in the highest tertile showed a greater than six-fold increase in the risk of SCA (eFig. 18.6).³³ In multivariable analysis, the extent of PET-defined sympathetic denervation, LV end-diastolic volume index, and creatinine were significantly associated with the risk of SCA.³³

In summary, the available evidence suggests that cardiac neuronal imaging with NE analogues including ¹²³I-MIBG and ¹¹C-HED are clinically useful tools for risk stratification of patients with heart failure.



EFIGURE 18.6 Stratification of arrhythmic risk by volume of scarred and denervated myocardium. Bull's-eye maps of myocardial perfusion (*left*), ¹⁸F-FDG viability (*middle*), and sympathetic innervation (*right*) in a patient that experienced sudden cardiac arrest. There is a large matched perfusion-metabolic defect involving the inferior and inferolateral walls, consistent with prior myocardial infarction. The ¹¹C hydroxyephedrine (HED) images demonstrate a larger myocardial volume of sympathetic denervation (reduced HED uptake) compared with the scarred area. This mismatch between infarct size (reduced ¹⁸F-FDG) and the volume of sympathetic denervation (larger HED defect) has been identified as an imaging marker for risk of ventricular arrhythmias. ANT, Anterior; INF, inferior; LAT, lateral; SEP, septum. (Courtesy Dr. James A. Fallavollita, University of Buffalo, NY.)

symptoms that cannot distinguish AL from ATTR-CA. AL amyloidosis is treated with chemotherapy. Wild-type TTR-CA is treated by TTR stabilization (tafamidis) and for hereditary TTR neuropathy is treated by silencing TTR gene products (patisiran and inotersen). Hence once a diagnosis of ATTR-CA is confirmed, genetic testing is indicated to exclude TTR gene mutation.

The diagnosis of cardiac amyloidosis is often delayed because of its perceived rarity and multifaceted clinical presentation (Fig. 18.34; see Fig. 72.13). An evaluation for cardiac amyloidosis includes clinical history and examination, cardiac biomarkers, evaluation for light chain amyloidosis, cardiac imaging, endomyocardial or organ biopsy, and genetic testing in patients with ATTR-CA.³⁴ Echocardiography and CMR (see Fig. 19.13) are important first tests that raise the suspicion of cardiac amyloidosis (see Chapters 16 and 19). Radio-nuclide scintigraphy (SPECT

bone-avid radiotracers or amyloid PET radiotracers)³⁴ is emerging as a key diagnostic study for ATTR-CA.

Although myocardial uptake of bone-avid radiotracers in cardiac amyloidosis has been recognized for almost 40 years, it is now established that such increased uptake is more consistently seen in ATTR-CA. Multiple studies have established the high accuracy of bone scintigraphy to diagnose ATTR-CA. About 20% to 25% of patients with AL cardiac amyloidosis also manifest significant myocardial uptake of bone-avid radiotracers. Exclusion of AL amyloidosis using serum free light chain assay, serum, and urine immunofixation electrophoresis is thus critical to maintain the high specificity of ^{99m}Tc-PYP/DPD/HMDP scan for ATTR-CA and to ensure timely consideration of chemotherapy if AL amyloidosis is diagnosed. A multicenter study of 1498 patients revealed that a grade 2 or 3 positive ^{99m}Tc-PYP/DPD/HMDP scan can identify cardiac ATTR amyloidosis with nearly 100% specificity and 71% sensitivity, if AL amyloidosis is excluded, avoiding an endomyocardial biopsy.³⁵ Furthermore, there is growing evidence that nearly 13% to 18% of older adults with HFpEF, and nearly 25% to

30% of those with severe aortic stenosis have underlying ATTR-CA by bone-avid tracer cardiac scintigraphy (see Chapters 51 and 72). These findings are particularly important now as ATTR-CA is a treatable cause of HFpEF.

A multisocietal expert consensus document recommends multimodality imaging in cardiac amyloidosis, including the key role of bone scintigraphy for identification of ATTR amyloidosis.³⁶ As per these recommendations, cardiac AL amyloidosis can be diagnosed by biopsy or clinical measures (Table 18.5) and cardiac ATTR amyloidosis can be diagnosed by biopsy or by imaging. Indications for ^{99m}Tc-PYP/DPD/HMDP imaging include Black patients age >60 with HFpEF or LV thickening; non-Black patients age >60 with HFpEF and LV thickening;

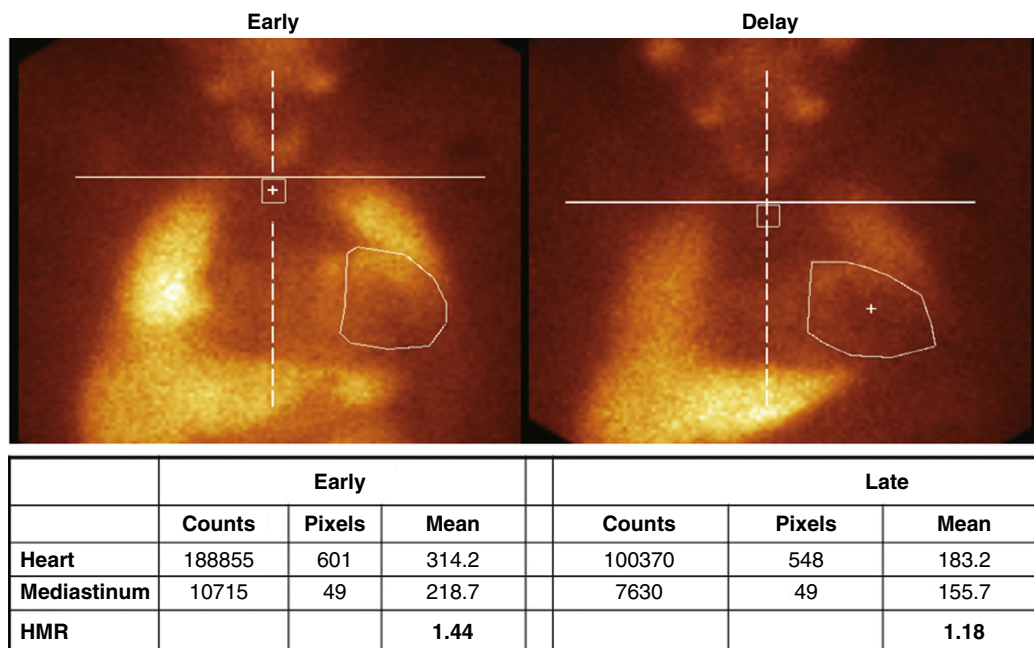
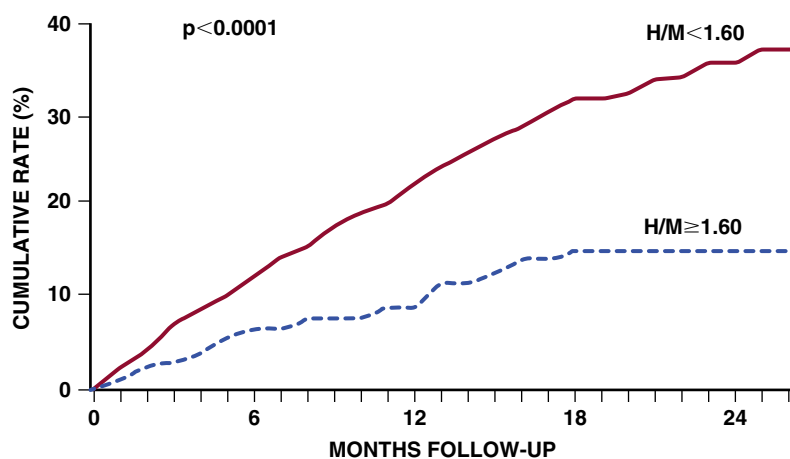


FIGURE 18.32 Assessment of heart to mediastinum ratio (HMR) with ¹²³I-MIBG. These planar chest images illustrate the calculation of HMR with MIBG imaging. Regions of interest are drawn over the heart and upper mediastinum on the early (15-minute) and delayed (4-hour) images, and corresponding mean counts used to calculate the HMR. (Images courtesy Dr. Mark Travin, Montefiore Medical Center, Bronx, NY.)

COMPOSITE PRIMARY ENDPOINT



n: H/M < 1.60	760	698	629	537	441	330	241	176	67
n: H/M ≥ 1.60	201	192	178	164	141	107	85	62	28

FIGURE 18.33 Prognostic value of ¹²³I-MIBG in heart failure. In the ADMIRE-HF study, 961 subjects with heart failure (New York Heart Association [NYHA] class II/III) and left ventricular ejection fraction (LVEF) of ≤35% underwent ¹²³I-MIBG imaging. The cumulative rate of events (time to first NYHA class progression, potentially life-threatening arrhythmia, or cardiac death) was significantly higher in patients with a heart to mediastinum ratio (H/M) < 1.6 than in those with H/M ≥ 1.6. (From Jacobson AF, et al. Myocardial iodine-123-meta-iodobenzylguanidine imaging and cardiac events in heart failure. Results of the prospective ADMIRE-HF (AdreView Myocardial Imaging for Risk Evaluation in Heart Failure) study. *J Am Coll Cardiol* 2010;55:2212-2221.)

However, it is still uncertain if such evidence is sufficient to guide selection of heart failure patients for primary prevention ICD implantation beyond LVEF and conventional clinical risk stratification parameters as recommended by practice guidelines.

Infiltrative Cardiomyopathy: Amyloidosis

Cardiac amyloidosis is a protein misfolding disorder in which misfolded proteins deposit in various organs as fibrils causing a diffuse infiltrative cardiomyopathy (see Chapter 53). The two common forms of amyloidosis that affect the heart are immunoglobulin light chain amyloidosis (AL amyloidosis, a plasma cell dyscrasia) and transthyretin amyloidosis (wild-type ATTR or hereditary ATTR).³⁴ Both AL and ATTR-CA present as heart failure with preserved EF (HFpEF), and a multitude of clinical

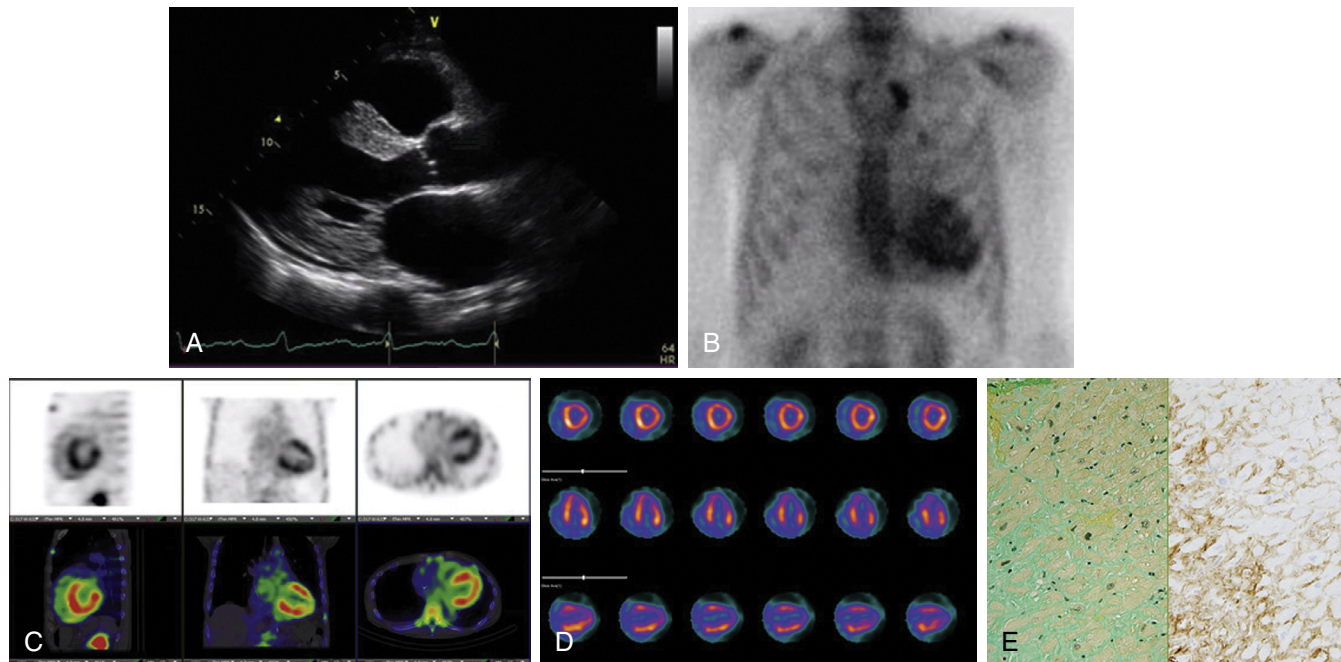


FIGURE 18.34 Role of bone scintigraphy in the diagnosis of cardiac amyloidosis. **A**, Echocardiogram in a 78-year-old man with heart failure and recently diagnosed cardiac amyloidosis showed severe concentric left ventricular (LV) thickening (18 mm) and moderately reduced LV ejection fraction (35%). **B**, The ^{99m}Tc -PYP SPECT/CT scan showed intense myocardial PYP uptake (grade 3) on the planar and **(C and D)** SPECT/CT images. **E**, Endomyocardial biopsy with sulfated Alcian blue staining and immunohistochemistry-confirmed transthyretin (TTR) cardiac amyloidosis. Serum free light chain assay and serum and urine immunofixation were normal and excluded light chain amyloidosis. A genetic test excluded TTR mutations and confirmed wild-type A TTR amyloidosis.

TABLE 18.5 Diagnostic Criteria for Cardiac Amyloidosis

Endomyocardial biopsy: documenting amyloid deposits with Congo red positivity and immunohistochemistry or mass spectrometry typing of fibril
Extracardiac biopsy: documenting amyloid deposits with Congo red positivity and immunohistochemistry or mass spectrometry typing of fibril AND
Cardiac AL or ATTR amyloidosis can be diagnosed by typical imaging features* (echo wall thickness >12 mm, late gadolinium enhancement, or expanded extracellular volume >0.40) OR Cardiac AL amyloidosis can be diagnosed by elevated cardiac biomarkers* (age-adjusted NT proBNP or troponin T)
Clinical diagnosis: cardiac ATTR amyloidosis can be diagnosed by endomyocardial biopsy or a strongly positive bone-avid cardiac scintigraphy (PYP/DPD/HMDP) in patients with typical imaging features* and without a plasma cell dyscrasia (normal serum free light chain assay as well as serum and urine immunofixation electrophoresis).

*When all other causes of imaging features or cardiac biomarker release are excluded. From Dorbala S, et al. ASNC/AHA/ASE/EANM/HFSA/ISA/SCMR/SNMIMI expert consensus recommendations for multimodality imaging in cardiac amyloidosis: Part 2 of 2-Diagnostic criteria and appropriate utilization. *J Nucl Cardiol* 2019;26:2065-2123.

heart failure with unexplained peripheral sensory neuropathy; known or suspected hereditary ATTR-CA; and follow-up of progressive symptoms in known AL amyloidosis or ATTR-CA. Once a diagnosis of ATTR-CA is made, the next step is to evaluate for TTR gene mutations as that may identify need for different therapies, a different prognosis, and implications for family members.³⁴

The typical imaging protocol for ^{99m}Tc bone scintigraphy includes the use of SPECT imaging (preferably SPECT/CT if available) 2 to 3 hours after the IV administration of the bone-avid radiotracer. Planar imaging with measurement of heart to contralateral lung ratio has been used and it can be helpful when negative. However, when positive planar imaging is limited it is difficult to distinguish blood pool from myocardial retention. ^{99m}Tc -PYP/DPD/HMDP images are typically interpreted visually comparing radiotracer uptake in myocardium in relation to that in the ribs using the following grading system: grade 0 = absent myocardial uptake, grade 1 = rib uptake, grade 2 = rib uptake,

and grade 3 = rib uptake (Fig. 18.35). Quantitative imaging of bone-avid scintigraphy with SPECT/CT is emerging as a novel technique,³⁷ which may allow detection of early disease, assessment of response to therapy, and determination of prognosis. Bone-avid scintigraphy can detect early amyloid deposition in the heart before increase in myocardial wall thickening,³⁴ but emerging data indicate that bone scintigraphy may be negative in certain hereditary forms of cardiac amyloidosis. Consequently, if hereditary ATTR-CA is suspected and the bone scintigram is negative, further evaluation including endomyocardial biopsy should be considered. Also, ^{99m}Tc -MDP, a common bone scanning tracer in the United States, has low sensitivity and is not recommended for evaluation of ATTR-CA.³⁴ The presence of ATTR-CA by bone scintigraphy has been associated with worse outcome.³⁸

Amyloid imaging using targeted PET radiotracers approved for diagnosis of Alzheimer disease is emerging as a novel method to accurately diagnose cardiac AL and ATTR amyloidosis.³⁹ Amyloid-targeted PET tracers are quantitative and provide a measure of whole-heart and whole-body amyloid load and can be repeated, making it a potentially promising tool to evaluate response to therapy. Notably, these tracers are the only clinically available tracers to image AL cardiac amyloidosis. ^{123}I -serum amyloid P-component SPECT is used in the United Kingdom for systemic AL amyloidosis imaging, but it does not image cardiac AL amyloidosis and is not available in the United States. Limited whole-body images (^{18}F -florbetapir,⁴⁰ and other tracers) have identified AL amyloid deposits in various organs before clinical suspicion of organ involvement. Importantly, recent data indicate that early cardiac AL amyloid deposits can be identified using ^{18}F -florbetapir⁴¹ (eFig. 18.7) and ^{11}C -Pittsburgh-B-Compound imaging³⁹ before clinically evident changes in cardiac structure (increased LV thickness) or cardiac biomarker release.

Inflammatory Cardiomyopathy: Sarcoidosis

Sarcoidosis is a granulomatous disorder of unknown etiology that affects multiple organs and cardiac involvement is present in approximately 20% to 25% of patients (see Chapter 52).⁷ Women and Black patients are specially predisposed to sarcoidosis.⁷ Sarcoidosis is characterized by focal noncaseating granulomas with multinucleated giant cells and macrophages formed as a result T cell-mediated immune response to an unknown trigger. The granulomas may remain

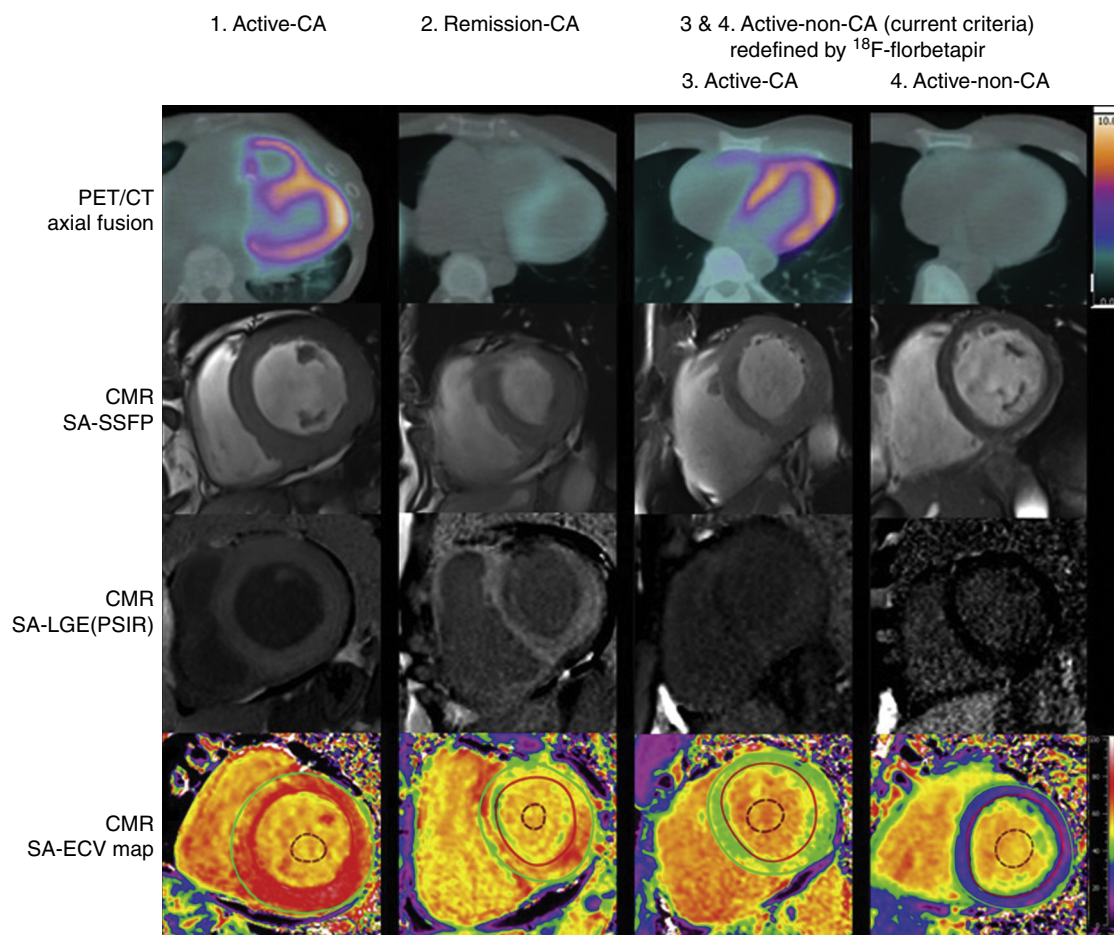


FIGURE 18.7 ^{18}F -florbetapir PET/CT for early detection of light chain cardiac amyloidosis. PET/CT, cardiac magnetic resonance (CMR) (steady-state free precession [SSFP]), CMR (late gadolinium enhancement [LGE], phase sensitive inversion recovery [PSIR]), and CMR (extracellular volume [ECV]) images of patients with active cardiac amyloidosis (CA) (positive cardiac biomarkers), remission (prior cardiac amyloidosis and bone marrow in remission), and active noncardiac amyloidosis (systemic light chain amyloidosis without cardiac involvement by conventional criteria, normal wall thickness, and normal cardiac biomarkers). ^{18}F -florbetapir PET/CT identified early cardiac amyloid deposition (column 3). SA, short axis. (From Cuddy SAM, et al. Improved quantification of cardiac amyloid burden in systemic light chain amyloidosis: redefining early disease? JACC Cardiovasc Imaging 2020;13:1325-1336.)

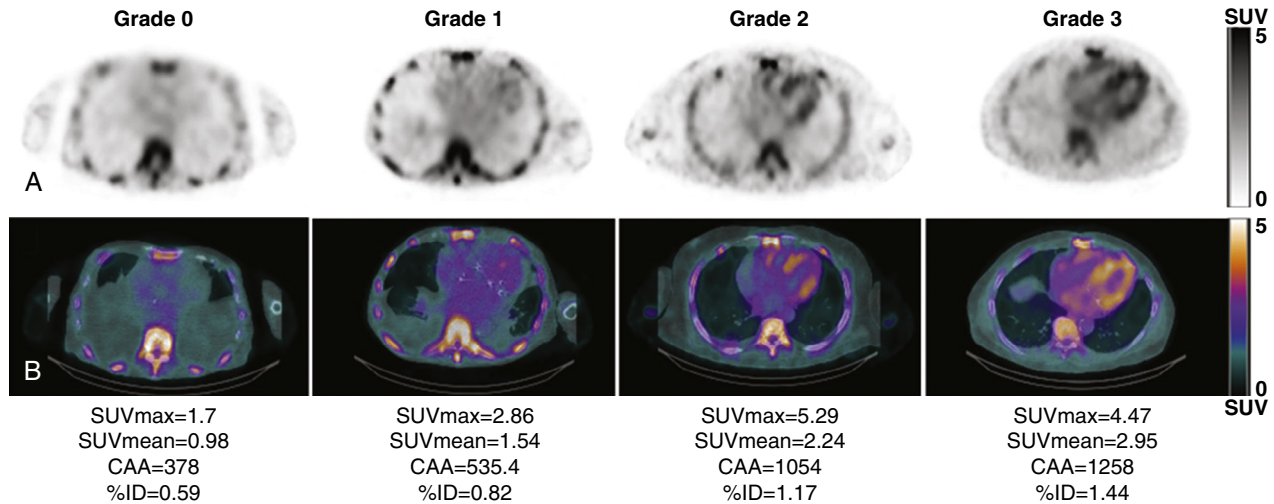


FIGURE 18.35 Quantification of ^{99m}Tc -PYP uptake. Selected cross-sectional ^{99m}Tc -PYP SPECT (A) and fused SPECT/CT (B) images of the chest illustrating visual grades of PYP uptake and their corresponding absolute quantitative metrics including standardized uptake value (SUV), cardiac amyloid activity (CAA), and percentage injected dose (%ID). (From Dorbala S, et al. Absolute quantitation of cardiac (^{99m}Tc)-pyrophosphate using cadmium zinc telluride-based SPECT/CT. *J Nucl Med* 2020;62:716-722.)

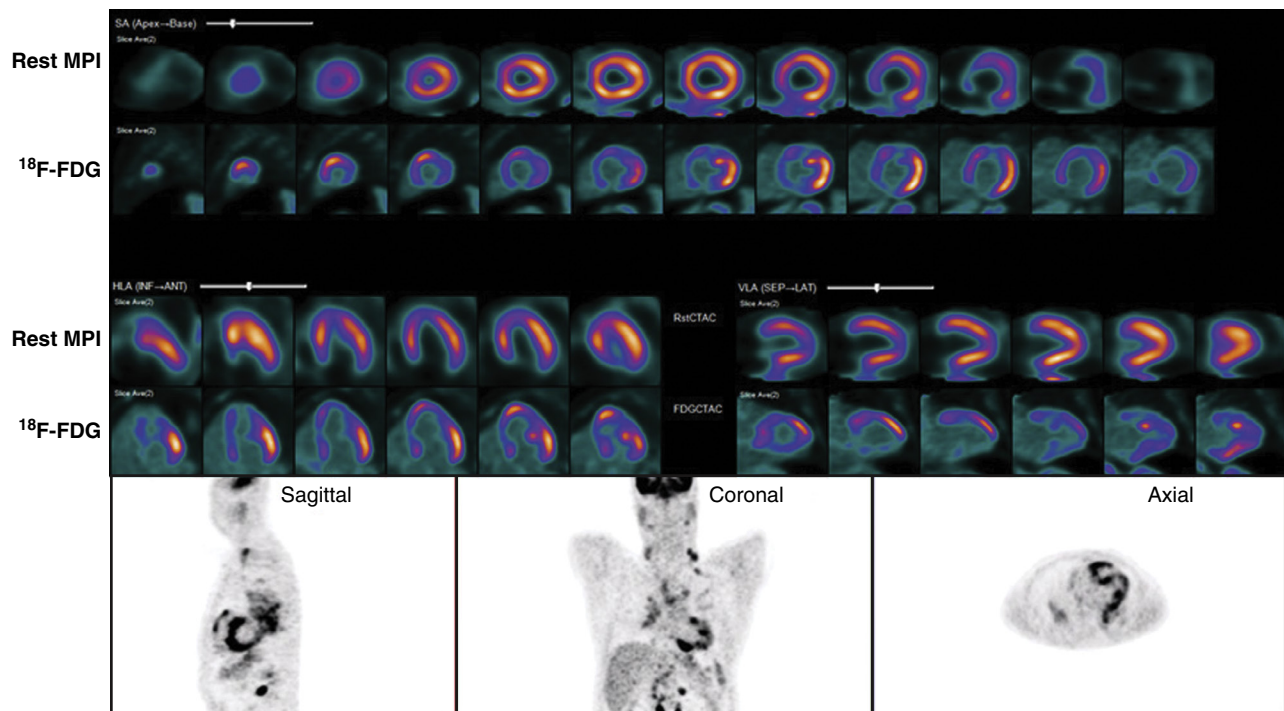


FIGURE 18.36 ^{18}F -FDG PET/CT in a patient with suspected cardiac sarcoidosis. Rest ^{99m}Tc -sestamibi SPECT/CT and ^{18}F -FDG PET/CT scan of a 43-year-old man with progressive dyspnea, prominent hilar lymphadenopathy on chest CT scan, and patchy subepicardial regions of late gadolinium enhancement involving the mid to basal inferoseptal wall of the left ventricle and the right ventricular (RV) free wall in the region of the RV outflow tract on cardiac magnetic resonance imaging (not shown). PET scan demonstrates multiple focal regions of intense myocardial uptake including the apical anteroseptal and mid and basal lateral walls (maximum standardized uptake value [SUVmax]: 7.3). There is also moderate RV uptake. In addition, there are multiple intensely ^{18}F -FDG-avid supraclavicular, mediastinal, and right-sided internal mammary lymph nodes (SUV max: 11.2). The perfusion images show a small perfusion defect in the basal inferoseptal wall without corresponding ^{18}F -FDG uptake (matched reduction in perfusion and metabolism ^{18}F -) consistent with myocardial scar. His left ventricular ejection fraction was 60%. The volume of inflamed myocardium (using an SUV threshold of 2.7) was 77 cc. Endomyocardial biopsy confirmed nonnecrotizing granulomas with focal granulomas consistent with sarcoidosis.

actively inflamed, resolve spontaneously, or progress to a fibrotic phase. Patients can be asymptomatic or present with syncope, sudden death, heart block, atrial or ventricular tachyarrhythmias, and heart failure (Fig. 18.36). RV endomyocardial biopsy has a low yield because of frequent sampling errors given the focal nature of the cardiac sarcoidosis most frequently affecting the left ventricle. Most importantly, any given patient may harbor active granulomas, healing granulomas, or scar and a biopsy with blind sampling may underestimate the burden and variety of pathologies in cardiac sarcoidosis. CMR and PET imaging play a critical role in the clinical diagnosis of cardiac sarcoidosis (Figs. 18.36 and 18.37; see Fig. 19.12).⁷ The diagnostic criteria for cardiac sarcoidosis are shown in Table 18.6.

^{18}F -FDG PET imaging has a significant advantage over endomyocardial biopsy in identifying cardiac and systemic involvement, identifying extracardiac sites for biopsy, and facilitating the evaluation of response to anti-inflammatory therapy. CMR is typically the first test when cardiac sarcoidosis is suspected with specific features that may suggest sarcoidosis (see Chapter 19). However, the presence of late gadolinium enhancement does not differentiate fibrosis from active inflammation, and T2-weighted edema signal is insensitive to diagnose active cardiac sarcoidosis. Currently, the only clinical test to image myocardial inflammation is ^{18}F -FDG PET, which is used when CMR is positive, unavailable, contraindicated, or inconclusive. ^{18}F -FDG PET is necessary, even when CMR is positive, to guide the potential need of anti-inflammatory therapy (Fig. 18.38).

TABLE 18.6 Criteria to Diagnose Cardiac Sarcoidosis

JAPANESE MINISTRY OF HEALTH AND WELFARE (JMHWW)	HEART RHYTHM SOCIETY (HRS)
Histologic Diagnosis Group	Histologic Diagnosis From Myocardial Tissue
CS confirmed by EMB, and histologic or clinical diagnosis of extracardiac sarcoidosis	Noncaseating granulomas on EMB with no alternative cause identified
Clinical Diagnosis Group	Clinical Diagnosis
Histologic or clinical diagnosis of extracardiac sarcoidosis AND	Probable diagnosis of CS exists IF
Two or more major criteria OR	There is histologic diagnosis of extracardiac sarcoidosis* AND
One major criterion and two or more minor criteria	One or more of the following is present
Major Criteria	Major Criteria
Advanced atrioventricular block	Cardiomyopathy or atrioventricular block responsive to immunosuppressive treatment*
	Unexplained reduced LVEF (<40%)
Basal thinning of intraventricular septum	Unexplained ventricular tachycardia
67-Ga uptake in heart	Mobitz II second- or third-degree heart block
Depressed LVEF (<50%)	¹⁸ F-FDG uptake on cardiac PET consistent with CS*
Minor Criteria	Minor Criteria
Electrocardiography: ventricular tachycardia, PVCs, RBBB, abnormal axis, abnormal Q wave	Late gadolinium enhancement on cardiac MRI consistent with CS
Echocardiography: structural or wall motion abnormality	Cardiac 67-Ga uptake AND
Nuclear medicine: perfusion defect, 201Tl, 99mTc*	Exclusion of other causes of cardiac manifestations
Cardiac MRI: late gadolinium enhancement	
EMB: moderate fibrosis or monocyte infiltration	

*Significant difference between Japanese Ministry Health Welfare and Heart Rhythm Society criteria.
 FDG, Fluorodeoxyglucose; LVEF, left ventricular ejection fraction; MRI, magnetic resonance imaging; PVC, premature ventricular contractions; RBBB, right bundle branch block; CS, cardiac sarcoidosis; EMB, endomyocardial biopsy; Ga, gallium; Tl, thallium; Tc, technetium.
 From Chareonthaitawee P, et al. Joint SNMMI-ASNC expert consensus document on the role of (18)F-FDG PET/CT in cardiac sarcoid detection and therapy monitoring. J Nucl Cardiol 2017;24:1741-1758.

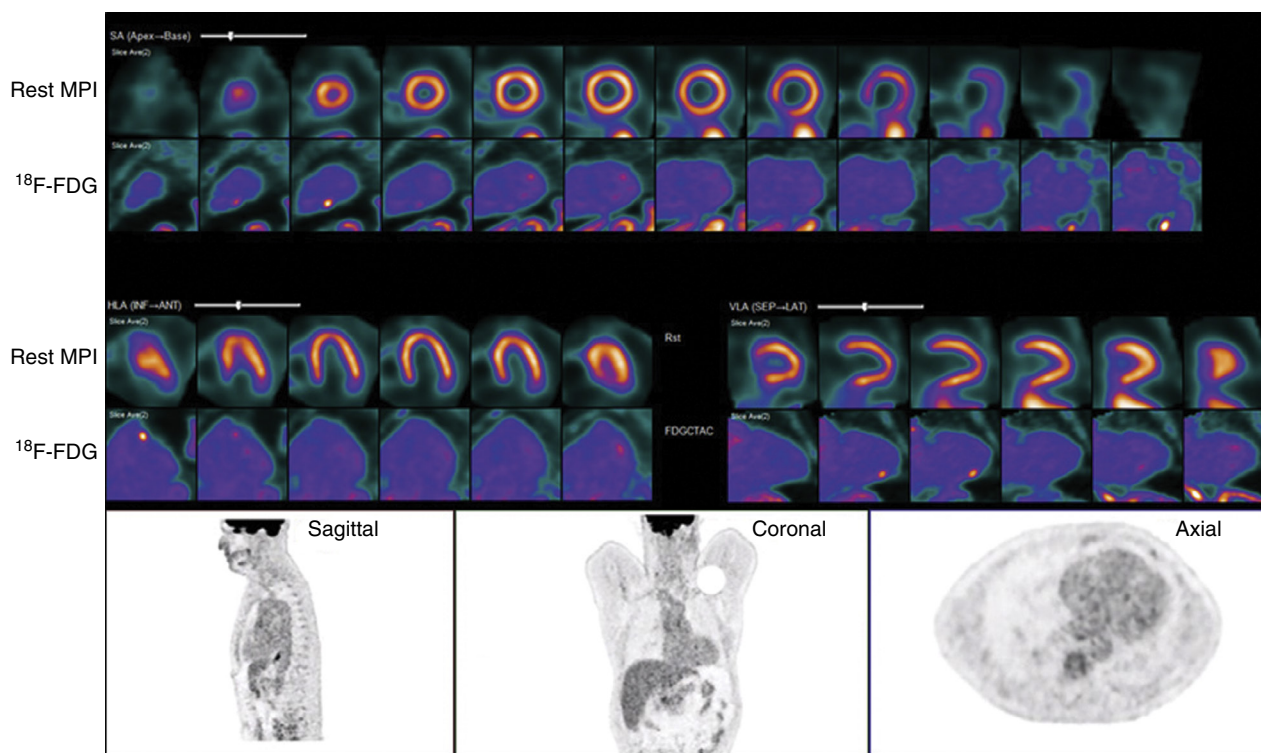


FIGURE 18.37 ¹⁸F-FDG PET/CT to assess treatment response in cardiac sarcoidosis. Follow-up PET images of the patient described in Fig. 18.36 after 6 months of anti-inflammatory therapy showed complete resolution of myocardial and extracardiac ¹⁸F-FDG uptake. The severe perfusion defect in the basal inferoseptal wall remained unchanged and consistent with focal myocardial scarring.

^{18}F -FDG PET uptake in the heart, however, is not specific for sarcoidosis and can represent normal myocardium, inflamed myocardium, malignancy, or hibernating myocardium. Hence the ^{18}F -FDG PET scan is performed with a special diet of low-carbohydrate and high-fat meals for 24 hours before the test followed by prolonged fasting of at least 12 hours.⁷ A myocardial perfusion scan is performed in conjunction with the ^{18}F -FDG PET study to identify areas of myocardial scar or burned out cardiac sarcoidosis. In patients with intracardiac devices, both attenuation-corrected, and non-attenuation-corrected images are interpreted to avoid artifactual focal uptake of ^{18}F -FDG in the regions with the metallic leads. Fig. 18.12 summarizes the typical patterns of myocardial perfusion and ^{18}F -FDG imaging in cardiac sarcoidosis.

^{18}F -FDG PET plays an important role in the evaluation and management of cardiac sarcoidosis. In relation to the Japanese Ministry

of Health and Welfare criteria or Japanese Heart Rhythm Society criteria, ^{18}F -FDG PET is highly sensitive and specific to diagnose cardiac sarcoidosis. In a meta-analysis, pooled sensitivity was 89% and pooled specificity was 78%. As ^{18}F -FDG PET may be more sensitive than the Japanese ministry criteria, the reference used in these meta-analyses, these estimates may be biased.⁷ Also, ^{18}F -FDG PET provides significant prognostic value. Among patients with known or suspected sarcoidosis, the presence of myocardial perfusion defects and focally increased ^{18}F -FDG uptake in the left and/or right ventricles are high-risk markers (Fig. 18.39).⁴² ^{18}F -FDG is performed at baseline before initiation of immunosuppressive therapy and to monitor response to therapy (see Fig. 18.37).⁴³ Quantitative ^{18}F -FDG PET imaging using SUV, volume of inflamed myocardium using an SUV threshold, and target to background ratio (myocardium to left atrium or blood pool ratio) are usually included in the evaluation of the response to therapy.^{43,44}

Infective Endocarditis

Infective endocarditis is a multisystem acute inflammatory/infectious disease that is increasing in prevalence and is associated with a very high mortality (see Chapter 80). Echocardiography, particularly transesophageal echocardiography (TEE), plays a central role in the evaluation and management of patients with infective endocarditis. However, as echocardiography is not tomographic and does not image the whole body, it is limited in evaluating complications of endocarditis. It is also limited in prosthetic valve/device/implanted prosthetic material infection caused by artifact from the prosthetic material.

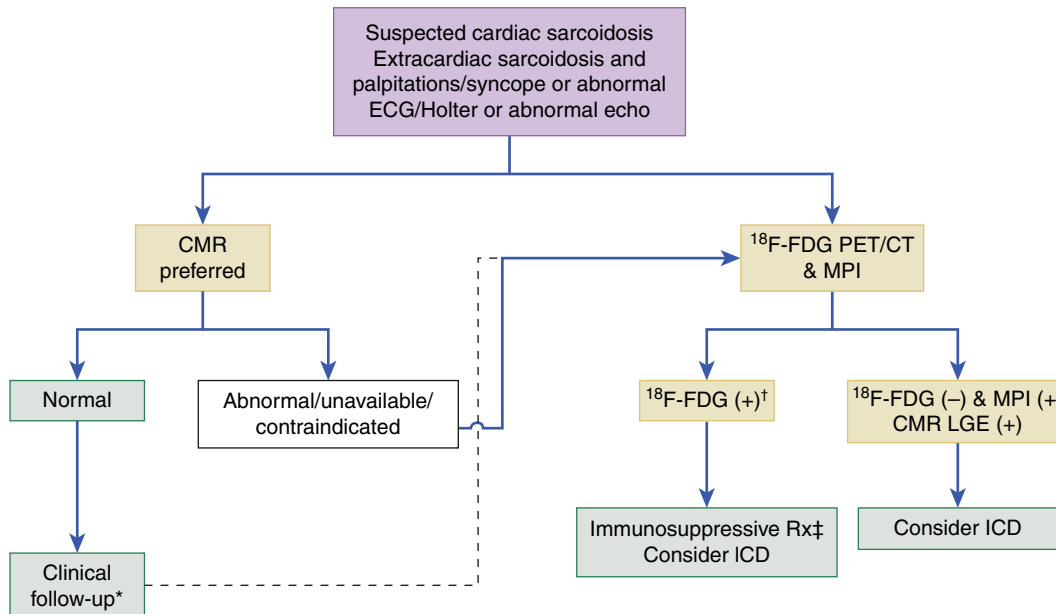


FIGURE 18.38 Role of ^{18}F -FDG PET/CT in sarcoidosis. This flowchart illustrates the role of ^{18}F -FDG PET in the evaluation of patients with suspected cardiac sarcoidosis. *High clinical suspicion. †Identifies coexistent inflammation. Immunosuppressive Rx may be considered, taking into account the amount of inflammation. CMR, Cardiac magnetic resonance imaging; ICD, implantable cardioverter defibrillator; MPI, myocardial perfusion imaging.

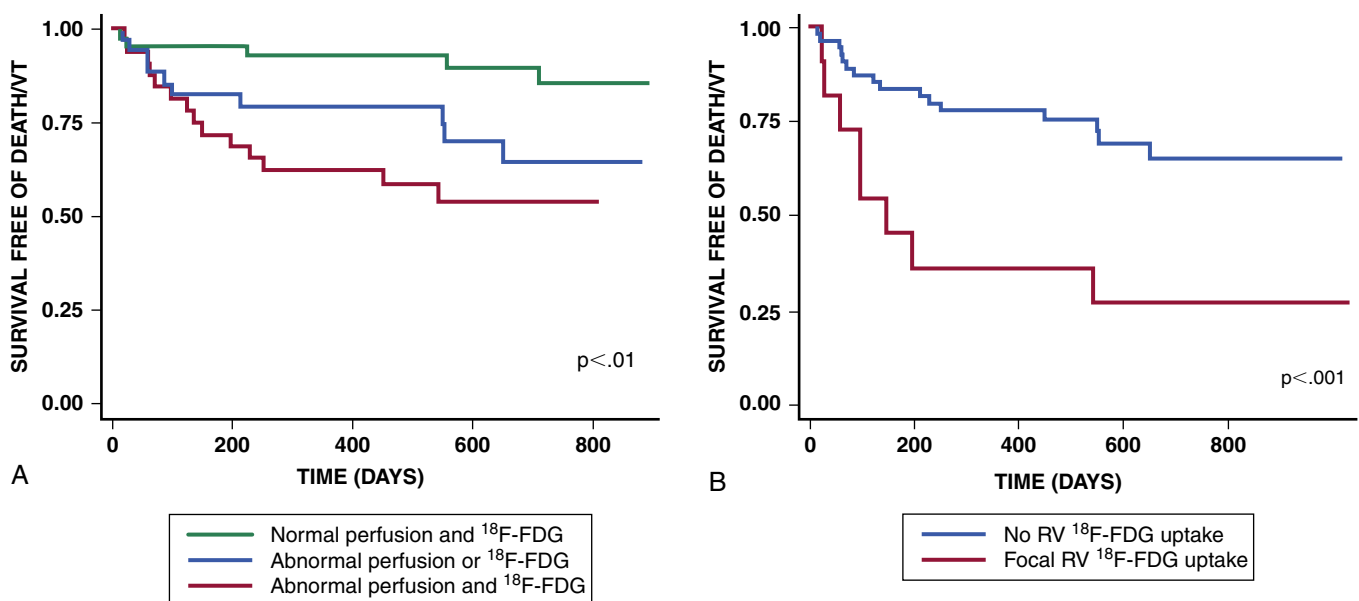
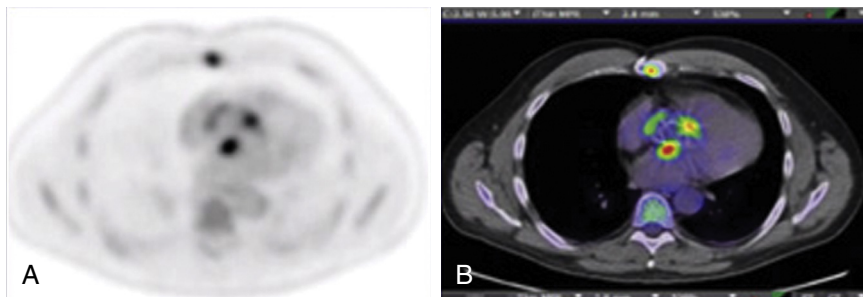
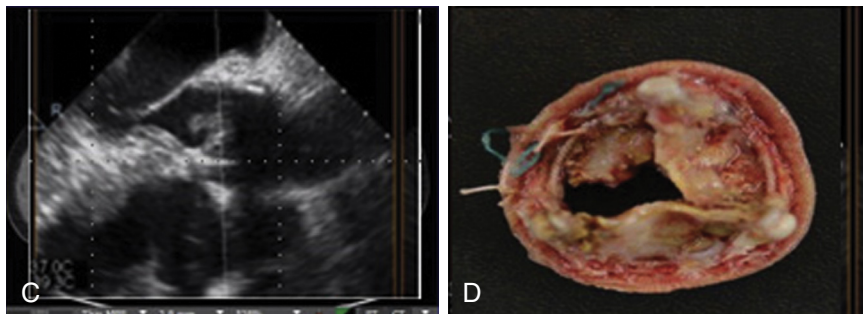


FIGURE 18.39 Prognostic value of ^{18}F -FDG PET/CT in cardiac sarcoidosis. Event-free survival of different patterns of ^{18}F -FDG uptake in the left ventricular (A) and right ventricular (B) myocardium in patients with known or suspected sarcoidosis referred for ^{18}F -FDG PET/CT. VT, Ventricular tachycardia. (From Blankstein R, et al. Cardiac positron emission tomography enhances prognostic assessments of patients with suspected cardiac sarcoidosis. J Am Coll Cardiol 2014;63:329-336.)

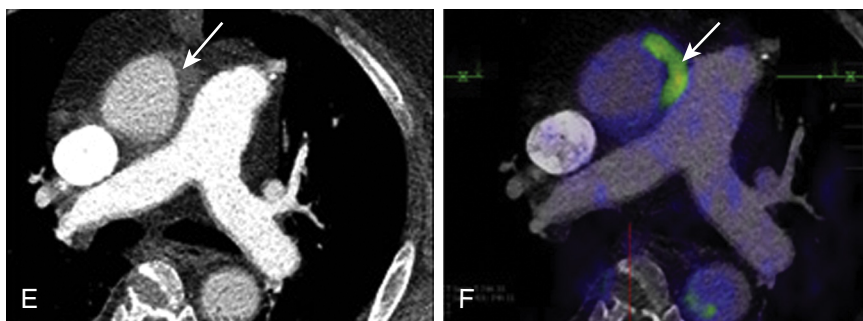
^{18}F -FDG PET/CT in prosthetic valve endocarditis



TEE and explanted valve with endocarditis



Value of contrast cardiac CT



^{18}F -FDG: Septic emboli

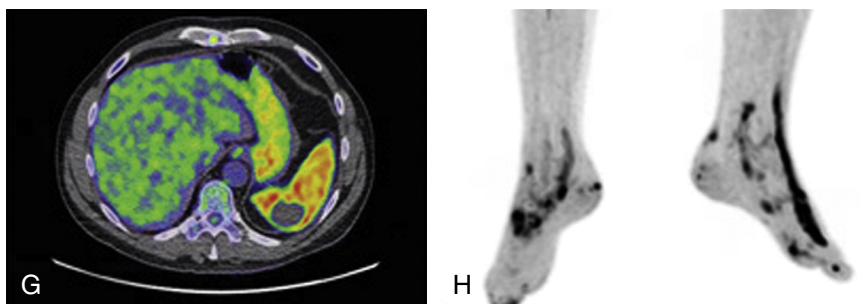


FIGURE 18.40 ^{18}F -FDG PET/CT and multimodality imaging of infective endocarditis. Images of a 54-year-old man with a history of bioprosthetic aortic valve and aortic root replacement who presented with multiple episodes of transient vision loss and bacteremia with *Cardiobacterium valvarum*. **A** and **B**, Selected axial ^{18}F -FDG PET and fused PET/CT images showing focal FDG uptake in the aortic valve annulus. **C**, Transesophageal echocardiogram (TEE) (120-degree long axis) shows a 1.25 × 1 cm vegetation on the bioprosthetic aortic valve and a thickened aortic root that could represent abscess. **D**, Explanted aortic valve showing valve destruction from endocarditis. **E** and **F**, Selected axial view of a CT angiogram and its corresponding ^{18}F -FDG image at the level of the pulmonary artery bifurcation shows increased soft tissue density around the aortic root (arrow) with increased metabolic activity suspicious for abscess. **G**, Selected axial whole-body ^{18}F -FDG PET image shows a focal region with absent ^{18}F -FDG uptake in the spleen consistent with a splenic infarct, likely embolic. **H**, ^{18}F -FDG images of the feet demonstrate multiple focal areas of uptake consistent with septic emboli.

^{18}F -FDG PET and cardiac CTA are emerging as important adjuncts to echocardiography to identify complications of endocarditis, prosthetic valve/device infection, and systemic embolization (Fig. 18.40). Contrast-enhanced CT along with ^{18}F -FDG PET enhances the evaluation of complications from infective endocarditis. In a recent study, the combination of ^{18}F -FDG PET and cardiac CTA yielded higher diagnostic performance compared with ^{18}F -FDG PET/CT alone (Fig. 18.41).⁴⁵ ^{18}F -FDG PET is also a useful method to image response to therapy in patients in whom removal of the infected prosthetic material is not feasible (e.g., conduits or descending aortic stents). As with sarcoidosis imaging, patients must be adequately prepared with a high-fat/low-carbohydrate diet and undergo dedicated cardiac imaging followed by whole-body imaging to delineate possible sites of septic embolization. Nonspecific ^{18}F -FDG uptake can be seen after surgery. The presence of focal (as opposed to diffuse) and intense radiotracer uptake is consistent with infection. Images are reconstructed with and without

attenuation correction. As with sarcoidosis, non-attenuation-corrected ^{18}F -FDG emission images are also reviewed in patients with mechanical heart valves and metallic cardiovascular implantable electronic devices to ensure that any focal uptake seen on the attenuation-corrected images does not represent an artifact from overcorrection of attenuation from a metallic object.

The incremental diagnostic value of ^{18}F -FDG PET for prosthetic valve and native valve endocarditis, intracardiac device infection, and LV-assist device infection was studied by several investigators⁴⁶ and summarized in a recent systematic review.⁴⁷ In addition, a recent study demonstrated the prognostic value of ^{18}F -FDG PET/CT. In this study, 173 patients with native ($n = 64$) or prosthetic valve ($n = 109$) endocarditis were followed for a mean of 225 days for major cardiac events (in hospital and 1-year death, recurrent infective endocarditis, unscheduled cardiovascular hospitalization, and new embolic events on antibiotics). MACE occurred in 94 patients, and on multivariable

analysis, C-reactive protein level ≥ 100 mg/L, a positive ^{18}F -FDG PET/CT, and a moderate to intense ^{18}F -FDG PET/CT valvular uptake remained independently associated with MACE. This study showed that moderate to severe ^{18}F -FDG uptake associated with predictive of new embolic events within the first year after diagnosis of infective endocarditis (hazard ratio [HR] 7.5; 95% confidence interval [CI]: 1.2 to 45.2; $P = 0.03$).⁴⁸ The 2015 European Society of Cardiology (ESC) guidelines on infective endocarditis⁴⁹ included an abnormal ^{18}F -FDG PET/CT (abnormal ^{18}F -FDG activity around the site of the prosthetic valve implantation detected by PET/CT only if prosthesis was implanted >3 months prior), or radiolabeled leukocyte SPECT/CT, or cardiac CT showing a definite paravalvular lesion as major criterion for infective endocarditis. In the ESC guidelines,⁴⁹ ^{18}F -FDG PET or leukocyte-labeled SPECT/CT was also indicated for cases with possible/rejected infective endocarditis with high clinical suspicion for prosthetic valve endocarditis. A recent algorithmic approach to the evaluation of infective endocarditis proposes using ^{18}F -FDG PET/CT after a positive or nondiagnostic TEE study, a positive cardiac CTA study, and a positive white blood cell scintigraphy study.⁴⁷

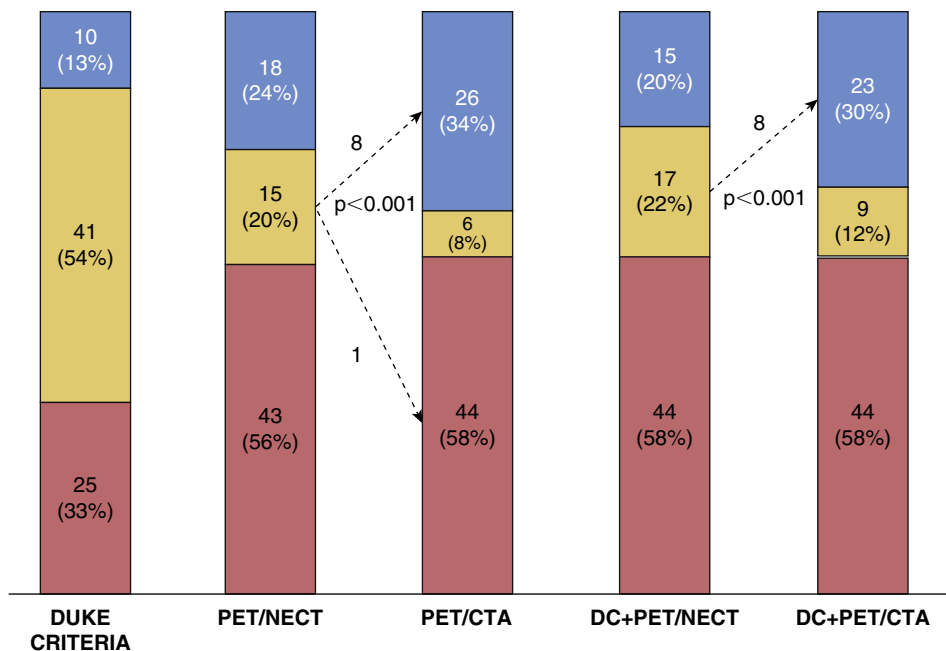


FIGURE 18.41 Value of ^{18}F -FDG PET/CTA in diagnosis of infective endocarditis. This stacked bar graph demonstrates the incremental value of ^{18}F -FDG PET/CTA over modified Duke criteria to enhance diagnostic certainty in patients with suspected prosthetic valve or cardiac device infection. (From Pizzi MN, et al. Improving the diagnosis of infective endocarditis in prosthetic valves and intracardiac devices with ^{18}F -fluorodeoxyglucose positron emission tomography/computed tomography angiography: initial results at an infective endocarditis referral center. *Circulation* 2015;132:1113-1126.)

Radionuclide Imaging in Vasculitis

Vasculitis can be challenging to diagnose. The initial evaluation in patients with suspected vasculitis typically includes clinical history and serum biomarkers, followed by anatomic assessment of vascular involvement by ultrasound, MRA, CTA or invasive angiography, and ^{18}F -FDG PET/CT imaging (see Chapters 43 and 97). The clinical manifestations of vasculitis and serum biomarker changes are usually nonspecific. A positive vascular biopsy is usually confirmatory but limited by false-negatives. Imaging plays a central role in the diagnosis and management of vasculitis. Anatomic imaging methods identify wall thickening, thrombus, luminal stenosis, and aneurysms, which typically represent advanced disease manifestations that may not be reversible.⁶⁷ Gallium-SPECT and radiolabeled white blood cell scans are obsolete because of poor sensitivity. ^{18}F -FDG PET/CT is the test of choice to ascertain the presence of inflammation in large-vessel vasculitis (Fig. 18.42).⁵⁰ Moreover, ^{18}F -FDG PET/CT can guide the most appropriate site of biopsy, identify disease at an inflammatory stage where it may be more amenable to therapy, and can quantify the extent and severity of inflammation that is useful in the evaluation of response to anti-inflammatory therapy. Typically, ^{18}F -FDG PET/CT is used in conjunction with MRA or CTA to evaluate the anatomic abnormalities from the vasculitis.

As with cardiac sarcoidosis, ^{18}F -FDG PET/CT for vasculitis is often performed after a high-fat, low-carbohydrate diet for 24 hours, especially for evaluation of the aortic root. Whole-body images are obtained a minimum of 90 minutes after injection of radiotracer. ^{18}F -FDG is interpreted visually in relation to liver uptake as grade 0 = no vascular uptake (\leq mediastinum), grade 1 = low-grade uptake ($<$ liver), grade 2 = vascular uptake = liver, and grade 3 = vascular uptake $>$ liver uptake.⁵⁰ Grade 0 (no uptake) or grade 1 (low-grade uptake) are considered negative for vasculitis, grade 2 (intermediate-grade uptake) is possible vasculitis, and grade 3 (high-grade uptake) is considered positive for vasculitis. In conjunction with magnetic resonance imaging (MRI) images, the vasculitis patterns can be classified as normal (both MRI and PET normal), inflammatory (PET uptake $>$ liver uptake and abnormal MRI), and fibrous (abnormal MRI, but PET uptake \leq liver uptake). Target to background SUV ratios (vessel to blood pool ratio) are used for quantitative evaluation.⁵⁰

^{18}F -FDG PET/CT has a pooled sensitivity and specificity of 90% and 98% for diagnosis of giant cell arteritis, and a pooled sensitivity and specificity of 80% and 89%, respectively, for the diagnosis of Takayasu arteritis.⁵⁰ Sensitivity of ^{18}F -FDG PET/CT to detect inflammation may be

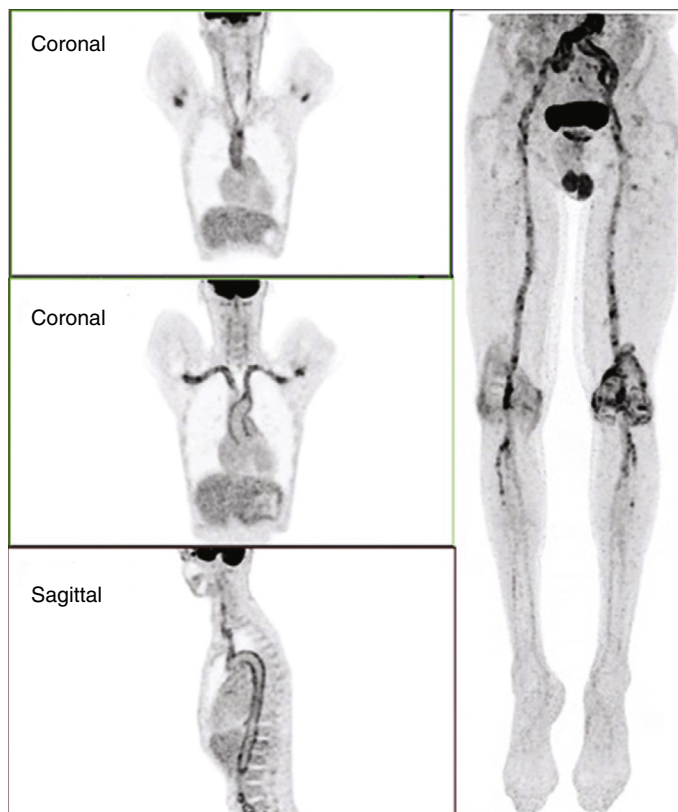


FIGURE 18.42 ^{18}F -FDG PET/CT imaging in large-vessel vasculitis. Selected ^{18}F -FDG PET images of a 69-year-old man with a history of ulcerative colitis and polymyalgia rheumatica presenting with night sweats and weight loss. CT angiography showed diffuse circumferential wall thickening of the aorta and main branches (images not shown). The PET images show intense ^{18}F -FDG uptake in the thoracic and abdominal aorta and subclavian, carotid, and femoral arteries bilaterally, consistent with large-vessel vasculitis. Giant cell arteritis was excluded and he was started on oral prednisone 60 mg/day with a reduction in C-reactive protein and erythrocyte sedimentation rate.

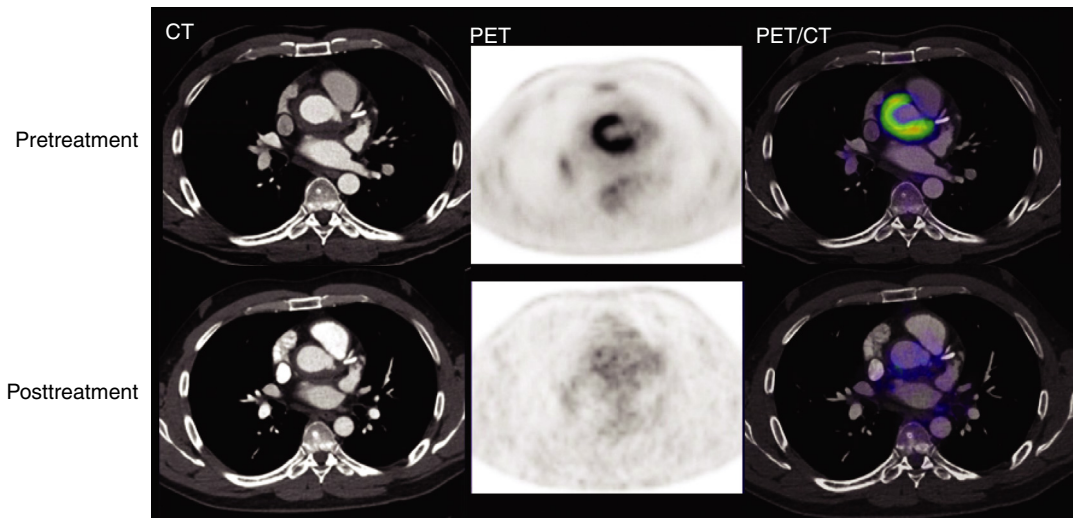


FIGURE 18.43 ^{18}F -FDG PET/CT imaging to assess response to therapy in aortitis. Selected axial chest CT angiograms (CTAs) (left), ^{18}F -FDG PET (middle), and fused CTA and ^{18}F -FDG PET images (right) of a patient with Behçet disease. Pretreatment images (top row) show peri-aortic thickening on the CT images with near circumferential intense ^{18}F -FDG uptake consistent with inflammation. Posttreatment scans (bottom row) demonstrate persistent wall thickening on the CT images, but near complete resolution of ^{18}F -FDG uptake indicating excellent response to therapy.

reduced after more than 3 days of glucocorticoid therapy.⁵⁰ ^{18}F -FDG offers the advantage to demonstrate change after successful immunosuppressive therapy (Fig. 18.43), whereas anatomic imaging methods may be limited as they may continue to demonstrate vessel wall abnormalities even in the fibrotic phase of vasculitis. However, the definitive role of ^{18}F -FDG to evaluate longitudinal disease course and response to therapy remains unclear, with some studies indicating decreased ^{18}F -FDG uptake after therapy and other studies finding no difference in relapsing and nonrelapsing patients.⁵⁰ In addition to large-vessel vasculitis, comprising giant cell arteritis and Takayasu arteritis, ^{18}F -FDG PET/CT can also be helpful in diagnosing and monitoring response to therapy in aortitis, Behçet disease, and IgG4-related disease.

Cardio-Oncology

Radionuclide imaging can be used to evaluate possible cardiovascular complications from chemotherapy and radiotherapy in patients with cancer (see Chapters 56 and 57). The incidence and prognosis of cardiotoxicity from cancer therapy can vary depending on the age at treatment, sex, agent(s) used, cumulative dose, concomitant treatment with other cardiotoxic therapies, and other factors, including underlying cardiovascular risk factors. There are several other forms of cardiotoxicity associated with cancer therapy including ventricular dysfunction, CAD, hypertension, myocarditis, valvular heart disease, pericardial disease, venous thromboembolic disease, arrhythmias, and conduction system abnormalities. Additionally, neoplasms can involve the heart as primary cardiac tumors, or as a site of metastases. The following is a brief description of the most common applications of radionuclide imaging in patients undergoing cancer treatment or in cancer survivors.

Assessment of Ventricular Function

The American Society of Clinical Oncology recommends assessment of LVEF at baseline in all patients who meet criteria for increased risk with reassessment within 1 year of completing anthracycline therapy. Patients at increased risk for ventricular dysfunction and heart failure include those receiving high-dose anthracycline therapy (e.g., doxorubicin ≥ 250 mg/m²); those receiving concomitant high-dose radiation therapy (≥ 30 Gy) with the heart in the treatment field; those receiving lower-dose anthracycline therapy in combination with lower-dose radiation therapy where the heart is in the field; those receiving lower-dose anthracycline or trastuzumab therapy alone and have any of the following risk factors including ≥ 2 cardiovascular risk factors, age ≥ 60 , or known cardiovascular disease; and those receiving treatment with lower-dose anthracycline followed by trastuzumab.⁵¹ The guideline

recommends discontinuation of doxorubicin if there is an absolute decrease in LVEF of $\geq 10\%$ from baseline to $\leq 50\%$.

Although echocardiography is currently the modality of choice for baseline and serial assessment of LV function in patients with cancer, gated blood pool scanning (also known as equilibrium radionuclide angiography) can also be used to determine regional and global LV function. The technique consists of radiolabeling the patient's own red blood cells, which are then re-injected for imaging. For a full description of the technique, please refer to the SNMMI Procedure Standard.⁵² Briefly, there are two methods for labeling the red blood cells: (1) *in vivo* or modified *in vivo/in vitro* methods (e.g., using 2 to 3 mg stannous pyrophosphate 15 minutes before injection of $^{99\text{m}}\text{Tc}$) and (2) commercial *in vitro* kit, which is the most commonly used. Radiolabeled blood cells are then re-injected and, after 1 to 2 minutes, ECG-gated equilibrium blood pool imaging is obtained with planar or SPECT imaging. End-diastolic and end-systolic volumes are then measured to calculate LVEF.

Evaluation of Coronary Artery Disease

CAD, a frequent comorbid illness in patients diagnosed with cancer, has increased in prevalence in cancer survivors as this population continues to live longer, and is a known form of cardiotoxicity of several cancer therapies.⁵³ Radiation therapy in particular has been associated with an increased risk of obstructive CAD. Because of this, guidelines recommend functional stress testing for the evaluation of obstructive CAD 5 to 10 years after exposure in high-risk patients, even if they are asymptomatic (e.g., lymphoma). Radiation therapy with the heart in the treatment field remains the cancer therapy associated with the highest risk for development of CAD. The risk of radiation-associated CAD increases linearly with mean radiation dose to the heart, with no apparent threshold. MPI with SPECT or PET is commonly used for this application similar to that described previously for noncancer patients. An advantage of PET is its ability to quantify myocardial blood flow and flow reserve, which increases the sensitivity for detection of myocardial ischemia.

Evaluation of Primary or Metastatic Cardiac Neoplasms

Cardiac neoplasms are rare and multimodality imaging plays a critical role in the evaluation and management of these patients. Although CMR is the modality of choice for the evaluation of cardiac masses, ^{18}F -FDG PET/CT can be helpful in the evaluation of both primary malignancies and metastatic disease to the heart. Imaging with ^{18}F -FDG PET to identify metabolically active tissue and integrated anatomic assessment with CT can provide useful diagnostic information and help plan therapeutic interventions such as surgical resection.

MACHINE LEARNING AND ARTIFICIAL INTELLIGENCE

Machine learning and artificial intelligence applications are transforming several aspects of cardiology and cardiovascular imaging (see [Chapter 11](#)). The use of artificial intelligence in nuclear cardiology can be applied to image processing, enhancement of image quality, image interpretation, and risk assessment. Machine learning approaches integrating imaging data with the vast amounts of clinical and stress data have been shown to improve diagnosis, risk assessment, and management of ischemic heart disease. The REFINE SPECT registry included high-efficiency solid-state CZT SPECT scanner MPI data with follow-up data for prognosis from 5 medical centers on 20,418 patients, and diagnostic data (patients without known CAD, MI, or coronary revascularization and with invasive coronary angiography) on 2079 patients from 9 centers. In one study from this registry, deep learning improved the identification of obstructive CAD⁵⁴ compared with conventional semiquantitative visual interpretation. In another analysis from this registry, a score developed from machine learning methods accurately predicted in which patients a rest MPI could be safely canceled.⁵⁵ Machine learning including clinical and imaging data demonstrated high accuracy for predicting 3-year risk of MACE and was superior to machine learning–based evaluation of imaging or conventional measures of stress or ischemic perfusion defects alone ([eFig. 18.8](#)).⁵⁶

TRANSLATIONAL MOLECULAR IMAGING

Cardiovascular molecular imaging is a cutting-edge field with several exciting translational research applications, some of which are discussed in the following section.

Peripheral Arterial Disease

PAD is prevalent and associated with high morbidity and mortality. (see [Chapter 43](#)). Conventional approaches to diagnosis of PAD including the ankle-brachial index (ABI) and angiography (invasive and noninvasive) can only assess the extent and severity of macrovascular atherosclerosis. There is growing recognition that microvascular abnormalities in PAD contribute to patient symptoms and portend adverse clinical outcomes including wound healing, infection, and limb amputation. However, microvascular abnormalities and associated skeletal muscle remodeling are poorly captured by standard diagnostic modalities. Radionuclide imaging with SPECT and PET provide accurate, quantitative assessments of the integrated effects of macrovascular and microvascular abnormalities on skeletal muscle perfusion, thereby complementing angiographic information.⁵⁷ Beyond skeletal muscle perfusion, radionuclide molecular imaging techniques are emerging as promising tools to evaluate the effects of novel cell-based and gene-based therapies.⁵⁷

Atherosclerosis

By integrating the detailed anatomic information from CT with the high sensitivity of radionuclide imaging to evaluate targeted molecular and cellular abnormalities in the myocardium and vasculature, hybrid imaging may play a key role in shaping the future of molecular diagnostics and therapeutics. One of the areas of greatest research interest has been centered on the evaluation of inflammation within atheroma (see [Chapter 24](#)). Because there is marked heterogeneity in the composition of human atherosclerotic plaques, targeted molecular imaging has been used to characterize the composition of such plaques, thereby allowing the determination of their risk for complications (e.g., erosion and rupture). Such imaging tools provide mechanistic insights into atherothrombotic processes, better risk stratification, optimal selection of therapeutic targets, and the means for monitoring therapeutic responses.

PET/CT is a powerful technique because it is highly sensitive in detecting low quantities of molecularly targeted radiotracers to assess biologic processes involved in atherosclerosis (e.g., inflammation, microcalcification). Although the use of radionuclide imaging in atherosclerosis remains a research tool at the moment, it is an area of very active investigation.

For example, ¹⁸F-FDG PET has been the most commonly applied imaging marker of vascular inflammation. In patients with carotid

disease, ¹⁸F-FDG uptake has been shown to accurately differentiate culprit and high-risk from lower-risk carotid atherosclerotic plaques. A meta-analysis of data from 539 patients in 14 studies showed that ¹⁸F-FDG uptake was significantly higher in culprit carotid arteries than in nonculprit arteries in patients with transient ischemic attack or stroke.⁵⁸ ¹⁸F-FDG is of limited value for imaging atherosclerotic disease activity in the coronary vasculature because under most physiologic conditions the tracer is avidly taken up by the myocardium.

Focus is beginning to shift toward other more specifically targeted PET ligands because of the limitations of plaque imaging using ¹⁸F-FDG.⁵⁹ For example, ¹⁸F-sodium fluoride (NaF) enables the study of vascular calcification resulting from intense plaque inflammation. Because it is not taken up by normal cardiomyocytes, ¹⁸F-NaF has demonstrated superior ability to differentiate high-risk coronary lesions compared with ¹⁸F-FDG.^{60,61} The mitochondrial membrane translocator protein (TSPO) receptor involved in cholesterol transport, immunomodulation, and apoptosis is widely expressed in the body, it is abundant in macrophages, and it has been evaluated in experimental and human atherosclerosis. ⁶⁸Ga-Pentixafor binds to C-X-C chemokine receptor 4 (CXCR4) and is the receptor for CXCL12 and the chemokine macrophage migration inhibitory factor that is expressed in endothelial cells, smooth muscle cells, monocytes, and other leukocytes. In patients with recent MI, ⁶⁸Ga-pentixafor retention was higher in culprit than nonculprit coronary lesions.⁶² Finally, the ⁶⁸Ga-dotatate has also been used to evaluate plaque inflammation. It targets the somatostatin receptor subtype-2 (*SSTR2*), which is overexpressed in activated macrophages and other inflammatory cells. Binding of ⁶⁸Ga-dotatate was demonstrated in CD68-positive macrophage-rich carotid plaque regions and there was a strong correlation between its *in vivo* retention signals and *SSTR2* and *CD68* gene expression.⁶³

Novel PET Perfusion Tracers

¹⁸F-flurpiridaz is a novel ¹⁸F-labeled PET perfusion tracer that binds to mitochondrial complex I, demonstrates rapid myocardial uptake, and has higher extraction than ¹³N-ammonia even at high myocardial blood flow rates.⁶⁴ It is produced by a cyclotron, but because of its long half-life (110 minutes) it can be transported as unit doses to various sites, vastly enhancing access to PET MPI globally. Data from a phase III study demonstrate its superior accuracy in relation to SPECT MPI. In the study, 795 patients (mean age 62.3 ± 9.5 years, 31% women, 55% obese, 71% pharmacologic stress) from 92 sites in the United States and Canada underwent ^{99m}Tc-SPECT, ¹⁸F-flurpiridaz PET, and invasive coronary angiography.⁶⁴ ¹⁸F-flurpiridaz PET MPI was more sensitive to ^{99m}Tc-SPECT MPI in diagnosing ≥50% obstructive CAD (sensitivity 71.9 [95% CI 67.0% to 76.3%] vs. 53.7% [95% CI 48.5% to 58.8%], *p* < 0.001). But its specificity did not meet prespecified criteria of noninferiority (76.2% [95% CI, 71.8% to 80.1%] vs. 86.6% [95% CI, 83.2% to 89.8%], *p* = nonsignificant [NS]). Perfusion defect size, image quality, and radiation dose were better delineated by ¹⁸F-flurpiridaz PET compared with ^{99m}Tc-SPECT MPI ([eFig. 18.9](#)). ¹⁸F-flurpiridaz PET was superior to SPECT in subgroups of women, obese individuals, patients undergoing pharmacologic stress, and in patients with small LV volumes.⁶⁴ Because of its long half-life, exercise PET is feasible and nearly 30% of the patients in the study underwent exercise PET.⁶⁴ A second phase III study is currently underway.

Whole-Body PET Imaging

PET using targeted radiotracers is the most sensitive method for imaging biologic processes. A novel PET scanner that is 194 cm long has been recently developed. This scanner provides high spatial and temporal resolution imaging, rapid imaging of the whole body (<2 minutes), very low radiation dose imaging (<1 mCi), delayed imaging of physiologic processes (10-hour imaging for ¹⁸F-FDG), and whole-body dynamic imaging.⁶⁵ Whole-body coverage allows for real-time tracking of blood flow to the heart and various organs opening novel clinical research applications. Atherosclerosis and several cardiovascular diseases are systemic diseases, and this system offers unprecedented opportunities to study cardiovascular pathophysiology including heart and brain connections. High temporal resolution allows for imaging tracers with short half-lives. The rapid imaging minimizes patient motion and freezes respiratory and cardiac motion further improving spatial resolution of the images. The high-count sensitivity allows for detection of radiotracer for several hours after injection and can provide novel applications to track metabolic processes over a long duration of several hours.⁶⁵ The whole-body PET scanner has transformed cardiovascular molecular imaging with several ongoing research studies ([eFig. 18.10](#)).

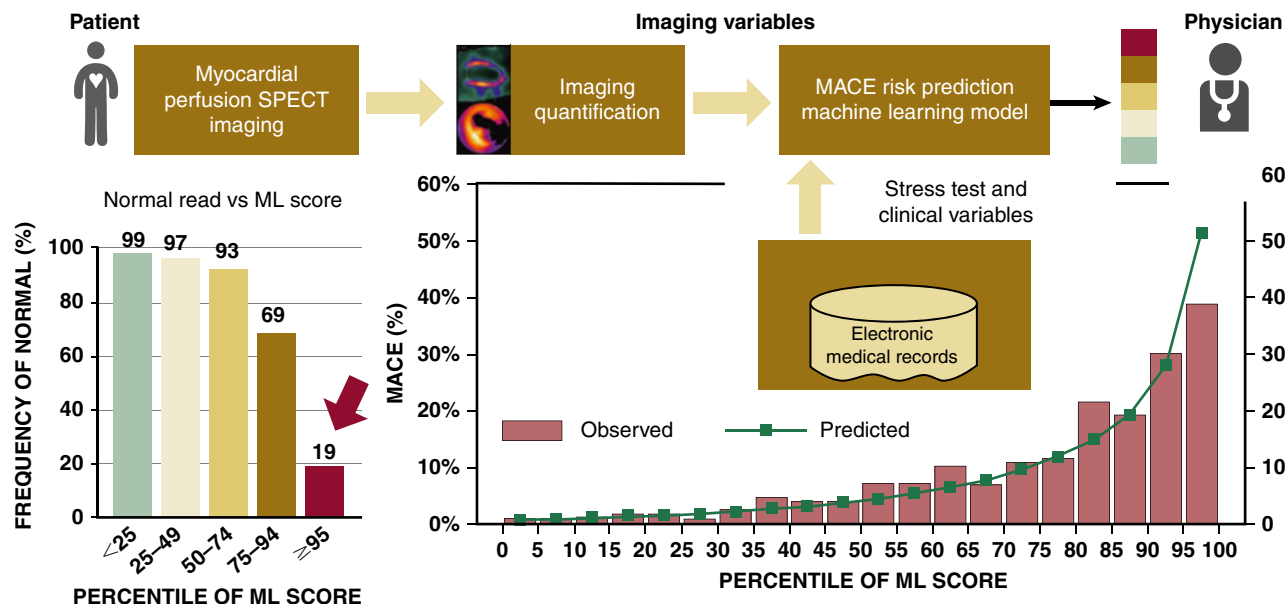


FIGURE 18.8 Machine learning to predict prognosis. Machine learning (ML) models, when combined with patient data, imaging quantification, and clinical data, were accurate in predicting major adverse cardiac events (MACE). Predicted MACE by machine learning methods (green line) very closely tracked observed MACE (pink bars) in this study. Notably, 19% of the patients with a normal scan interpretation were identified by the machine learning algorithm as high risk. (From Betancur J, et al. Prognostic value of combined clinical and myocardial perfusion imaging data using machine learning. *JACC Cardiovasc Imaging* 2018;11:1000-1009.)

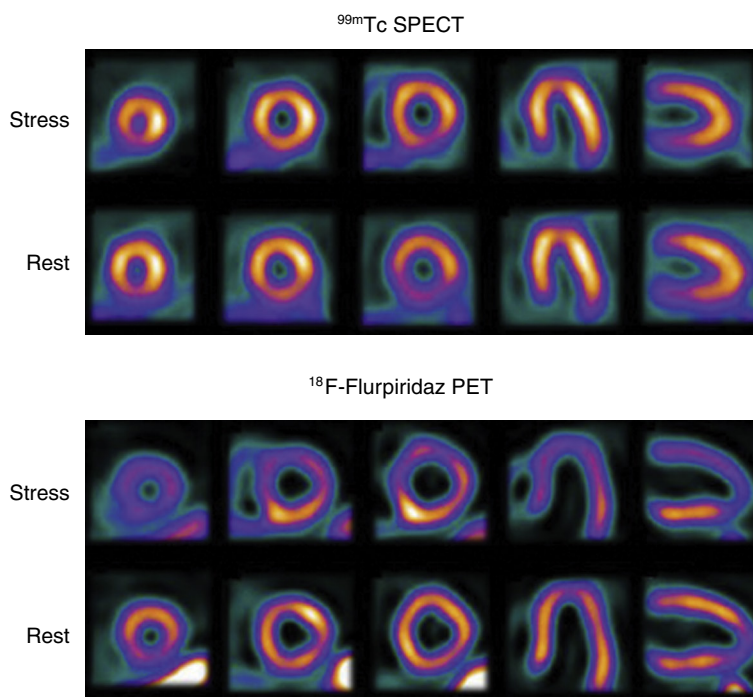
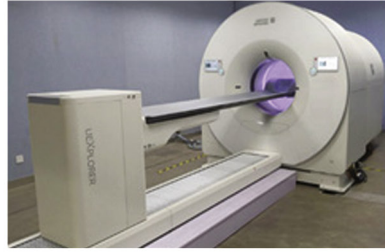
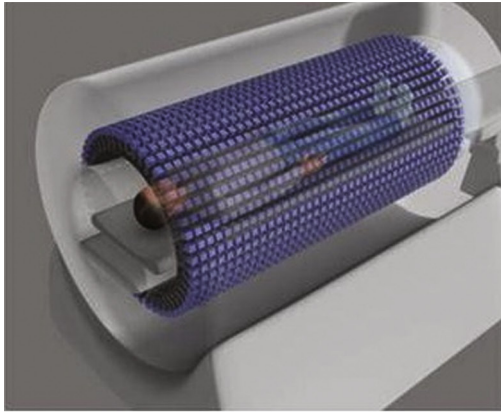
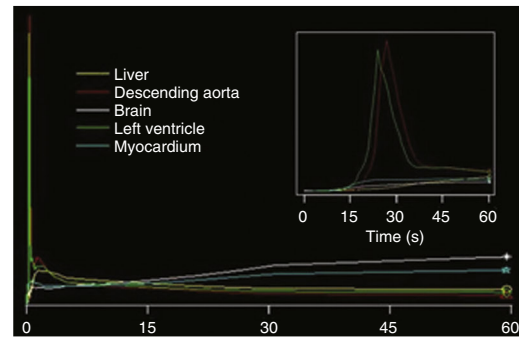
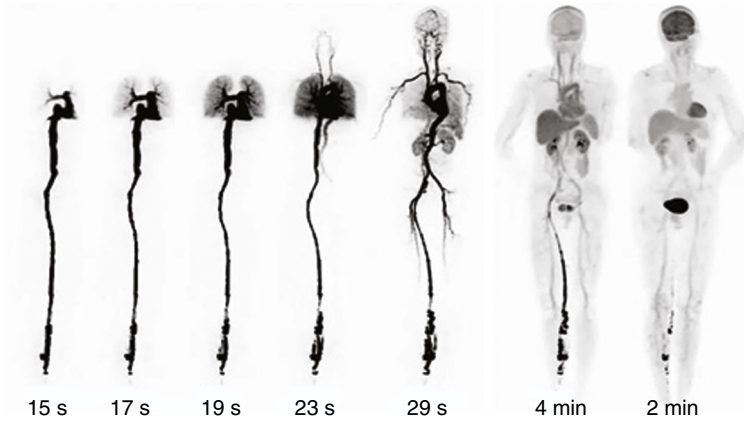


FIGURE 18.9 ¹⁸F-flurpiridaz PET/CT versus ^{99m}Tc-SPECT MPI. Stress/rest ^{99m}Tc-sestamibi images (top) and ¹⁸F-flurpiridaz PET/CT images (bottom) of the same patient. SPECT images were normal, whereas PET/CT images showed a large region of ischemia in the anterior wall, anteroseptal wall, and apex. (From Berman DS, et al. Phase II safety and clinical comparison with single-photon emission computed tomography myocardial perfusion imaging for detection of coronary artery disease: flurpiridaz F18 positron emission tomography. *J Am Coll Cardiol* 2013;61:469-747.)



- High quality imaging
- Scan duration <2 min
- Ultra low dose imaging <1 mCi
- Late imaging ¹⁸F-FDG 10 hr
- Whole body dynamic imaging



EFIGURE 18.10 Whole-body PET/CT scanner. Whole-body PET scanner with a z-axis length of nearly 1.7 m. This scanner offers advantages of high-quality images, scan duration of less than 2 minutes, ultralow-dose imaging (<1 mCi), late imaging at 10 hours ¹⁸F-FDG PET, and whole-body dynamic images. (From Badawi RD, et al. First human imaging studies with the EXPLORER Total-Body PET Scanner. *J Nucl Med* 2019;60:299-303; and Cherry SR, et al. Total-body imaging: transforming the role of positron emission tomography. *Sci Transl Med* 2017;9:eaaf6169.)



Aortic Valve Disease

Calcific aortic valve stenosis is one of the most common valvular disease of aging (see Chapter 72). Currently, the only effective therapy is aortic valve replacement, which is most effective when applied before onset of irreversible interstitial myocardial fibrosis. Echocardiography is usually the first imaging test in the evaluation of valvular heart disease and aortic disease and provides information of EF, mass, and global longitudinal strain (see Chapter 16). CMR additionally provides evidence of extracellular volume expansion (see Chapter 19). Radionuclide imaging is playing an emerging role in imaging inflammation, microvascular calcification, ATTR amyloidosis (see Fig. 72.13), infection, and microvascular dysfunction in patients with aortic valve disease.

Patients with severe aortic stenosis may remain asymptomatic and accurate prediction of disease progression remains challenging. Inflammation and microcalcification have been proposed as potential mechanisms that lead to progressive aortic stenosis. In one study 30 patients with aortic stenosis underwent ¹⁸F-NaF and ¹⁸F-FDG PET/CT.⁶⁶ In 12 of these patients the excised valves after surgery were evaluated for inflammation (CD68 staining) and microcalcification (alkaline phosphatase and osteocalcin) and 18 patients underwent aortic valve calcium scoring at baseline and after 1 year (see Fig. 72.12). ¹⁸F-FDG imaging did not correlate with CD68 staining.⁶⁶ Baseline ¹⁸F-NaF but not ¹⁸F-FDG, correlated closely with increase in aortic valve calcification on CT ($r = 0.66$; $P < 0.01$).⁶⁶ Ongoing studies will inform us whether ¹⁸F-NaF-guided management of aortic stenosis is superior to current clinical management. eFig. 18.11 shows ¹⁸F-NaF PET in a patient with native and prosthetic valve aortic stenosis (see also Fig. 72.12).

Severe aortic stenosis increases LV wall thickness, wall stress, and afterload, each of which decreases coronary microvascular function. Advanced phenotyping of patients with severe asymptomatic aortic stenosis using myocardial perfusion reserve is identifying an advanced disease phenotype that may benefit from valve replacement before advanced irreversible LV remodeling. In a study of 43 patients with aortic stenosis or sclerosis and a matched cohort of 43 patients without aortic valve disease, global MFR decreased with increasing aortic valve stenosis.⁶⁷ Reduced MFR was associated with worse function (global longitudinal strain) and survival free of MACE after a median follow-up of 7 years. Adjusted annualized MACE rates were determined by MFR and global longitudinal strain, and they were highest in patients with both abnormal values and lowest in those with both normal values (30.99% vs. 1.86%, $P = 0.002$).⁶⁷

Wild-type ATTR-CA and aortic stenosis are both diseases of aging and a prevalent cause of heart failure in the elderly. Transcatheter aortic valve replacement (TAVR) has revolutionized the treatment of aortic stenosis making it accessible to patients with severe comorbidities precluding surgery (see Chapter 74). In aortic stenosis the left ventricle is thickened because of myocyte hypertrophy, whereas in amyloidosis the left ventricle is thickened because of infiltration by amyloid fibrils. Both conditions are characterized by high intraventricular pressures, high wall stress, high filling pressures, subendocardial and microvascular ischemia, heart failure, arrhythmia, contractile dysfunction, angina, syncope, and death (see Chapters 53 and 72). Patients with very advanced aortic stenosis may manifest features of myocardial disease, reduced cardiac output, and poor prognosis. Both diseases can potentiate heart failure and small initial reports suggested that patients with dual pathology of ATTR-CA and aortic stenosis were at higher risk of post-TAVR mortality.⁶⁸ More recent studies refute those initial reports and suggest no differences in post-TAVR mortality. A recent two-center study of 204 patients undergoing TAVR for severe aortic stenosis showed that after a mean follow-up of 2 years, post-TAVR survival was similar in aortic stenosis patients with and without ATTR-CA.⁶⁹ However, 1-year heart failure hospitalization rate was higher in those with dual aortic stenosis and ATTR-CA.⁶⁹

REFERENCES

Principles of Imaging, Interpretation of Images, and Radiation Dose

- Dorbala S, Ananthasubramanian K, Armstrong JS, et al. Single Photon Emission Computed Tomography (SPECT) myocardial perfusion imaging guidelines: instrumentation, acquisition, processing, and interpretation. *J Nucl Cardiol*. 2018;25:1784–1846.
- Dilsizian V, Bacharach SL, Beanlands RS, et al. ASNC imaging guidelines/SNMMI procedure standard for Positron Emission Tomography (PET) nuclear cardiology procedures. *J Nucl Cardiol*. 2016;23:1187–1226.

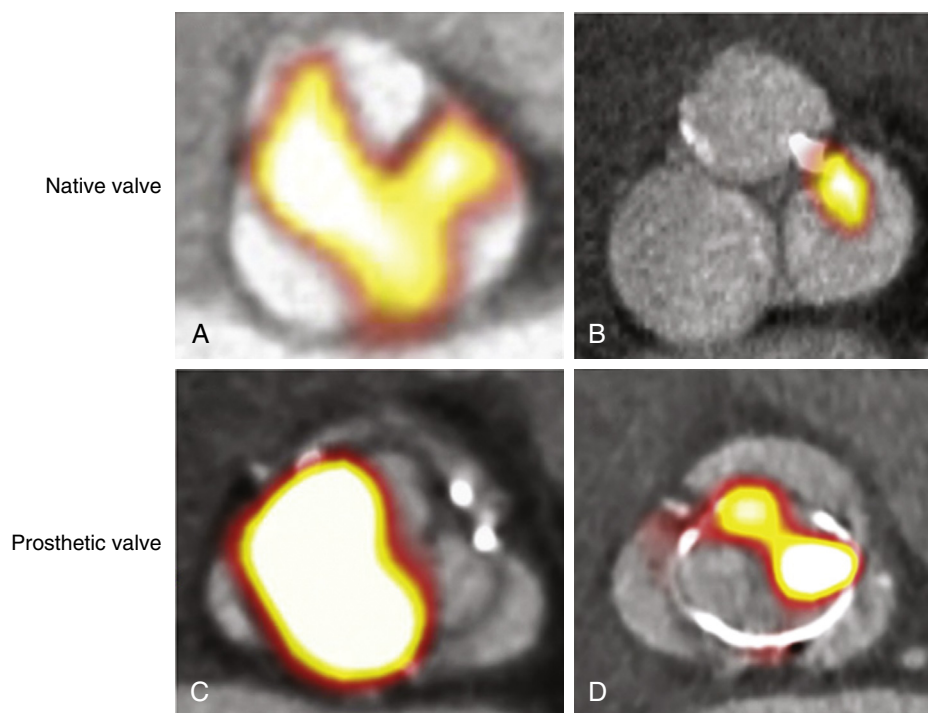
- Taegtmeyer H, Young ME, Lopaschuk GD, et al. Assessing cardiac metabolism: a scientific statement from the American Heart Association. *Circ Res*. 2016;118:1659–1701.
- Viola A, Munari F, Sanchez-Rodriguez R, et al. The metabolic signature of macrophage responses. *Front Immunol*. 2019;10:1462.
- Duncker DJ, Koller A, Merkus D, Cauty Jr JM. Regulation of coronary blood flow in health and ischemic heart disease. *Prog Cardiovasc Dis*. 2015;57:409–422.
- Henzlava MJ, Duvall WL, Einstein AJ, et al. ASNC imaging guidelines for SPECT nuclear cardiology procedures: stress, protocols, and tracers. *J Nucl Cardiol*. 2016;23:606–639.
- Chareonthaitawee P, Beanlands RS, Chen W, et al. Joint SNMMI-ASNC expert consensus document on the role of (18)F-FDG PET/CT in cardiac sarcoid detection and therapy monitoring. *J Nucl Cardiol*. 2017;24:1741–1758.
- Dorbala S, Ando Y, Bokhari S, et al. ASNC/AHA/ASE/EANM/HFSA/ISA/SCMR/SNMMI expert consensus recommendations for multimodality imaging in cardiac amyloidosis: Part 1 of 2-evidence base and standardized methods of imaging. *J Nucl Cardiol*. 2019;26:2065–2123.
- Murthy VL, Bateman TM, Beanlands RS, et al. Clinical quantification of myocardial blood flow using PET: joint position paper of the SNMMI cardiovascular council and the ASNC. *J Nucl Cardiol*. 2018;25:269–297.
- Dorbala S, Di Carli MF, Beanlands RS, et al. Prognostic value of stress myocardial perfusion positron emission tomography: results from a multicenter observational registry. *J Am Coll Cardiol*. 2013;61:176–184.
- Dorbala S, Blankstein R, Skali H, et al. Approaches to reduce radiation dose from radionuclide myocardial perfusion imaging. *J Nucl Med*. 2015;56:592–599.
- Einstein AJ, Pascual TN, Mercuri M, et al. Current worldwide nuclear cardiology practices and radiation exposure: results from the 65 country IAEA Nuclear Cardiology Protocols Cross-Sectional Study (INCAPS). *Eur Heart J*. 2015;36:1689–1696.

Clinical Applications—Ischemic Heart Disease

- Medical Advisory S. Single photon emission computed tomography for the diagnosis of coronary artery disease: an evidence-based analysis. *Ont Health Technol Assess Ser*. 2010;10:1–64.
- Takx RA, Blomberg BA, El Aidi H, et al. Diagnostic accuracy of stress myocardial perfusion imaging compared to invasive coronary angiography with fractional flow reserve meta-analysis. *Circ Cardiovasc Imaging*. 2015;8:e002666.
- Driessen RS, Danad I, Stuijzand WJ, et al. Comparison of coronary computed tomography angiography, fractional flow reserve, and perfusion imaging for ischemia diagnosis. *J Am Coll Cardiol*. 2019;73:161–173.
- Neglia D, Rovai D, Caselli C, et al. Detection of significant coronary artery disease by noninvasive anatomical and functional imaging. *Circ Cardiovasc Imaging*. 2015;8:e002179.
- Danad I, Rajmakers PG, Driessen RS, et al. Comparison of coronary CT angiography, SPECT, PET, and hybrid imaging for diagnosis of ischemic heart disease determined by fractional flow reserve. *JAMA Cardiol*. 2017;2:1100–1107.
- Shaw LJ, Hage FG, Berman DS, Hachamovich R, Iskandrian A. Prognosis in the era of comparative effectiveness research: where is nuclear cardiology now and where should it be? *J Nucl Cardiol*. 2012;19:1026–1043.
- Patel KK, Spertus JA, Chan PS, et al. Extent of myocardial ischemia on positron emission tomography and survival benefit with early revascularization. *J Am Coll Cardiol*. 2019;74:1645–1654.
- Murthy VL, Naya M, Foster CR, et al. Improved cardiac risk assessment with noninvasive measures of coronary flow reserve. *Circulation*. 2011;124:2215–2224.
- Charytan DM, Skali H, Shah NR, et al. Coronary flow reserve is predictive of the risk of cardiovascular death regardless of chronic kidney disease stage. *Kidney Int*. 2018;93:501–509.
- Naya M, Murthy VL, Foster CR, et al. Prognostic interplay of coronary artery calcification and underlying vascular dysfunction in patients with suspected coronary artery disease. *J Am Coll Cardiol*. 2013;61:2098–2106.
- Shah NR, Charytan DM, Murthy VL, et al. Prognostic value of coronary flow reserve in patients with dialysis-dependent ESRD. *J Am Soc Nephrol*. 2016;27:1823–1829.
- Mahmari JJ, Shaw LJ, Filipchuk NG, et al. A multinational study to establish the value of early adenosine technetium-99m sestamibi myocardial perfusion imaging in identifying a low-risk group for early hospital discharge after acute myocardial infarction. *J Am Coll Cardiol*. 2006;48:2448–2457.
- Taqeti VR, Everett BM, Murthy VL, et al. Interaction of impaired coronary flow reserve and cardiomyocyte injury on adverse cardiovascular outcomes in patients without overt coronary artery disease. *Circulation*. 2015;131:528–535.
- Al-Khatib SM, Stevenson WG, Ackerman MJ, et al. 2017 AHA/ACC/HRS guideline for management of patients with ventricular arrhythmias and the prevention of sudden cardiac death: a report of the American College of Cardiology/American Heart Association task force on clinical practice guidelines and the Heart Rhythm Society. *Circulation*. 2018;138:e272–e391.
- Gupta A, Harrington M, Albert CM, et al. Myocardial scar but not ischemia is associated with defibrillator shocks and sudden cardiac death in stable patients with reduced left ventricular ejection fraction. *JACC Clin Electrophysiol*. 2018;4:1200–1210.
- Partington SL, Valente AM, Bruyere Jr J, et al. Reducing radiation dose from myocardial perfusion imaging in subjects with complex congenital heart disease. *J Nucl Cardiol*. 2019. <https://doi.org/10.1007/s12350-019-01811-y>.

Clinical Applications—Heart Failure and Cardiomyopathies

- Panza JA, Ellis AM, Al-Khalidi HR, et al. Myocardial viability and long-term outcomes in ischemic cardiomyopathy. *N Engl J Med*. 2019;381:739–748.
- Mc Ardle B, Shukla T, Nichol G, et al. Long-term follow-up of outcomes with F-18-Fluorodeoxyglucose positron emission tomography imaging-assisted management of patients with severe left ventricular dysfunction secondary to coronary disease. *Circ Cardiovasc Imaging*. 2016;9:e004331.
- Bonow RO, Maurer G, Lee KL, et al. Myocardial viability and survival in ischemic left ventricular dysfunction. *N Engl J Med*. 2011;364:1617–1625.
- Jacobson AF, Senior R, Cerqueira MD, et al. Myocardial iodine-123 meta-iodobenzylguanidine imaging and cardiac events in heart failure. Results of the prospective ADMIRE-HF (AdreView Myocardial Imaging for Risk Evaluation in Heart Failure) study. *J Am Coll Cardiol*. 2010;55:2212–2221.
- Fallavollita JA, Heavey BM, Luisi Jr AJ, et al. Regional myocardial sympathetic denervation predicts the risk of sudden cardiac arrest in ischemic cardiomyopathy. *J Am Coll Cardiol*. 2014;63:141–149.
- Dorbala S, Cuddy S, Falk RH. How to image cardiac amyloidosis: a practical approach. *JACC Cardiovasc Imaging*. 2020;13:1368–1383.
- Gillmore JD, Maurer MS, Falk RH, et al. Nonbiopsy diagnosis of cardiac transthyretin amyloidosis. *Circulation*. 2016;133:2404–2412.
- Dorbala S, Ando Y, Bokhari S, et al. ASNC/AHA/ASE/EANM/HFSA/ISA/SCMR/SNMMI expert consensus recommendations for multimodality imaging in cardiac amyloidosis: Part 2 of 2-Diagnostic criteria and appropriate utilization. *J Nucl Cardiol*. 2019;26:2065–2123.
- Dorbala S, Park MA, Cuddy S, et al. Absolute quantitation of cardiac (99m)Tc-pyrophosphate using cadmium zinc telluride-based SPECT/CT. *J Nucl Med*. 2020. <https://doi.org/10.2967/jnumed.120.247312>.
- Singh V, Falk R, Di Carli MF, et al. State-of-the-art radionuclide imaging in cardiac transthyretin amyloidosis. *J Nucl Cardiol*. 2019;26:158–173.



EFIGURE 18.11 Molecular imaging of aortic stenosis and bioprosthetic valve degeneration. Selected hybrid ^{18}F -sodium fluoride (NaF) positron emission tomography and contrast-enhanced, electrocardiogram-gated computed tomography angiograms demonstrate increased tracer activity localizing to the valve leaflet as a marker of increased calcification activity in aortic stenosis (**A** and **B**) and bioprosthetic valves (**C** and **D**). (Images courtesy Dr. Mark Dweck, University of Edinburgh, Scotland.)

39. Rosengren S, Skibsted Clemmensen T, Tolbod L, et al. Diagnostic accuracy of [(11)C]PIB positron emission tomography for detection of cardiac amyloidosis. *JACC Cardiovasc Imaging*. 2020;13:1337–1347.
40. Ehman EC, El-Sady MS, Kijewski MF, et al. Early detection of multiorgan light-chain amyloidosis by whole-body (18)F-florbetapir PET/CT. *J Nucl Med*. 2019;60:1234–1239.
41. Cuddy SAM, Bravo PE, Falk RH, et al. Improved quantification of cardiac amyloid burden in systemic light chain amyloidosis: redefining early disease? *JACC Cardiovasc Imaging*. 2020;13:1325–1336.
42. Blankstein R, Osborne M, Naya M, et al. Cardiac positron emission tomography enhances prognostic assessments of patients with suspected cardiac sarcoidosis. *J Am Coll Cardiol*. 2014;63:329–336.
43. Slart R, Glaudemans A, Lancellotti P, et al. A joint procedural position statement on imaging in cardiac sarcoidosis: from the cardiovascular and inflammation & infection Committees of the European Association of Nuclear Medicine, the European Association of Cardiovascular Imaging, and the American Society of Nuclear Cardiology. *J Nucl Cardiol*. 2018;25:298–319.
- Clinical Applications—Endocarditis, Vasculitis, Cardio-Oncology**
44. Miller RJH, Cadet S, Pournazari P, et al. Quantitative assessment of cardiac hypermetabolism and perfusion for diagnosis of cardiac sarcoidosis. *J Nucl Cardiol*. 2020. <https://doi.org/10.1007/s12350-020-02201-5>.
45. Pizzi MN, Roque A, Fernandez-Hidalgo N, et al. Improving the diagnosis of infective endocarditis in prosthetic valves and intracardiac devices with 18F-fluorodeoxyglucose positron emission tomography/computed tomography angiography: initial results at an infective endocarditis referral center. *Circulation*. 2015;132:1113–1126.
46. Swart LE, Gomes A, Scholtens AM, et al. Improving the diagnostic performance of (18)F-fluorodeoxyglucose positron-emission tomography/computed tomography in prosthetic heart valve endocarditis. *Circulation*. 2018;138:1412–1427.
47. Gomes A, Glaudemans A, Touw DJ, et al. Diagnostic value of imaging in infective endocarditis: a systematic review. *Lancet Infect Dis*. 2017;17:e1–e14.
48. San S, Ravis E, Tessonier L, et al. Prognostic value of (18)F-fluorodeoxyglucose positron emission tomography/computed tomography in infective endocarditis. *J Am Coll Cardiol*. 2019;74:1031–1040.
49. Habib G, Lancellotti P, Antunes MJ, et al. 2015 ESC guidelines for the management of infective endocarditis: the task force for the management of infective endocarditis of the European Society of Cardiology (ESC). Endorsed by: European Association for Cardio-Thoracic Surgery (EACTS), the European Association of Nuclear Medicine (EANM). *Eur Heart J*. 2015;36:3075–3128.
50. Slart R. FDG-PET/CT(A) imaging in large vessel vasculitis and polymyalgia rheumatica: joint procedural recommendation of the EANM, SNMMI, and the PET Interest Group (PIG), and endorsed by the ASNC. *Eur J Nucl Med Mol Imaging*. 2018;45:1250–1269.
51. Armenian SH, Lacchetti C, Barac A, et al. Prevention and monitoring of cardiac dysfunction in survivors of adult cancers: American Society of Clinical Oncology clinical practice guideline. *J Clin Oncol*. 2017;35:893–911.
52. Farrell MB, Galt JR, Georgoulis P, et al. SNMMI procedure standard/EANM guideline for gated equilibrium radionuclide angiography. *J Nucl Med Technol*. 2020;48:126–135.
53. Lancellotti P, Nkomo VT, Badano LP, et al. Expert consensus for multi-modality imaging evaluation of cardiovascular complications of radiotherapy in adults: a report from the European Association of Cardiovascular Imaging and the American Society of Echocardiography. *Eur Heart J Cardiovasc Imaging*. 2013;14:721–740.
- Artificial Intelligence and Translational Molecular Imaging**
54. Betancur J, Comandeur F, Motlagh M, et al. Deep learning for prediction of obstructive disease from fast myocardial perfusion SPECT: a multicenter study. *JACC Cardiovasc Imaging*. 2018;11:1654–1663.
55. Hu LH, Miller RJH, Sharif T, et al. Prognostically safe stress-only single-photon emission computed tomography myocardial perfusion imaging guided by machine learning: report from REFINE SPECT. *Eur Heart J Cardiovasc Imaging*. 2020. <https://doi.org/10.1093/ehjci/jeaa134>.
56. Betancur J, Otaki Y, Motwani M, et al. Prognostic value of combined clinical and myocardial perfusion imaging data using machine learning. *JACC Cardiovasc Imaging*. 2018;11:1000–1009.
57. Stacy MR, Paeng JC, Sinusas AJ. The role of molecular imaging in the evaluation of myocardial and peripheral angiogenesis. *Ann Nucl Med*. 2015;29:217–223.
58. Chowdhury MM, Tarkin JM, Evans NR, et al. (18)F-FDG uptake on PET/CT in symptomatic versus asymptomatic carotid disease: a meta-analysis. *Eur J Vasc Endovasc Surg*. 2018;56:172–179.
59. Tarkin JM, Joshi FR, Rudd JH. PET imaging of inflammation in atherosclerosis. *Nat Rev Cardiol*. 2014;11:443–457.
60. Dweck MR, Chow MW, Joshi NV, et al. Coronary arterial 18F-sodium fluoride uptake: a novel marker of plaque biology. *J Am Coll Cardiol*. 2012;59:1539–1548.
61. Joshi NV, Vesey AT, Williams MC, et al. 18F-fluoride positron emission tomography for identification of ruptured and high-risk coronary atherosclerotic plaques: a prospective clinical trial. *Lancet*. 2014;383:705–713.
62. Derlin T, Sedding DG, Dutzmann J, et al. Imaging of chemokine receptor CXCR4 expression in culprit and nonculprit coronary atherosclerotic plaque using motion-corrected [(68)Ga]pentixafor PET/CT. *Eur J Nucl Med Mol Imaging*. 2018;45:1934–1944.
63. Tarkin JM, Joshi FR, Evans NR, et al. Detection of atherosclerotic inflammation by (68)Ga-DOTATATE PET compared to [(18)F]FDG PET imaging. *J Am Coll Cardiol*. 2017;69:1774–1791.
64. Maddahi J, Lazewatsky J, Udelson JE, et al. Phase-III clinical trial of fluorine-18 flurpiridaz positron emission tomography for evaluation of coronary artery disease. *J Am Coll Cardiol*. 2020;76:391–401.
65. Badawi RD, Shi H, Hu P, et al. First human imaging studies with the EXPLORER total-body PET scanner. *J Nucl Med*. 2019;60:299–303.
66. Dweck MR, Jenkins WS, Vesey AT, et al. 18F-sodium fluoride uptake is a marker of active calcification and disease progression in patients with aortic stenosis. *Circ Cardiovasc Imaging*. 2014;7:371–378.
67. Zhou W, Bajaj N, Gupta A, et al. Coronary microvascular dysfunction, left ventricular remodeling, and clinical outcomes in aortic stenosis. *J Nucl Cardiol*. 2019. <https://doi.org/10.1007/s12350-019-01706-y>.
68. Falk RH, Dorbala S. Transthyretin cardiac amyloidosis in patients with severe aortic stenosis. *Eur Heart J*. 2020;41:2768–2770.
69. Rosenblum H, Masri A, Narotsky DL, et al. Unveiling outcomes in coexisting severe aortic stenosis and transthyretin cardiac amyloidosis. *Eur J Heart Fail*. 2020. <https://doi.org/10.1002/ehfj.1974>.